AD-A053 584 MASSACHUSETTS INST OF TECH CAMBRIDGE DEPT OF ELECTRI--ETC F/G 20/12
CLUSTER MODEL INVESTIGATION OF DEFECTS IN SOLIDS.(U)
APR 78 G W PRATT N00014-75-C-0785

UNCLASSIFIED NL

1 OF 2
AD
A053584

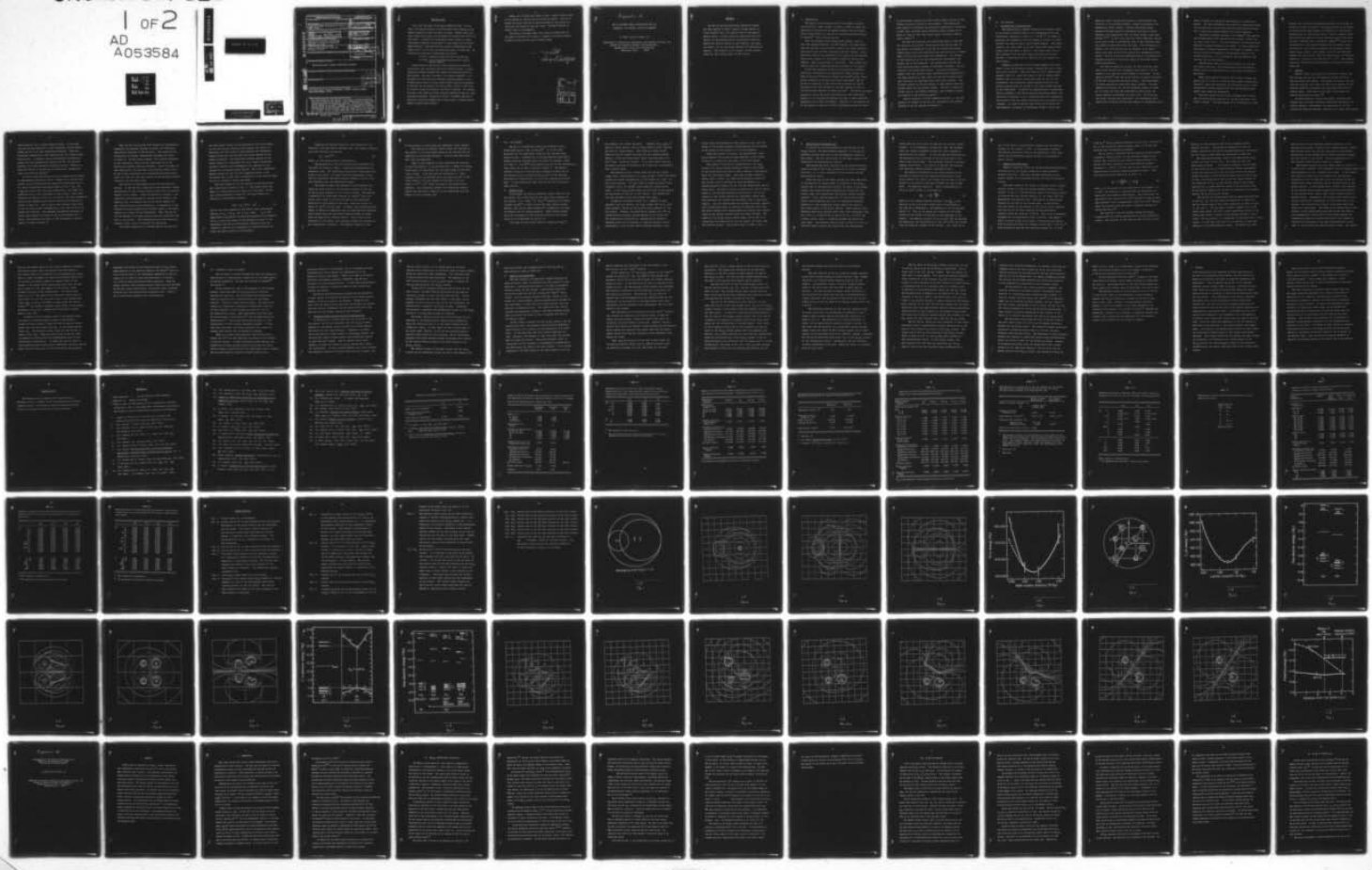

SECURITY CLASSIFICATION OF THIS PAGE (When Data Entered)

REPORT DOCUMENTATION PAGE

READ INSTRUCTIONS BEFORE COMPLETING FORM

1. REPORT NUMBER
2. GOVT ACCESSION NO.
3. RECIPIENT'S CATALOG NUMBER

4. TITLE (and Subtitle)
Cluster Model Investigation of Defects in Solids

5. TYPE OF REPORT & PERIOD COVERED
Final Technical Report
1 Feb 75 - 31 Jan 77

6. PERFORMING ORG. REPORT NUMBER

7. AUTHOR(s)
George W. Pratt

8. CONTRACT OR GRANT NUMBER(s)
N00014-75-C-0785

9. PERFORMING ORGANIZATION NAME AND ADDRESS
Massachusetts Institute of Technology
Department of Electrical Engineering
Cambridge, MA 02139

10. PROGRAM ELEMENT, PROJECT, TASK AREA & WORK UNIT NUMBERS
121102

11. CONTROLLING OFFICE NAME AND ADDRESS
Office of Naval Research (Code 427)
Arlington, VA 22217

12. REPORT DATE
Apr 78

13. NUMBER OF PAGES
180

14. MONITORING AGENCY NAME & ADDRESS (if different from Controlling Office)

15. SECURITY CLASS. (of this report)
Unclassified

15a. DECLASSIFICATION/DOWNGRADING SCHEDULE

16. DISTRIBUTION STATEMENT (of this Report)

Approved for public release, distribution unlimited

17. DISTRIBUTION STATEMENT (of the abstract entered in Block 20, if different from Report)

18. SUPPLEMENTARY NOTES

19. KEY WORDS (Continue on reverse side if necessary and identify by block number)
Solid State Theory, Crystalline Defects, F-center, Radiation Damage, High Pulsed Magnetic Fields.

20. ABSTRACT (Continue on reverse side if necessary and identify by block number)

The SCF-Xα method has been applied to the study of crystalline defects. First the LiF molecule was studied. The Xα method gave the correct internuclear separation and vibrational frequency. This work was extended to the LiF crystal via a cluster treatment. The correct lattice constant was derived and the electronic structure was in agreement with experiment. The final phase of the work dealt with the removal of an F_2^- ion creating an F_2^- center. The Xα - cluster method gave a good description of this defect.

DD FORM 1 JAN 73 1473 EDITION OF 1 NOV 65 IS OBSOLETE
S/N 0102-014-6601

SECURITY CLASSIFICATION OF THIS PAGE (When Data Entered)

220045

ONR FINAL REPORT

This is the Final Report of ONR Contract N00014-75-C-0785. The main focus of the research has been on solid state theory with an emphasis on the magnetic properties of matter and defect in crystals. Magnetic phase transitions, energy hand structures, and the formation of vacancies and interstitials were studied. In addition very large magnetic pulses suitable for remote electromagnetic detection were generated in a joint program with the National Magnet Laboratory. These pulses had peak currents of 22,000 ampues, pulse lengths from 0.1 uc to 30 usec. and maximum pulse power of 48 mega watts. The following Ph.D. theses were completed under this contract.

1. Eric Li, "Electronic Energy Structure of F_eS_2 and N_iS_2"
2. D. Choo, "SCF Xα Cluster Model Calculations for Crystals and Point Defects"

A detailed study of the electronic states associated with impurities, iso-electronic traps, and vacancy and interstial defects was made. A cluster technique developed by Professor Keith Johnson was extended and applied to these problems. This work is included in this report as Appendices I - III. The objective of this program was to develop a technique adequate in scope to handle defect problems in nuclear reactor materials where the condensation of individual lattice vacancies into voids and then a lattice of voids leads to a swelling of materials exposed to high levels of radiation. This swelling, by as much as 25%, leads to a serious structural weakening and hence to a dangerous made of operation. The ability of the SCF - Xα method to describe vacancies and interstitials suggests that it may be useful in studying radiation damage in nuclear reactor materials.

Perhaps, one of the most basic defects is the F - center in alholi holides. LiF was selected as a practical case to initiate the research. First the LiF molecule was treated, then the LiF crystal simulated by a Li_4F_4 cluster and finally one F was removed to study the F center. The results obtained are stated in detail in the appendices.

The principal investigator would like to express his appreciation for the support of the ONR in this research. A proposal is now being considered by ERDA to continue with the study of radiation damage.

Principal Investigator

Appendix I.

SCF Xα CLUSTER MODEL CALCULATIONS FOR LiF MOLECULE, LiF CRYSTAL, AND ITS F-CENTER*

D. Choo† and G.W. Pratt, Jr.

Department of Electrical Engineering and Computer Science, and
Center for Materials Science and Engineering
Massachusetts Institute of Technology
Cambridge, Mass. 02139

ABSTRACT

The SCF Xα multiple-scattering method of Johnson has been applied to small, neutral cluster models of a LiF molecule and a LiF crystal with an overlapping-sphere scheme. In both cases the calculated bulk properties at equilibrium, such as internuclear distance, vibrational quantum energy or bulk modulus, and cohesive energy, are in very good agreement wth experimental results. The F-center in LiF crystal is also studied using the same cluster model of the crystal.

I. INTRODUCTION

The purpose of the present work[1] is to model a crystalline solid by a small cluster of atoms in order to study the electronic structures of the perfect crystal and the crystal with a point defect via the SCF Xα multiple-scattering method of Johnson[2-7] from first principles.

Over the decades various energy-band methods, such as APW, OPW, pseudo-potential, and KKR methods, have been developed and applied to many perfect crystals for their electronic structures which includes long-range periodic effects. Still some basic equilibrium properties of a crystal can be obtained from a small portion of the crystal through its short-range effects, which will be shown in this paper. Such a model will also be ideal for investigating point defects in the crystal.

It has been possible to solve the point-defect problems from first principles by the energy-band method through the Green's function formalism of Koster and Slater[8], e.g. the single and di-vacancies in silicon by Callaway and Huges[9], and the Pb and Te vacancies in lead telluride by Parada and Pratt[10]. Calculation was also carried out for the F-center in LiF by the LCAO method recently by Chaney and Lin[11]. The SCF Xα multiple-scattering method has great advantages over such traditional methods in its straight-forwardness and ease in self-consistent computation with rapid convergence. However, in the applications of the method to crystals, careful considerations must be given

to the boundary conditions of the cluster models because of the inherent molecular nature of the clusters. This method has been applied to calculate the electronic properties of vacancies in PbS, PbTe, and SnTe using relatively large clusters of 27 atoms in order to make them nearly neutral including several atomic layers.[12]

LiF has both molecular and crystalline forms so that the LiF molecule can be first tested on how much and how well we can obtain its properties by the SCF Xα multiple-scattering method before we go into simulating the LiF crystal by a cluster model to calculate the crystal bulk properties. The changes of the properties as the LiF molecules are transformed into crystal can be also examined. The constituent atoms of LiF have relatively small numbers of electrons, therefore, the calculations can be performed easily. Also alkali halides in general have been studied rather thoroughly, both theoretically and experimentally, so that there are much data already available including the knowledge about their point defects. The F-center problem in the LiF crystal is also studied using the cluster model for the perfect crystal. The LiF is almost entirely ionic in its bonding character; more covalent crystals are treated in the following papers.[1]

The LiF molecule is first treated in Section II, and the perfect LiF crystal in Section III, followed by the F-center problem in the LiF crystal in Section IV.

II. LiF MOLECULE

A. Calculational Considerations

The heteronuclear diatomic molecule LiF is mostly ionic in its bonding character when it is in equilibrium with the internuclear distance of 2.854 a.u. (1.51 Å).[13] In order to determine the geometry of the LiF molecular cluster, we first consider the sizes of the Li and F atomic spheres. The atomic (neutral) and ionic radii of Li and F which were deduced from crystal data are shown in Table I. The atomic radii are so much different from the ionic radii that they will not be suitable in describing the LiF molecule (or LiF crystal for that matter).

Suppose we make the Li and F atomic spheres touch each other to form the molecular cluster, keeping the raio of their ionic radii constant. Then the radius of the F atomic sphere becomes 1.888 a.u., while the radius of the Li atomic sphere becomes 0.965 a.u.,which is too small even for the Li^+ ion. Furthermore, the interatomic region becomes relatively too large occupying about two thirds of the total volume enclosed by the outersphere. In muffin-tin approximation of potentials, which is adopted in the SCF Xα multiple-scattering method, the interatomic potential is only volume-averaged and consequently less accurate than the atomic potentials which are spherically averaged. In order to correct some errors which arises from this geometry, we employ an overlapping scheme in which the

spherical atomic regions are allowed to extend beyond the situation of the touching spheres, thereby overlapping with neighboring atomic regions. Similar overlapping-sphere schemes have been applied to molecules resulting in better agreement with experiments than the cases without using such schemes.[14,15] It will also allow the atomic spherical regions to be large enough to accommodate most of the electrons which are primarily associated with the atoms. The overlapping is, however, not to be carried too far because, if an atomic center gets deep into the core region of a neighboring atomic center, its core charge will adversely affect the spherically averaged potential in the outer region of the atomic center under consideration.

For the LiF molecular cluster, we start from the ionic radii which results in an overlapping scale factor 1.33 and varies it such that the virial theorem is satisfied. It was shown by Slater[16] that the virial theorem is exactly satisfied by the SCF X_α multiple-scattering method. The outer-sphere is always adjusted to touch both atomic spheres. The overlapping scale factor for the LiF molecular cluster is fixed at 1.4 after the first few iterations at which point the virial theorem is satisfied to within 0.2%. If we satisfy the virail theorem more accurately, the overlapping scale factor will be larger and the core charge of a neighboring atom

start to affect the potential erroneously by a significant amount. The same overlapping scale factor is used consistently for the molecular cluster with various internuclear distances. Fig. 1 shows the cluster geometry for the LiF molecule.

The atomic exchange parameter α of Schwarz[17] are used for the corresponding atomic centers of the cluster (0.78147 for Li, and 0.73732 for F). For the interatomic and extramolecular regions, a weighted average of the atomic α's with respect to the number of valence electrons in the atoms is adopted since we are primarily interested in the electron states of the valence electrons. It is 0.74468 for the LiF molecule (and the same for the LiF cyrstal).

The molecular basis functions are made of Li s,p and F s,p atomic functions. The contributions from the excited atomic levels are negligible due to the rapid convergence of the method.

Among the molecular orbitals, the 1σ and 2σ states are practically F 1s and Li 1s core electron states respectively. Therefore, their wave functions are calculated only in their corresponding atomic regions which for this purpose extend beyond their spherical boundaries.

The total energy of the cluster converges more slowly than the one-electron energies, as the self-consistent iterations proceed. The total energy of a LiF molecule is about

200 Ry, and it has to be computed accurately to the order of 0.001 Ry in order to obtain an accurate picture of the change of the molecular total energy as a function of internuclear distance near its equilibrium value. Such an accuracy could be achieved by performing enough iterations which runs about 15 with a modified Pratt improvement scheme[18,19] which were incorporated in the original program for the present study. At the end of the iteration procedure the potential convergence factor, which is the largest ratio of the difference between the starting and resultant potentials to the starting potential, becomes of the order of $10^{-3} \sim 10^{-4}$. The normalization of the partial-wave components for electron states was also made.

B. Results

Table II shows the results of the non-SCF (atomic) and SCF calculations for the LiF molecular cluster by the $X\alpha$ multiple-scattering method. The non-SCF calculation was done with the original ionic radii for the atomic spheres and the starting potential calculated from the charge densities of neutral atoms. Also shown in the table is the result of LCAO-MO calculation by Ransil.[20]

As self-consistent iterations proceed, the electronic charges tend to be more uniformly distributed throughout the cluster regions. Consequently the magnitudes of all the statistical energies decrease, resulting in a lower total energy

(more negative) and a larger cohesive energy. At the same time the constant potential in the interatomic region becomes higher and so do all the one-electron energies. These are the general tendencies of SCF iterations for any cluster model calculations. In general, the Xα one-electron energies are higher than the corresponding Hartree-Fock(HF) one-electron energies for either molecular clusters or atoms. There is a basic difference in the meaning of one-electron energies between the Xα and HF methods.[7]

We first study the molecule with its internuclear distance at experimental equilibrium value. Except the 1σ and 2σ core states, the only bound electron states of the molecule are 3σ, 4σ, and 1π states which are mostly made of F 2s, F $2p_z$, and F $2p_x$-type atomic wave functions respectively, with small contributions from s and p functions of the Li atom. Their wave functions are shown in Figs. 2a, 2b, and 2c; and their normalized partial-wave components and electron charge distributions are listed in Table III. The 3σ and 4σ wave functions show nodes in the Li atomic center corresponding to the node of the Li 2s atomic wave function. This apparent antibonding character of the 4σ state causes the rising of the 4σ level above the 1π level, thus reversing the order of the corresponding LCAO-MO result, as shown in Table II.

Next the SCF calculations were pursued for homogeneously compressed and expanded clusters to obtain the theoretical equilibrium properties of the molecule. The results of the calculations at several internuclear distances are shown in Table IV. As the cluster expands, the constant potential in the interatomic region and the magnitudes of all the statistical energies obviously decrease. Since the atoms are more separated at the same time, each electron energy level of the cluster approaches the corresponding electron energy level of a free ion, and the ionicity of the molecule slightly increases over the range shown.

The ionicity of each atomic center was calculated as follows. At the end of an iteration we get electronic charge distribution for each valence electron state over the various regions of the cluster. Since the electronic charges in the interatomic and extramolecular regions do not belong to any specific atom, we reassign them to the atomic centers for each valence electron state separately, in proportion to the valence electronic charges which already exists in the atomic ceneters as a result of the calculation. Then, the sum of all the charges in an atomic center gives the ionicity of the atom in the cluster. This redistributions of the electronic charges is done only to calculate the ionicities.

The virial coefficient is defined here as the ratio of

the total kinetic energy to the magnitude of the total energy. For all the cluster configurations treated, the virial coefficients are very close to unity because the overlapping-sphere scheme was used such that the virial theorem can be closely satisfied. The coefficient becomes smaller as the atomic centers are overlapped more for a given internuclear distance, however, more overlapping than used here is not pursued for the reason stated earlier. The virial coefficient becomes closer to unity for more expanded cluster, since the system then is more like a collection of free ions for which the virial theorem is better satisfied.

The total energy of the LiF molecule is plotted against the internuclear distance in Fig. 3. The figure shows that there is a stable equilibrium state over the range. We now use a simple parabolic formula for the total energy as a function of internuclear distance,

$$E(R) = E_o + \frac{k}{2} (R - R_o)^2 , \qquad (1)$$

and fit the total energies at the latter three internuclear distance of R_e, 1.02 R_e, and 10.5 R_e, where R_e is the experimental equilibrium internuclear distance of the molecule. The E_o is the total energy of the molecular cluster at the theoretical equilibrium internuclear distance R_o, and the constant k then can be interpreted as a spring constant between two atomic centers of the molecule.

Assuming the harmonic motion for the vibration of the molecule at the equilibrium configuration, the angular frequency ω_v of the vibration is given by

$$\omega_v = (k/\mu)^{1/2} , \qquad (2)$$

where μ is the reduced mass of the molecule.

The properties of the LiF molecule thus calculated from the model are listed in Table V along with corresponding experimental data. The theoretical equilibrium internuclear distance is only about 1.3% larger than the experimental value, and the calculated vibrational quantum energy is also in very good agreement with the experimental value.

The cohesive energy was obtained as the difference between the total energy of the molecular cluster and the sum of the Xα total energies of a Li and an F atoms. The exchange α parameters for atoms were computer by Schwarz[17] such that the Xα total energy of an atom is equal to the restricted Hartree-Fock total energy of the atom which was listed in a report by Mann[21] for all atoms. In Table V the calculated total energy is smaller in magnitude than the experimentally observed total energy while the calculated cohesive energy is larger than the experimental cohesive energy. This is due to the difference in the atomic total energies between the theoretical and experimental situations. The cohesive energies of the

of the molecule in both cases are reasonably close, however.

The theoretical electric dipole moment was obtained as the product of the calculated values of the ionicity and the equilibrium internuclear distance. It is in very good agreement with the experiment.

There is one remark to be made concerning the accuracy of the calculations. As we see from Fig. 3, there is a rather large margin of uncertainty for the total energy of the molecular cluster. (Also see previous subsection A.) More accuracy can not be attained since the relative error of the total energy at the last stages of iterations is of the order of $10^{-5} \sim 10^{-6}$ which is close to the minimum error possible. The uncertainty affects the vibrational quantum energy most seriously, which has to be interpreted with the margin of error of about $\pm$20%.

III. LiF CRYSTAL

The LiF in a crystalline form is an insulator with a direct band gap of 1.000 ± 0.004 Ry[22]. It is of a NaCl structure and its constituent atoms are the lightest among alkali halides. Consequently it has the smallest equilibrium nearest-neighbor distance among the family of crystals, which is 3.998 a.u. (2.01 Å)[23] being exactly the sum of the Zachariasen's ionic radii for Li and F as given in Table I. The nearest-neighbor distance for LiF has been increased by about 25% as the molecules form a crystal primarily due to the isotropic electrostatic interactions of ions in the crystalline environment. In the crystalline form, the LiF will still maintain a high ionicity.

A. Cluster Model

If we choose the smallest possible cluster model for the LiF crystal while retaining the full point group symmetry of the crystal, it is $(LiF_6)^{-5}$ or $(FLi_6)^{+5}$ necessarily including a Watson sphere[24] in order to make the whole system neutral. However, they are too much unbalanced in composition of atoms to simulate the LiF crystal properly. These cluster models are also unsuitable for the F-center problem of the crystal which will be considered in Section IV.

If we add two more atomic layers of atoms to $(FLi_6)^{+5}$,

for example, the cluster structure becomes $(FLi_6 F_{12}Li_8)^{+1}$, which is almost neutral but an extra electron still requires the use of a Watson sphere. This could be a good cluster model for the LiF crystal and also for the F-center problem. However, it has two inequivalent atomic sites for each of Li and F atoms unlike the crystal. It is also rather large for the present purpose of simulating the crystal by a conveniently small cluster model.

The smallest neutral cluster model for the LiF crystal larger than a mere molecule is a Li_4F_4 cluster in which the atomic centers are placed tetrahedrally at the corners of a cube for each atomic species. The next layer of atoms contains 24 atoms altogther which, if included, would make the cluster quite large. In the Li_4F_4 cluster model, all the atoms of each species are equivalent as they are in LiF crystal. The compositions are also the same in both the cluster and crystal.

In general a balanced cluster for a compound is less symmetric than the crystal; the Li_4F_4 cluster has the T_d point group symmetry instead of the O_h point group symmetry of the LiF crystal. However, the reduction of symmetry will not by itself present a serious problem because we can always use the compatibility relations for representations between a symmetry group and its subgroup to identify electron states. Furthermore, in any cluster model regardless whether it has

a full point group symmetry of the crystal or not, only the states of the highest symmetry representations can be related to the states of the crystal if it is ever possible.

Since the cluster is neutral, the electrostatic interaction between the cluster and the remainder of the crystal is kept at a minimum for the given size of the cluster.

The results of the SCF Xα claculations for the Li_4F_4 cluster with various nearest-neighbor distance within $\pm$20% of the experimental equilibrium value revealed no equilibrium state for the cluster model. Only when an empty spherical center (call O center) was added at the geometric center of the cluster could an equilibrium state be reached at a nearest-neighbor distance not far from the experimental equilibrium value. The empty O center is treated just like an atomic center in the multiple-scattering calculations, and its inclusion in the cluster reduces the interatomic region where wave functions are treated less accurately than in the atomic regions. Also the bonding behaviors between the atomic centers will be described better by linking the scattered waves from the atomic centers more closely, especially because the O center takes up the central position among the atomic centers. The model will be called OLi_4F_4 cluster model, and we use it to investigate the properties of the LiF crystal and later study the F-center problem. The cluster model is shown in Fig. 4.

B. Calculational Considerations

In the SCF X_α multiple-scattering calculations for the OLi_4F_4 cluster, the same exchange parameter α's of the LiF molecular cluster were used in the corresponding regions of the cluster. The α in the O center is the same α used in the interatomic and extramolecular regions.

The symmetrized basis functions for the valence electron states are made of the s and p functions of Li and F together with the s, p, d, and f functions for the O center and the extramolecular region.

Since the size of the atomic centers are more restricted by the presence of larger number of neighbors in the OLi_4F_4 cluster than in the molecular cluster, the radii of the atomic centers were calculated more rigorously as follows for the cluster model with experimental equilibrium nearest-neighbor distance. First, the touching radii of the Li and F atomic centers were determined such that the spherically averaged potentials in any neighboring atomic centers are equal at the contact point of the atomic spheres. These touching radii remained essentially constant after only a few iterations; they are 1.675 a.u. (0.866 Å) for Li and 2.123 a.u. (1.123 Å) for F atomic center, being intermediate between the atomic and ionic radii. The touching radius of the O center is 1.166 a.u. (0.619 Å) which is about 50% larger than the corresponding

radius when the ionic radii are used for the Li and F atomic centers. In the subsequent interations, then, the touching radii are linearly expanded so that the virial theorem is satisfied for the cluster. In this process the potentials of the neighboring atomic centers at the touching radii still remain practically equal. This procedure results in an overlapping scale factor, 1.14, and it is used for the clusters with different nearest-neighbor distances as well.

The Madelung corrections to the atomic potentials are included to account for the neglected electrostatic interaction between the ions in the cluster and the ions in the remainder of the crystal which were excluded from the cluster model. The Madelung correction term to the potential in the $\underline{i}$ th atomic center is calculated by

$$V_M^{\underline{i}} = 2 \alpha_M^{cl} \frac{q_{ion}^{\underline{i}}}{R} , \qquad (3)$$

where R is the nearest-neighbor distance, and $q_{ion}^{\underline{i}}$ is the ionicity of the $\underline{i}$ th atomic center which is calculated in the same way as described in the Subsection B of the previous Section II. That is, we assign the ionicity of the atomic centers of the cluster to the ions in the remainder of the crystal. The Madelung constant of the cluster α_M^{cl} was obtained by subtracting the contributions of the ions within the cluster from the Madelung constant of the crystal; this turns out to

be a 0.2915 which is significantly reduced from the Madelung constant of the crystal, 1.7476. In the present treatment the Madelung correction terms to the potentials in the interatomic and extramolecular regions as well as the central O region vanish.

C. Results and Discussions

Table VI lists the results of the SCF $X\alpha$ multiple-scattering calculations for the OLi_4F_4 cluster with various nearest-neighbor distances. They show the same tendencies as the cluster expands as we discussed earlier with the LiF molecular cluster.

The total energy of the cluster is plotted against lattice constant (which is twice the nearest-neighbor distance in LiF crystal) in Fig. 5. The equilibrium state of the OLi_4F_4 cluster is attained when the lattice constant is 7.4% larger than the experimental equilibrium value. This result is satisfactory considering the size of the cluster used. At equilibrium the total energy of the cluster is -214.322 Ry which, compared with the sum of the total energies of free atoms, gives cohesive energy per molecule, 0.638 Ry. This is in an excellent agreement with an experimental value, 0.644 Ry. The experimental cohesive energy with respect to free atoms was deduced from the cohesive energy with respect to free ions, -0.787 Ry,[25] with corrections made for the ionization energy of a Li atom,

0.396 Ry,[26] and the electron affinity of an F atom, -0.253 Ry.[27] Out of the calculated cohesive energy, about 0.1 Ry was contributed from the Madelung correction.

Now in order to calculate the bulk modulus we again assume a parabolic formula of Eq. (1) for the total energy of the cluster near equilibrium, and obtain a spring constant k by fitting the total energies at the three nearest-neighbor distances R = 1.05 Re, 1.074 Re, and 1.10 Re, where Re is the experiemental equilibrium nearest-neighbor distance. Then the equilibrium bulk modulus B_o is given by

$$B_o = V_o \left.\frac{d^2E(R)}{dV^2}\right|_o = \frac{1}{72}\frac{k}{R_o} \qquad (4)$$

where V is the volume for four molecules in the crystal, i.e. $V = 8R^3$, and subscript o indicates that the parameters are taken from the cluster at equilibrium. Thus calculated, the equilibrium bulk modulus 6.66×10^{11} dyne/cm^2 is also in very good agreement with an experimental value 6.98×10^{11} dyne/cm^2 which was obtained from the elastic stiffness constants of Brisco and Squire.[28]

The ionicity of the LiF crystal through the OLi_4F_4 cluster model is 0.899 at equilibrium in units of electronic charge. The reduction of the ionicity from 0.92 for the LiF

molecule is seen primarily due to the increased nearest-neighbor distance. The quilibrium properties of the LiF crystal obtained by the SCF Xα multiple-scattering calculations for the OLi_4F_4 cluster model are summarized in Table VII.

The one-electron energy levels of the equilibrium OLi_4F_4 cluster are shown in Fig. 6(a). The levels for the core electrons and mostly F 2s atomic electrons are not shown. In the figure the set of valence electron levels corresponds to the top valence band of the LiF crystal while the excited levels correspond to the conduction band levels of the crystal. In fact, the symmetries of the $3t_2$ and $3a_1$ states conform to the symmetries of the Γ_{15} top electron state of the valence band and the Γ_1 bottom electron state of the conduction band of the crystal respectively through the compatibility relations between the T_d and O_h point groups.

The partial-wave coefficients and the charge distributions of the $3t_2$, $3a_1$, and $4t_2$ states are described in Table VIII, and the contour maps of their wave functions are shown in Figs. 7a, 7b, and 7c. The $3t_2$ state is mostly composed of an F 2p atomic basis state, but with a small contribution from a Li 2s atomic basis state it gives a slight bonding between F and Li atoms. The $3a_1$ state is in a large part an extramolecular s state having a little more than half of its electronic charge probability in the extramolecular region. The higher $4t_2$ state

has even more of its electronic charge probability in the extramolecular region, primarily as an extramolecular p state. The excited states, $3a_1$ and $4t_2$, have more or less uniform distribution of the probability of finding electrons throughout the regions of the cluster. This is characteristic of the conduction band electron states of a crystal.

The bandgap derived from the cluster model is 0.54 Ry. It is quite small compared to the bandgap of the LiF crystal (about 1 Ry). This discrepancy can be explained as follows. In the crystal the conduction band levels are pushed up by the repulsive interactions from the electrons which has already filled the valence band levels completely and are located mostly in the atomic regions. In the cluster model, however, the electrons of the excited states largely escape from the atomic regions to the extramolecular region where little valence electronic charge resides. Consequently the excited state electrons can be more comfortably accommodated in the cluster than in the crystal, thus lowering their energy levels below where they would be in the crystal. The width of the valence band of the cluster is also significantly more narrow than the width of the corresponding valence band of the crystal because the interactions among the valence electrons in the cluster are limited by the presence of the empty extramolecular region, that is, by omitting some nearest-neighbor atoms. Now suppose

that all the energy levels of the valence electrons, including the excited levels, were contracted by the same degree in the cluster model by the presence of the extramolecular region. Then, in order to compare our results with energy band of the LiF crystal, we linearly expand the energy levels of the cluster in the ground state configuration such that its band-gap is equal to 1 Ry, the bandgap of the crystal, while aligning the tops of the valence bands. The linear scale factor is 1.85. The width of the resultant valence band of the cluster is 0.137 Ry, now quite close to the valence band width, about 0.125 Ry, of Brener's energy bands for the LiF crystal.[29] The linearly expanded energy levels of the cluster are shown in Fig. 8(a), compared with the Brener's energy bands in Fig. 8(b).

In order to find an exciton level in the present model we consider a transition-state cluster, using Slater's transition-state concept,[7] which has half an electron transferred from the top valence state, $3t_2$, to the lowest excited state, $3a_1$. The resultant energy levels of this cluster is shown in Fig. 6(b). Here the energy level of the $3a_1$ state is lowered by 0.044 Ry from the corresponding level in the ground-state configuration. It seems that the $3a_1$ state in the transistion-state configuration represents the first exciton state, while the $3a_1$ state in the ground-state configuration

represents the bottom of the conduction band of the crystal. Experimentally it was shown by Roessler and Walker[22] that the first exciton level in the fundamental absorption of the LiF crystal is at 0.927 Ry (with the half-width of 0.024 Ry), i.e. 0.073 Ry below the band-to-band transition. When the energy levels of the transition-state cluster are also expanded by the same linear scale factor, the exciton level is placed 0.081 Ry below the bottom of the conduction band. This is now in quite good agreement with the experiment.

IV. F-CENTER IN THE LiF CRYSTAL

The F-centers in alkali halides have been the subjects of many extensive investigations largely due to the significance in optical properties, and they are reviewed by Markham[30] and Fowler.[31]

On the theoretical side of the approach to the F-center problem, there have been calculations using a modified Hartree-Fock equation. One is the point-ion approximation based on neglecting the orthogonalization of the defect electron states to other electron states. The results obtained by a variational technique give absorption energies of the F-centers in alkal halides to within 10 ∿ 15% of the experimental values. Some improvements have been made by the extended-ion approximation[32] and the pseudo-potential approximation.[33] More crude semi-continuum model is also satisfactory for the F-center absorption problem. In fact, just about any model involving a potential well gives reasonably good results for the absorption energies.

There is a recent first-principle LCAO calculation by Chaney and Lin[11] for the electronic structure of the F-center in the LiF crystal. In this calculation atomic orbitals are approximate as being Gaussian-type to facilitate the multi-center integrals associated with the Hamiltonian matrix elements. The multiple-scattering method provides another first-

principle approach to the problem, and it is simpler and more straight-forward while keeping the orthogonality of the electron states in the system. There is no need to calculate difficult multicenter integrals, therefore, the SCF calculations can be performed rapidly. In this case approximation is made in modeling a cluster suitable for the crystal containaing the vacancy.

The SCF Xα multiple-scattering method can be applied to a large cluster for complete analysis of the F-center problem. However, we do not intend to be complete. Rather we will start from the small cluster model for the perfect LiF crystal, and show how much information we can obtain with such a minimal size of the cluster containing the F-vacancy.

A. F-Vacancy Model and Calculational Considerations

In formulating a cluster model for the F-vacancy in the LiF crystal, we will be consistent with the OLi_4F_4 cluster modeled for the perfect crystal so that we can also compare the results of both cases directly. Therefore, we remove the F atom from an F atomic center in the OLi_4F_4 cluster, and the resultant empty F atomic center (now called VacF center) is just like the O center. This F-vacancy cluster model becomes a cluster of $O{\cdot}VacF{\cdot}ALi{\cdot}Li_3{\cdot}F_3$ (called VacF cluster for convenience). It has a unique symmetry axis which connects the geometric centers of the VacF center and the O center, and

the ALi atomic center is a Li atomic enter on the axis, thereby being inequivalent to the other three Li atomic centers, which are equivalent among themselves. The remaining three F atomic centers are also equivalent. The symmetry of the VacF cluster belongs to the C_{3v} point group, a subgroup of the T_d point group for the OLi_4F_4 cluster.

In the SCF Xα multiple-scattering calculations for the VacF cluster, the same Madelung correction as was used for the OLi_4F_4 cluster is kept with the same ionicity. The exchange α parameter for the VacF center is the same α as we adopted for the O center as well as for the interatomic and extramolecular regions of the OLi_4F_4 cluster. Otherwise, the exchange α parameters and geometrical factors of the OLi_4F_4 cluster in its equilibrium state are retained.

The defect electron states due to the F-vacancy will be described in the extramolecular regions where neighboring atoms are missing as well as in the atomic centers and the interatomic region. In that sense the VacF cluster model is not quite ideal, however, it will be the smallest possible neutral cluster model for the F-vacancy, and in the present framework the defect electron states are equally well treated as the valence electron states of the VacF cluster or the OLi_4F_4 cluster.

The electron states of the VacF cluster and the OLi_4F_4 cluster can be correlated through the use of the compatibility

relations between the representations of the C_{3v} and T_d point groups as shown in Table IX.

B. Results and Discussions

The VacF cluster is an open-shell system obviously because the total number of electrons are odd, being 39 in all. Therefore, a spin-polarized scheme is in order to calculate electron states for the cluster. Calculations with spin-restricted scheme for the VacF cluster and $(VacF)^{+1}$ ionic cluster (the one missing electron from the F-center is now frozen on a Watson sphere, which is geometrically the same as the outersphere, to make the total system neutral) are also done for a comparative study. The results for the various clusters are described in Table X, and their electron energy level structures are shown in Fig. 9 compared with that of the OLi_4F_4 cluster.

As an F atom is removed from the OLi_4F_4 cluster, the top valence band loses six electron states counting degeneracy which accounts for a missing six-fold degenerate F 2p atomic level. At the same time only five valence electrons are lost, therefore, one electron is left over after the valence band is completely filled. This extra electron, which is associated with the F-center, is consequently accomodated by the next-higher $4a_1$ state in the VacF cluster. It is largely contained in the VacF center in the VacF cluster as one can

see by comparing the ionicities of the VacF center in the VacF cluster and the $(VacF)^{+1}$ cluster.

In the transition of the OLi_4F_4 cluster to the $(VacF)^{+1}$ cluster by losing an F^- ion, the width of the valence band decreases from 0.074 Ry to 0.065 Ry since six valence electron states are lost. At the same time the lost six electrons from cluster account for the lowering of the valence and conduction band levels by decreasing electron-electron interactions for the remaining electrons. Particularly, the $4a_1$ level is lowered deep into the bandgap from the conduction band by concentrating its wave function in the VacF center which would accommodate excited electrons more comforatably than any other region of the cluster.

The introduction of an electron into the $(VacF)^{+1}$ cluster, thus freeing the electron on the Watson sphere to make the system the VacF cluster, raises the valence band levels by increasing electron-electron interaction. However, the conduction band states are lowered a little because the new electron moves towards the inside of the cluster away from the Watson sphere around which the wave functions of the conduction band states are large.

Next, spin-polarization of the VacF cluster lowers all the spin-up electron levels (the $4a_1$ defect electron's spin is arbitrarily assumed to be up) and raises all the spin-

down electron levels, though changes in the valence band are negligible. The energy level structure of the spin-down electrons of the VacF cluster is quite similar to that of the OLi_4F_4 cluster. For all the VacF cluster configurations the width of the balence band remains fairly constant.

The wave functions of the top valence band state, 4e, and the excited states, $4a_1$, $5a_1$, and 5e, for both spins are shown in Figs. $10a_1$ through $10d_2$ by their contour map; and their normalized partial-wave components and electronic charge distributions are listed in Tables XIa and XIb.

The $4e^{\uparrow}$ and $4e^{\downarrow}$ states are almost identical to each other and similar to the top valence state, $3t_2$, of the OLi_4F_4 cluster, except in the centers along the symmetry axis including the VacF center. In terms of a spin-restricted perturbation, the $3t_2$ state of the OLi_4F_4 cluster is split into an a_1 and an e states as its symmetry is reduced from the T_d to C_{3v} point group with the introduction of the VacF center. The e state of the F-vacancy retains most of the characters of the $3t_2$ state of the OLi_4F_4 cluster except along the symmetry axis. However, the a_1 state which had its wave function concentrated along the axis previously in the OLi_4F_4 cluster is now so much perturbed by the F-vacancy that its energy level is driven up enormously (not shown in Fig. 9c). This a_1 state together with another e state from the valence band accounts for the

six electron states lost from the band as we discussed earlier.

The wave function of the $4a_1^{\uparrow}$ state is largely centered around the F-vacancy region as we see from Fig. $10b_1$, thereby simulating the F-center defect electron state of the LiF crystal. Its electronic charge is fairly uniformly distributed in the VacF center with the total of about half an electron. The wave function is mostly s-type with most of the contributiions coming from the VacF s and extramolecular s basis functions. The $4a_1$ states of both spins are the perturbed states of the $3a_1$ state of the OLi_4F_4 cluster due to the F-vacancy.

The difference between the $4a_1^{\uparrow}$ and $4a_1^{\downarrow}$ states is seen to result mainly from the difference in potentials in the F-vacancy region between spin-up and spin-down electrons, as shown in Fig. 11. The potential for a spin-up electron is rather low and approximately constant at about -0.65 Ry. On the other hand the potential for a spin-down electron becomes higher toward the center of the F-vacancy region, and it seems similar to the one which could be an effective (pseudo-) potential for the bottom conduction band state, $3a_1$, of the OLi_4F_4 cluster in the corresponding region. Consequently the $4a_1^{\uparrow}$ electron is more concentrated in the VacF center and lower in its energy than the $4a_1^{\downarrow}$ state.

The $4t_2$ state of the OLi_4F_4 cluster is now split to the 5e and $5a_1$ states when the F-vacancy is introduced. Let us first look at the $5a_1^{\uparrow}$ and $5a_1^{\downarrow}$ states. They are similar to each other in many aspects. But, while the primary extramolecular p character of the original $4t_2$ state of the OLi_4F_4 cluster is well preserved by the $5a_1^{\downarrow}$ state of the VacF cluster, a significant amount of s function sets in to distort such p character in the extramolecular region for the $5a_1^{\uparrow}$ state. The extramolecular s component is an extension of the s-type fucntion of the $5a_1^{\uparrow}$ state in the VacF center which also extends to the nearest-neighbor Li atomic centers of the cluster. Such character of the $5a_1^{\uparrow}$ wave function proves that the extramolecular region can approximately simulate missing neighboring atomic centers of the F-vacancy in the present cluster model. The s-type wave functions centered around the F-vacancy for the $5a_1$ states are less localized than those for the $4a_1$ states.

The $5e^{\uparrow}$ and $5e^{\downarrow}$ states are quire identical to each other, and mostly made of extramolecular p basis functions as in the case for the original $4t_2$ state of the OLi_4F_4 cluster. The contour map of the $4t_2$ wave function of the OLi_4F_4 cluster, which is shown in Fig. 7c, has p_z-type basis function in the extramolecular region. We can always combine this wave function with the other two equivalent P_x- and p_y-types to obtain new wave functions whose extramolecular p

functions are directed differently, for example, along the new symmetry axis of the VacF cluster as its 5e wave functions. Similar agruments can be made also for the $5a_1$ wave functions. For the $5a_1$ and 5e states also, the energy differences between the spin-up and spin-down electrons are attributed primarily to the difference in potentials in the F-vacancy region.

As the potential for a spin-up electron suggests, the F-center problem for the defect electron corresponds qualitatively to a three-dimensional potential-well problem. In view of a simple infinite square well model[34] or a hydrogenic model for the F-centers in alkali halides, the $4a_1^{\uparrow}$ state of the VacF cluster corresponds to the 1s state, and the $5a_1^{\uparrow}$ and $5e^{\uparrow}$ states correspond to the 2s and 2p states respectively. In these models the optical absorption of the F-center is the result of an electron excitation from the 1s to the 2p state.

The excitation energy from the $4a_1^{\uparrow}$ to the $5e^{\uparrow}$ state in the VacF cluster model is 0.178 Ry as the energy difference between the two energy levels. The transition energy calculated by Slater's transition-state scheme is 0.175 Ry, not much different from the above value. The difference in total energies between the clusters in ground and excited state configurations gives also similar figure for the excitation energy. However, if we expand the energy levels of ground-state VacF cluster linearly by the same scale factor of 1.85 as we did for the energy levels of the OLi_4F_4 cluster, the excitation energy be-

comes 0.33 Ry, close to an experimental result which indicates that the F-center absorption in a LiF crystal is peaked at 0.382 Ry with the half-width of 0.044 Ry.[35]

In the transition from the $(VacF)^{+1}$ cluster to the spin-restricted VacF cluster, total energy increases (in magnitude) by 0.181 Ry. Spin-polarization in the VacF cluster makes the total energy still larger (also in magnitude) by 0.033 Ry more.

The formation energy of the F-center in LiF is 0.674 Ry in the cluster model as the difference in total energies between the OLi_4F_4 cluster and a system of the VacF cluster plus a free F atom. However, the experimental formation energy is given with respect to an F atom adsorbed on the surface of the crystal; it is $0.172 \sim 0.197$ Ry.[36] Because such adsorption energy is not available, a comparison between the cluster model calculation and experiment for the formation energy of an F-center can not be made at present.

V. SUMMARY

A LiF molecule was first examined by direct application of the SCF Xα multiple-scattering method, and the results for molecular properties were shown in excellent agreement with experiments. Then we applied the method to the smallest-possible neutral cluster model of OLi_4F_4, consisting of only eight atoms and a centrally located empty spherical region whose existence is essential in achieving an equilibrium state for the cluster. Some modifications were made to calculate the sphere radii of the overlapping atomic centers self-consistently, and also to include a Madelung correction to atomic potentials due to the ions of the crystal which are not represented by the cluster model. The normalization of the partial-wave components and acceleration of convergence by a modified Pratt improvement scheme were also made in the program. From this model bulk properties of the LiF crystal at equilibrium were obtained in very good agreement with experiments. To conform to the energy-band structure of the crystal, the one-electron energy levels of the cluster were linearly expanded. The F-center problem of the crystal was also treated by introducing an F-vacancy at an F atomic center of the OLi_4F_4 cluster, and the consequent change of the electronic structures and the optical absorption due to the F-center were studied.

The results show that the SCF Xα multiple-scattering method can be used for small cluster models to simulate crystals (for a mostly covalent crystal, a GaP crystal is treated in a following paper[1]) and to study point defects. Larger cluster models may be used in such investigations to get more accurate quantitative results.

The total energies of clusters made of heavy atoms are too large to be accurate within 1 eV, which is the order of magnitude for the important thermodynamic parameters such as cohesive energies of crystals and formation or migration energies of point defects. To reduce the magnitude of total energies by subtracting common terms, we can freeze core electrons so that a nucleus and its core electrons enter as only one entity in calculating various terms of the total energies. Then accurate total energies can be compared to produce the thermodynamic parameters for any manageable-size clusters of any atoms. The change of total energy by changing the atomic positions in the OLi_4F_4 cluster was not accurate enough to incorporate relaxation effects of the F-vacancy in the present study; this situation can also be remedied by adopting the proposed scheme of calculating the total energies.

ACKNOWLEDGMENT

The authors wish to express their appreciation to Professor Keith H. Johnson of MIT for providing the original computer program of the SCF Xα multiple-scattering method and also for helpful discussions on many occasions.

REFERENCES

* Work supported by the Office of Naval Research (Contract no. N00014-75-C-0785).

† Based in part on this author's Ph.D. dissertation submitted in the Fall, 1975, to the Department of Electrical Engineering and Computer Science, Massachusetts Institute of Technology.

1. A paper on PbTe and its intrinsic point defects, and another on GaP and its nitrogen isoelectric trap follow.
2. K.H. Johnson, J. Chem. Phys. 45, 3085 (1966).
3. K.H. Johnson, Int. J. Quantum Chem. 1s, 361 (1967); 2s, 233 (1968); 4, 153 (1971).
4. K.H. Johnson and F.C. Smith, Jr., Phys. Rev. Lett. 24, 139 (1970).
5. K.H. Johnson, Adv. Quantum Chem. 7, 143 (1973).
6. J.C. Slater and K.H. Johnson, Phys. Rev. B 5, 844 (1972).
7. J.C. Slater, The Self-Consistent Field for Molecules and Solids: Quantum Theory of Molecules and Solids, Vol. 4, McGraw Hill, New York (1974).
8. G.F. Koster and J.C. Slater, Phys. Rev 95, (1967); 96, 1208 (1954).
9. J. Callaway and A.J. Hughes, Phys. Rev. 156, 860 ; 164 1043 (1967).
10. N.J. Parada and G.W. Pratt, Jr., Phys. Rev. Lett. 22, 180 (1969). N.J. Parada, Phys. Rev. B 3, 2042 (1971).

11. R.C. Chaney and C.C. Lin, Phys. Rev. B 13, 843 (1976).

12. L.A. Hemstreet, Phys. Rev B 11, 2260; 12,1212 (1975).

13. Tables of Interatomic Distances and Configurations in Molecules and Ions, Special Publ. No. 11, Chem. Soc. London, 1958.

14. N. Rösch, W.G. Klemperer, and K.H. Johnson, Chem. Phys. Lett. 23,149 (1973).

15. F. Herman, A.R. Williams, and K.H.Johnson, J. Chem. Phys. 61, 3508 (1974).

16. J.C. Slater, J. Chem. Phys. 57, 2389 (1972).

17. K. Schwarz, Phys. Rev. B 5, 2466 (1972).

18. G.W. Pratt, Jr., Phys. Rev. 88, 1217 (1952).

19. F. Herman and S. Skillman, Atomic Structure Calculations, Prentice Hall, Englewood Cliffs, New Jersey (1963).

20. B.J. Ransil, Rev. Mod. Phys. 32, 239; 32, 245 (1960).

21. J.B. Mann, Los Alamos Scientific Lab. Rept. LA 3690 (1967).

22. D.M. Roessler and W.C. Walker, J. Phys. Chem. Solids 28, 1507 (1967).

23. R.W.G. Wyckoff, Crystal Structures, second edition, Vol. 1, Interscience Publ., New York (1963).

24. R.E. Watson, Phys. Rev. 111, 1108 (1958).

25. C. Kittel, Introduction to Solid State Physics, fourth edition, John Wiley and Sons, New York (1971), p. 121.

26. D.E. Gray (coord. ed.), American Institute of Physics Handbook, McGraw Hill, New York (1972), pp. 7-10.

27. B.L. Moiseiwitch, Advan. in Atomic and Molecular Phys. 1, 61 (1965).

28. C.V. Briscoe and C.F. Squire, Phys. Rev. 106, 1175 (1957).

29. N.E. Brener, Phys. Rev.B 7, 1721 (1973).

30. J.J. Markham, F-Centers in Alkali Halides, Solid State Phys. Suppl. 8, Academic Press, New York and London (1966).

31. W.B. Fowler, Physics of Color Centers, Academic Press, New York and London (1968).

32. R.F. Wood and H.W. Joy, Phys Rev. 136, A451 (1964).

33. J.K. Kübler and R.J. Friauf, Phys. Rev. 140, A1742 (1965).

34. C.Z. van Doorn, Philips Res. Rept. Suppl. 4 (1962).

35. H. Rabin and M. Reich, Phys. Rev. 135, A101 (1964).

36. E. Baris, et al., Proc. Brit. Ceram. Soc. 9, 203 (1967). T.G. Stoebe, et al., ibid., 9,171 (1967).

TABLE I

Atomic and ionic radii of Li and F, in a.u.

	Li	F
Atomic radius in compounds[a]	2.740	0.945
Atomic radius in tetrahedral covalent bond[b]	--	1.209
Ionic radius of Zachariasen[c]	1.285	2.513

[a] J.C. Slater, J. Chem. Phys. 41, 3199 (1964).

[b] L. Pauling, The Nature of the Chemical Bond, third ed., Cornell Univ. Press, New York (1960), p. 246.

[c] From C. Kittle, Introduction to Solid State Physics, fourth ed., John Wiley & Sons, New York (1971), p. 129.

TABLE II

Results of the SCF Xα cluster model calculation for the LiF molecule with the experimental equilibrium internuclear distance (2.854 a.u.), compared with the SCF LCAO-MO results of Brener (ref. 29).

	Xα Cluster Non-SCF	Xα Cluster SCF	LCAO-MO SCF
Radius (a.u.)			
Li center	1.285	1.351	
F center	2.513	2.643	
outersphere	3.326	3.456	
Overlapping scale factor	1.331	1.4	
One-electron energies (Ry)			
1σ (F 1s core)	-49.168	-48.207	-52.252
2σ (Li 1s core)	- 3.819	- 3.658	- 4.862
3σ	- 2.498	- 1.803	- 2.689
4σ	- 1.141	- 0.477	- 0.806
1π	- 1.151	- 0.491	- 0.697
Constant potential in the interatomic region (Ry)	- 0.440	- 0.317	
Statistical energies (Ry)			
U_{NN} (Nucleus-Nucleus)	18.924	18.924	
U_{EN} (Electron-Nucleus)	-571.021	-554.683	
U_{EE} (Electron-Electron)	140.617	131.047	
U_X (Exchange correlation)	- 25.550	- 24.204	
U_K (Kinetic)	223.150	214.694	
E_T (Total energy)	213.879	-214.223	-212.763
Virial coefficient ($-U_K/E_T$)	1.043	1.002	
Ionicity	0.97	0.92	

TABLE III

Normalized partial-wave coefficients (C_L^j) and electronic charge distributions (Q) of the valence electron states of the LiF molecular cluster with experimental equilibrium internuclear distance.

			3σ	4σ	1π
C_L^j:	F	s	0.993	0.010	--
		p	-0.007	0.974	0.965
	Li	s	0.061	0.094	--
		p	-0.059	-0.135	0.048
	Out[a]	s	-0.038	0.059	--
		p	-0.035	0.115	0.156
		d	-0.004	0.101	0.055
		f	-0.007	0.003	0.019
Q[b]:	F		0.987	0.949	0.931
	Li		0.007	0.027	0.002

[a] "Out" stands for "extra-molecular".

[b] The rest of the electronic charges are distributed in the interatomic and extramolecular regions of the cluster.

TABLE IV

Results of the SCF Xα cluster model calculations for the LiF molecule with various internuclear distances. Overlapping scale factor is 1.4.

Internuclear distance	0.98 R_e [a]	R_e	1.02 R_e	1.05 R_e
One-electron energies (Ry)				
1σ (F 1s core)	-48.215	-48.207	-48.202	-48.195
2σ (Li 1s core)	- 3.634	- 3.658	- 3.681	- 3.713
3σ	- 1.811	- 1.803	- 1.795	- 1.784
4σ	- 0.483	- 0.477	- 0.472	- 0.464
1π	- 0.500	- 0.491	- 0.482	- 0.470
Constant potential in the interatomic region (Ry)	- 0.332	- 0.317	- 0.303	- 0.284
Statistical energies (Ry)				
U_{NN}(Nucleus-Nucleus)	19.3101	18.9239	18.5528	18.0227
U_{EN}(Electron-Nucleus)	-555.5654	-554.6833	-553.8552	-552.6865
U_{EE}(Electron-Electron)	131.4323	131.0467	130.6818	130.1655
U_X (Exchange correlation)	- 24.2235	- 24.2040	- 24.1866	- 24.1631
U_K (Kinetic)	214.8266	214.6943	214.5844	214.4404
E_T (Total energy)	-214.2200	-214.2225	-214.2227	-214.2208
Virial coefficient ($-U_K/E_T$)	1.0028	1.0022	1.0017	1.0010
Ionicity (electronic charge)	0.9164	0.9203	0.9237	0.9280

[a] R_e indicates the experimental equilibrium internuclear distance.

TABLE V

The equilibrium properties of the LiF molecule as calculated by the SCF $X\alpha$ multiple-scattering method, compared with experimental data.

	Calculation	Experiment
Internuclear distance (Å)	1.53	1.51
Vibrational quantum energy, $\hbar\omega_v$ (eV)	0.1197	0.1124[a]
Total energy (Ry)	-214.223	-215.004[a]
Cohesive energy (Ry)	-0.539	-0.440[b]
Dipole moment (Debye)[c]	6.777	6.6 ± 0.3[a]

[a] From ref. 20.

[b] A.G. Gaydon, Dissociation Energies, rev. ed. (1953).

[c] 1 (Debye) = 10^{-8} (esu) = 1/4.803 (e·Å) = 0.5564 (a.u.)

TABLE VI

Results of the SCF Xα multiple-scattering calculations for the OLi_4F_4 cluster with various nearest-neighbor distances.

Nearest-neighbor distance	R_e [a]	1.05 R_e	1.074 R_e	1.1 R_e	1.15 R_e
One-electron energies (Ry)					
Core					
F 1s	-48.345	-48.333	-48.327	-48.318	-48.299
Li 1s	- 3.624	- 3.660	- 3.677	- 3.694	- 3.725
Valence (Td group)					
$1a_1$ (F 2s)	- 1.988	- 1.959	- 1.946	- 1.933	- 1.908
$1t_2$ (F 2s)	- 1.973	- 1.948	- 1.937	- 1.925	- 1.903
$2a_1$ (F 2p)	- 0.716	- 0.682	- 0.668	- 0.652	- 0.622
1e (F 2p)	- 0.675	- 0.646	- 0.634	- 0.621	- 0.595
$2t_2$ (F 2p)	- 0.672	- 0.646	- 0.635	- 0.622	- 0.597
$1t_1$ (F 2p)	- 0.632	- 0.612	- 0.603	- 0.593	- 0.573
$3t_2$ (F 2p)	- 0.620	- 0.602	- 0.594	- 0.584	- 0.566
Constant potential in the inter-atomic region	- 0.363	- 0.329	- 0.315	- 0.300	- 0.274
Statistical Energies(Ry)					
U_M(Madelung correction)	- 0.3857	- 0.3905	- 0.3916	- 0.3921	- 0.3914
U_{NN}(Nucleus-Nucleus)	404.4785	385.2187	376.6104	367.7087	351.7214
U_{EN}(Electron-Nucleus)	-2873.1807	-2834.3291	-2817.0615	-2799.1934	-2767.1826
U_{EE}(Electron-Electron)	850.9722	831.9631	823.5098	814.7700	799.1123
U_X (Exchange correlation)	- 96.4353	- 96.3403	- 96.3048	- 96.2679	- 96.2084
U_K (Kinetic)	857.3088	856.5955	856.3496	865.0928	855.6870
E_T (Total energy)	-857.2419	-857.2825	-857.2881	-857.2817	-857.2612
Virial coefficient $(-U_K/E_T)$	1.0001	0.9992	0.9989	0.9986	0.9982
Ionicity (electronic charge)	0.8812	0.8935	0.8988	0.9041	0.9133

[a] R_e is the experimental nearest-neighbor distance at equilibrium.

TABLE VII

The equilibrium properties of the LiF crystal as calculated by the SCF Xα multiple-scattering method for the OLi_4F_4 cluster model, compared with experimental data.

	OLi_4F_4 cluster calculation	LiF crystal experiment
Radii of atomic centers (Å)		
Li	1.086(0.952)[a]	
F	1.376(1.207)	
Nearest-neighbor distance (Å)	2.159	2.01[b]
Bulk modulus (dyne/cm^2)	6.66×10^{11}	6.98×10^{11}[c]
Energies per molecule (Ry)		
Total energy	-214.322	
Cohesive energy	0.638	0.644[c]
Ionicity (electronic charge)	0.899	

[a] The numbers outside the parentheses are the radii of the atomic spheres determined through SCF calculations by satisfying the virial theorem. The overlapping scale factor is 1.14. The numbers inside the parentheses are the radii of the touching atomic spheres which are reduced from the overlapping atomic spheres so that the overlapping scale factor is unity.

[b] From ref. 23.

[c] See text.

TABLE VIII

Normalized partial-wave coefficients (C_L^j) and electronic charge distributions (Q) of the $3t_2$, $3a_1$, and $4t_2$ states of the OLi_4F_4 cluster.

			$3t_2$	$3a_1$	$4t_2$
C_L^j	F	s	-0.026	0.278	-0.139
		p	0.862, 0.465	-0.013	-0.126, 0.033
	Li	s	-0.021	-0.237	-0.120
		p	-0.044, 0.044	0.035	0.118, 0.004
	O	s	--	0.064	--
		p	-0.043	--	0.009
	Out[a]	s	--	0.766	--
		p	0.085	--	0.890
		d	-0.047	--	0.050
		f	0.027	0.046	-0.022
Q	F		0.959	0.077	0.036
	Li		0.004	0.057	0.028
	O		0.002	0.004	0.0
	In[b]		0.024	0.272	0.141
	Out[a]		0.010	0.589	0.794

[a] "Out" stands for "extramolecular".

[b] "In" represents the interatomic region of the cluster.

TABLE IX

Compatibility relations between the representations of the Td and C_{3v} point groups.

Td	C_{3v}
a_1	a_1
a_2	a_2
e	e
t_1	$a_2 + e$
t_2	$a_1 + e$

TABLE X

Results of the SCF Xα multiple-scattering calculations for the VacF (F-vacancy) cluster in various configurations.

Cluster configuration	$(VacF)^{+1}$	(VacF) spin-restricted	(VacF) spin-polarized spin ↑	(VacF) spin-polarized spin ↓
One-electron energies (Ry)				
Core states				
F 1s	-48.369	-48.341	-48.340	-48.340
Li 1s	- 3.811	- 3.713	- 3.707	- 3.702
ALi 1s	- 3.672	- 3.672	- 3.674	- 3.674
Valence states				
$1a_1$ (F 2s)	- 1.982	- 1.962	- 1.956	- 1.955
$1e$ (F 2s)	- 1.975	- 1.955	- 1.949	- 1.948
$2a_1$ (F 2p)	- 0.697	- 0.674	- 0.671	- 0.665
$2e$ (F 2p)	- 0.672	- 0.652	- 0.648	- 0.644
$3a_1$ (F 2p)	- 0.663	- 0.644	- 0.640	- 0.635
$3e$ (F 2p)	- 0.655	- 0.635	- 0.631	- 0.627
$1a_2$ (F 2p)	- 0.641	- 0.620	- 0.616	- 0.613
$4e^2$ (F 2p)	- 0.632	- 0.612	- 0.608	- 0.605
Excited states				
$4a_1$	- 0.188	- 0.183	- 0.225	- 0.076
$5a_1$	- 0.031	- 0.053	- 0.066	- 0.012
$5e$	- 0.013	- 0.034	- 0.047	- 0.001
Constant potential in the interatomic region	- 0.327	- 0.337	- 0.354	- 0.306
Statistical energies (Ry)				
U_M (Madelung correction)	- 0.3555	- 0.3760	- 0.3797	
U_{NN} (Nucleus-Nucleus)	245.0178	245.0178	245.0178	
U_{EN} (Electron-Nucleus)	-2057.0527	-2071.1079	-2071.4536	
U_{EE} (Electron-Electron)	573.6860	587.4375	587.7170	
U_X (Exchange correlation)	- 75.5144	- 75.6286	- 75.6914	
U_K (Kinetic)	656.6375	656.8948	655.9946	
E_T (Total energy)	-657.5808	-657.7620	-657.7947	
Ionicty (electronic charge)				
VacF	- 0.022	- 0.769	- 0.794	
F	- 0.884	- 0.914	- 0.912	
Li	0.924	0.871	0.878	
ALi	0.903	0.898	0.898	

TABLE XIa

Normalized partial-wave coefficients (C_L^j) and electronic charge distributions (Q) of the 4e and 5e states for both spins in the equilibrium VacF cluster.

			$4e^{\uparrow}$	$4e^{\downarrow}$	$5e^{\uparrow}$	$5e^{\downarrow}$
C_L^j:	F	s	-0.024	-0.022	-0.164	-0.140
		p_1	0.738	0.733	-0.076	-0.055
		p_2	0.382	0.387	-0.092	-0.082
		p_3	0.516	0.522	0.012	-0.004
	Li	s	-0.013	-0.012	-0.179	-0.135
		p_1	0.021	0.020	0.014	0.034
		p_2	-0.041	-0.042	0.107	0.081
		p_3	0.003	0.003	0.078	0.053
	ALi	p	-0.052	-0.051	0.058	0.054
	VacF	p	-0.008	-0.006	0.166	0.086
	O	p	-0.044	-0.043	0.016	0.012
	Out[a]	p	-0.082	0.076	0.779	0.879
		d_1	-0.004	-0.004	0.118	0.054
		d_2	-0.049	-0.047	0.104	0.066
Q:	F	(3)	0.957	0.960	0.041	0.029
	Li	(3)	0.002	0.002	0.050	0.029
	ALi		0.003	0.003	0.003	0.003
	VacF		0.0	0.0	0.028	0.007
	O		0.002	0.002	0.0	0.0
	In[b]		0.027	0.025	0.246	0.151
	Out[a]		0.009	0.008	0.632	0.870

[a] "Out" stands for "extramolecular".

[b] "In" represents the interatomic region of the cluster.

TABLE XIb

Normalized parial-wave coefficients (C_L^j) and electronic charge distributions (Q) of the $4a_1$ and $5a_1$ states for both spins in the equilibrium VacF cluster.

			$4a_1^{\uparrow}$	$4a_1^{\downarrow}$	$5a_1^{\uparrow}$	$5a_1^{\downarrow}$
C_L^j:	F	s	0.125	0.207	0.223	-0.149
		p_1	0.020	0.012	-0.055	0.076
		p_2	-0.158	-0.091	0.081	-0.101
	Li	s	-0.216	-0.248	-0.096	-0.002
		p_1	-0.191	-0.093	0.119	-0.116
		p_2	0.040	0.045	-0.035	0.070
	ALi	s	-0.027	-0.076	-0.150	0.134
		p	0.011	0.004	-0.051	0.058
	VacF	s	0.660	0.390	-0.153	0.206
		p	0.0	-0.007	-0.036	0.032
	O	s	0.110	0.100	0.026	-0.004
		p	0.048	0.022	-0.016	0.018
	Out[a]	s	0.306	0.602	0.636	-0.407
		p	0.242	0.215	-0.458	0.720
		d	-0.138	-0.077	0.087	-0.062
Q:	F (3)		0.041	0.051	0.059	0.038
	Li (3)		0.085	0.074	0.025	0.018
	ALi		0.001	0.006	0.025	0.021
	VacF		0.436	0.152	0.025	0.044
	O		0.014	0.010	0.001	0.0
	In[b]		0.252	0.294	0.243	0.191
	Out[a]		0.171	0.141	0.622	0.687

[a] "Out" stands for "extramolecular"

[b] "In" represents the interatomic region of the cluster.

FIGURE CAPTIONS

Fig. 1 Cluster model for a LiF molecule.

Fig. 2a Contour map of the 3σ wave function of the LiF molecule. The spheres of the atomic centers and the outersphere are also shown. The contour lables indicate the wave function values whose magnitudes are equally spaced in logarithmic scale between extrema. The coordinates are in a.u., centered at the center of the outersphere.

Fig. 2b Controu map of the 4σ wave function of the LiF molecule.

Fig. 2c Controu map of the 1π wave function of the LiF molecule.

Fig. 3 Calculated total energy of the LiF molecular cluster vs. internuclear distance in units of the experimental equilibrium internuclear distance. The vertical bars indicate the ranges of the total energies at the later stages of iterations. The dotted curve extends a parabolic fit.

Fig. 4 The OLi_4F_4 cluster model for a LiF crystal.

Fig. 5 Calculated total energy of the OLi_4F_4 cluster vs. lattice constant in units of the experimental equilibrium lattice constant of the LiF crystal. The vertical bars indicate the ranges of the total energies at the later stages of iterations.

Fig. 6 One-electron energy levels of the OLi_4F_4 cluster in the ground state configuration (a), and in the transition state configuration (b). ---- represents the constant potential in the interatomic region of the cluster. The numbers in parentheses indicates the occupation numbers of the band edge states; all the levels below them are completely filled, and those above them are empty.

Fig. 7a Contour map of the $3t_2$ wave function of the OLi_4F_4 cluster. It is plotted in the $1\bar{1}0$ plane (refer to Fig. 4) which bisects two Li and two F atoms, and the broken-line circles are the projections of the atomic centers (including the O center) and the outersphere of the cluster. The contour labels indicate the wave function values whose magnitudes are equally spaced in logarithmic scale between extrema.

Fig. 7b Contour map of the $3a_1$ wave function of the OLi_4F_4 cluster.

Fig. 7c Contour map of the $4t_2$ wave function of the OLi_4F_4 cluster.

Fig. 8 Linearly expanded one-electron energy levels of the OLi_4F_4 cluster in (a) to fit the bandgap of the LiF

crystal whose energy bands are shown in (b) as calculated by Brener (ref. 29).

Fig. 9 One-electron energy levels of the VacF (F-vacancy) cluster in various configurations (b,c, and d), compared with those of the OLi_4F_4 cluster (a). ---- represents the constant potential in the interatomic region of the cluster. The names of the valence electron states for the VacF cluster in all the configurations are the same in the same order. Shaded levels are the highest occupied ones with their occupation numbers being indicated by the portions of the shades.

Fig. $10a_1$ Contour map of the $4e^{\uparrow}$ wave function of the VacF cluster. It is plotted in the plane which bisects the F-vacancy, ALi atom, and each one of the Li and F atoms. (It is the same plane as the one used for the contour maps of the wave functions of the OLi_4F_4 electron states -- Figs. 7a, 7b, and 7c -- while the upper right F atomic center is now replaced by the F-vacancy.) The broken-line circles are the projections of the atomic centers and the outersphere of the cluster. The contour labels indcate the wave function values whose magnitudes are equally spaced in logarithmic scale between extrema.

Fig. $10a_2$ Contour map of the $4e^{\downarrow}$ wave function of the VacF cluster.

Fig. $10b_1$ Contour map of the $4a_1^{\uparrow}$ wave function of the VacF cluster.

Fig. $10b_2$ Contour map of the $4a_1^{\downarrow}$ wave function of the VacF cluster.

Fig. $10c_1$ Contour map of the $5a_1^{\uparrow}$ wave function of the VacF cluster.

Fig. $10c_2$ Contour map of the $5a_1^{\downarrow}$ wave function of the VacF cluster.

Fig. $10d_1$ Contour map of the $5e^{\uparrow}$ wave function of the VacF cluster.

Fig. $10d_2$ Contour map of the $5e^{\downarrow}$ wave function of the VacF cluster.

Fig. 11. Potentials for spin-up and spin-down electrons in the F-vacancy region of the VacF cluster. The horizontal lines indicate the constant potentials in the interatomic region of the cluster.

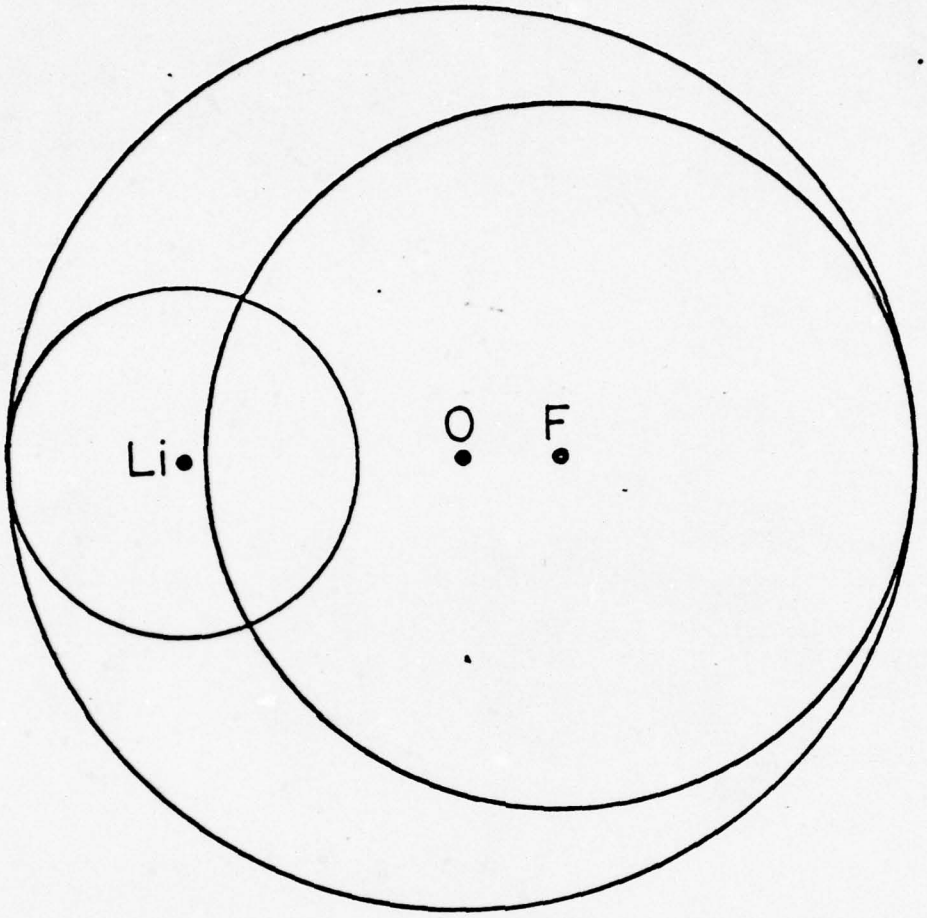

Overlapping scale factor = 1.4

LiF

Fig. 1

56

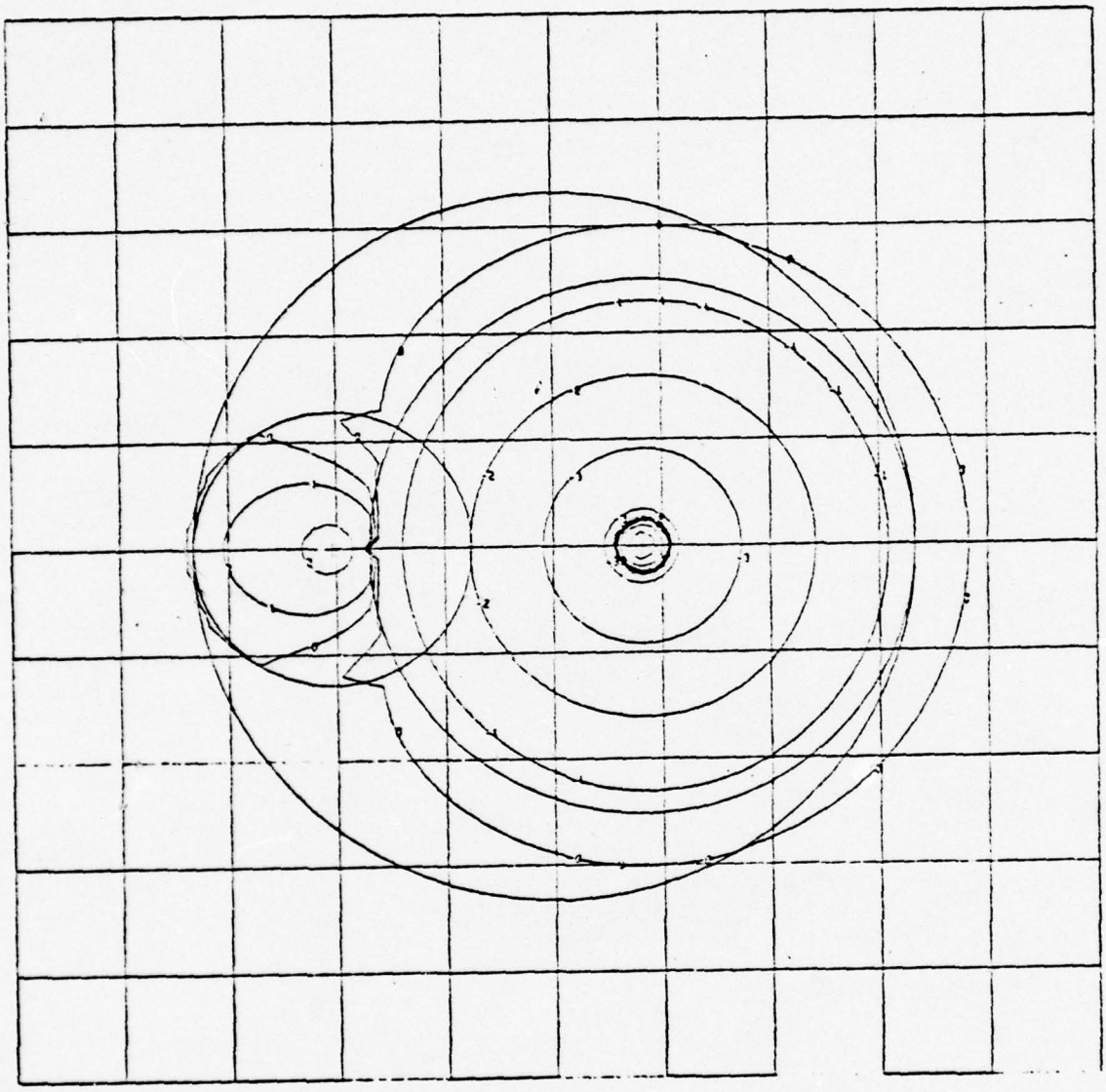

57

LiF

Fig. 2a

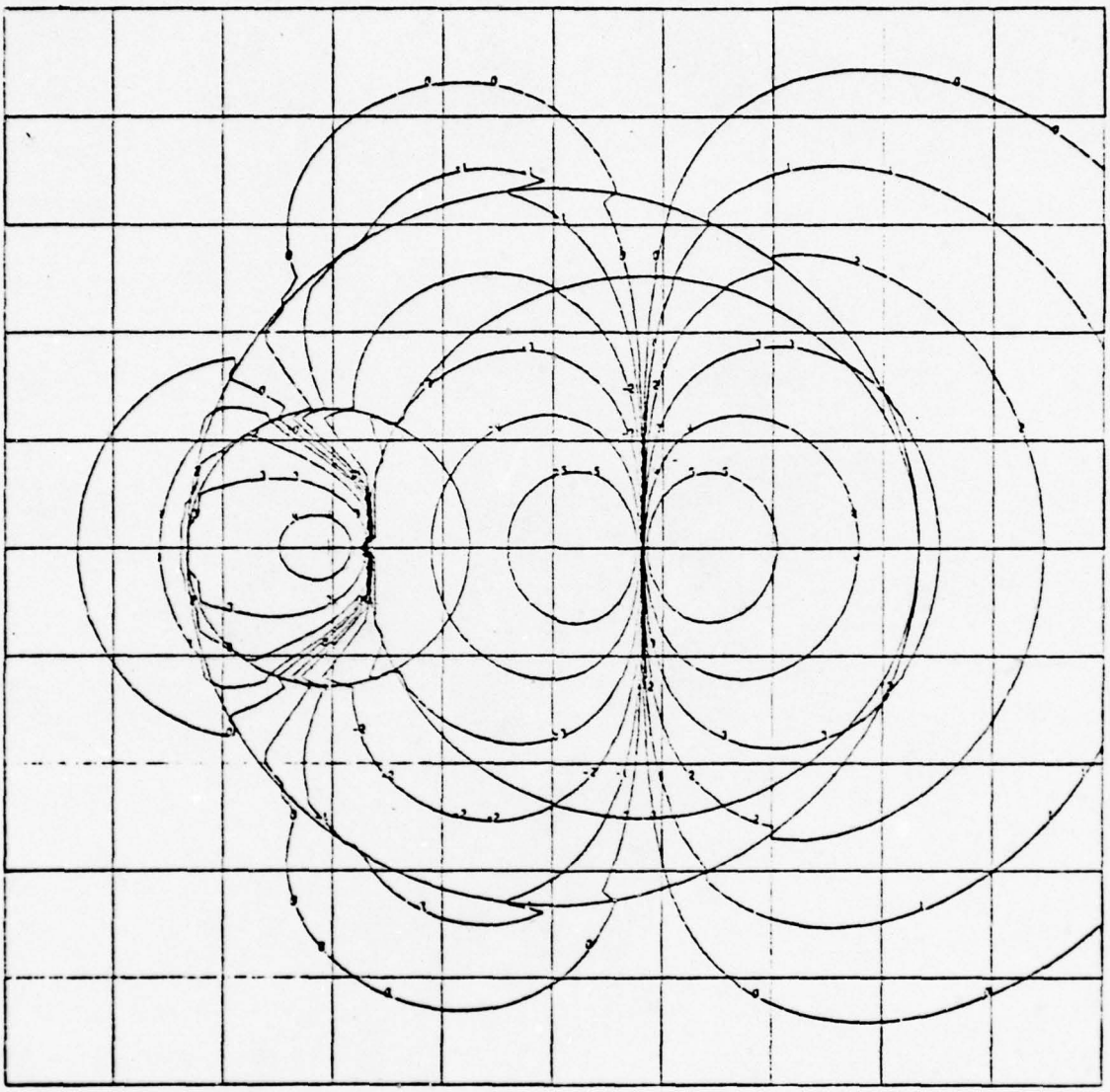

LiF

Fig. 2b

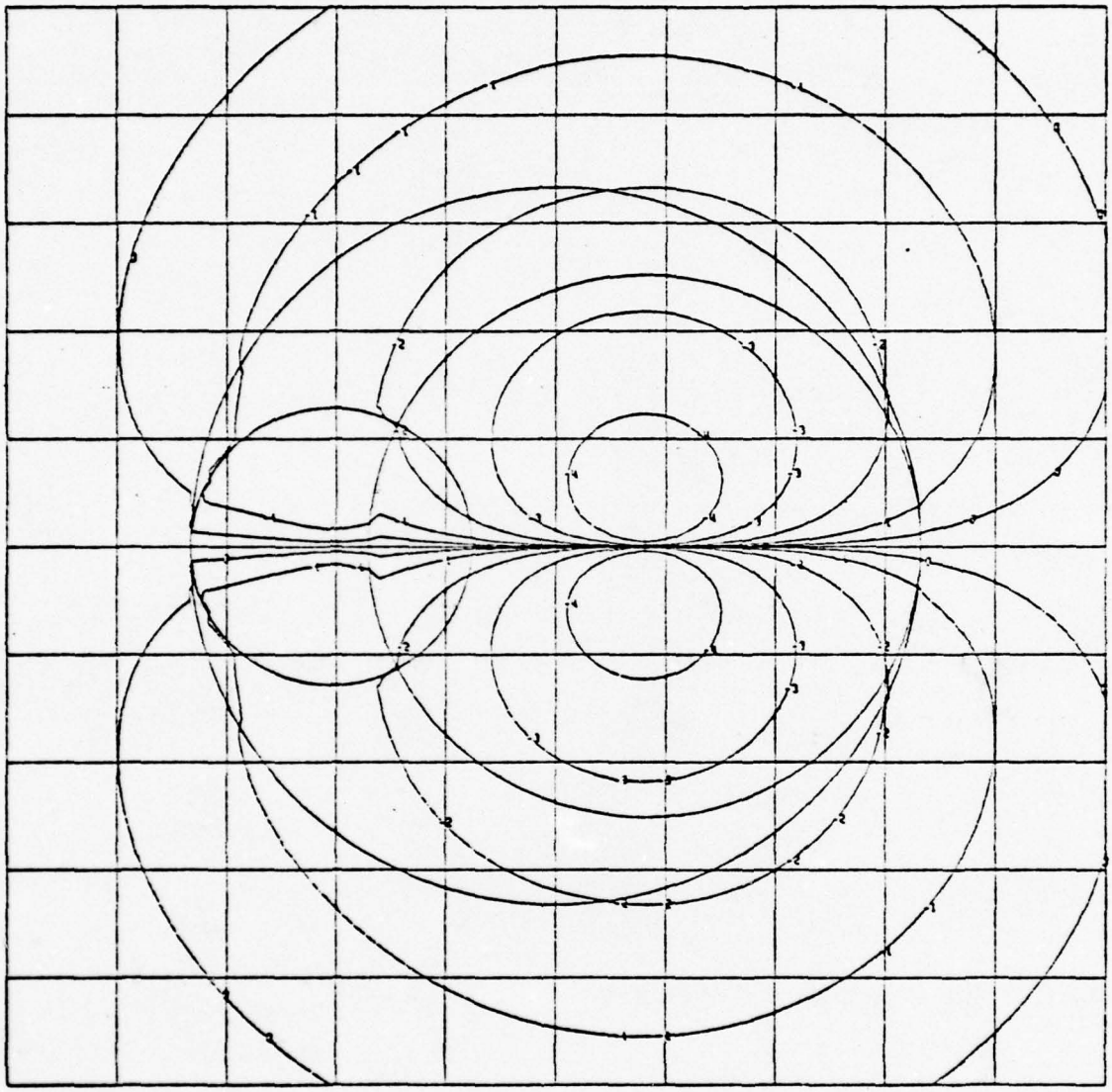

LiF

Fig. 2c

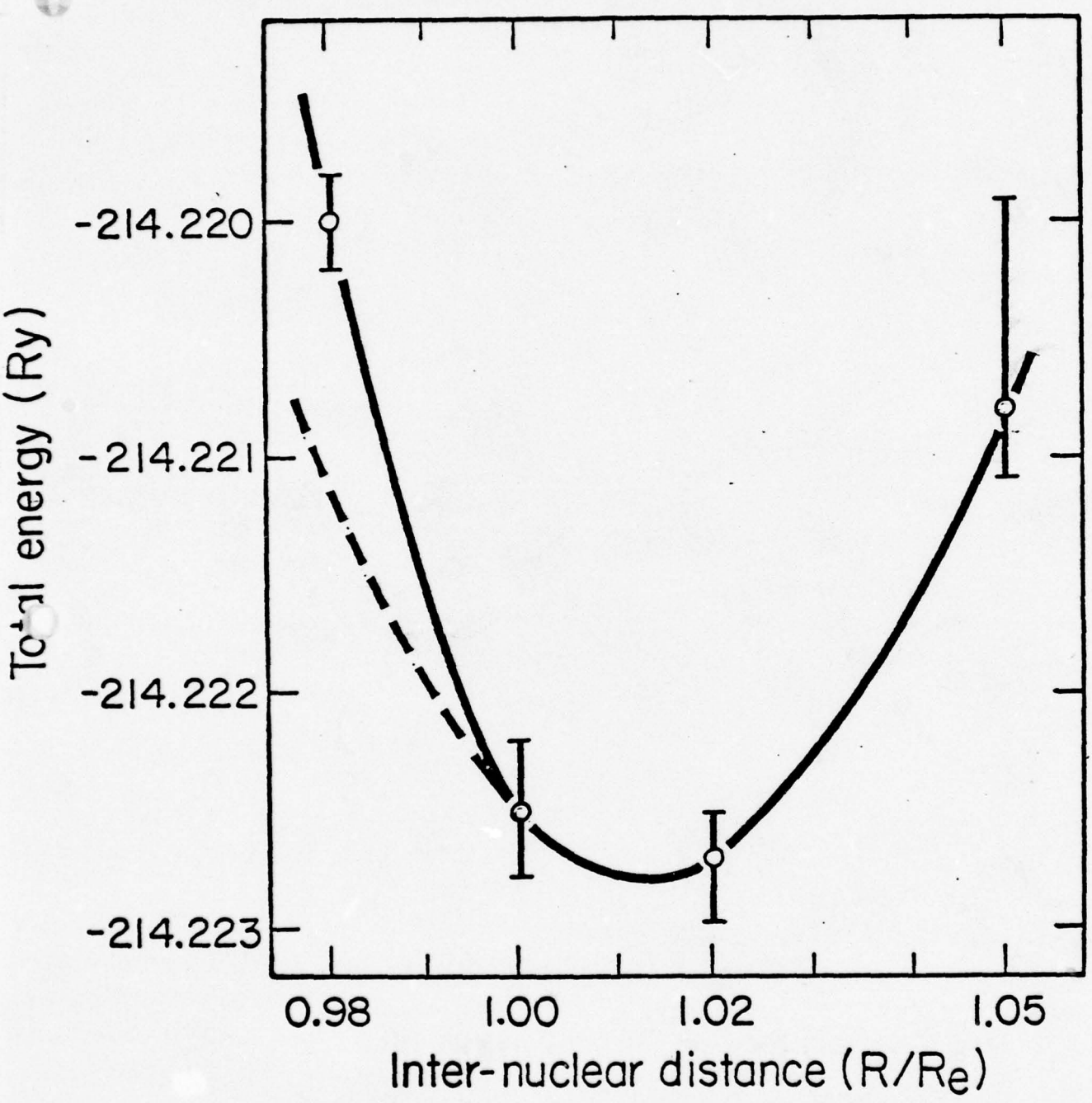
-214.220
-214.221
-214.222
-214.223
Total energy (Ry)
0.98
1.00
1.02
1.05
Inter-nuclear distance (R/Re)

Li F

Fig. 3

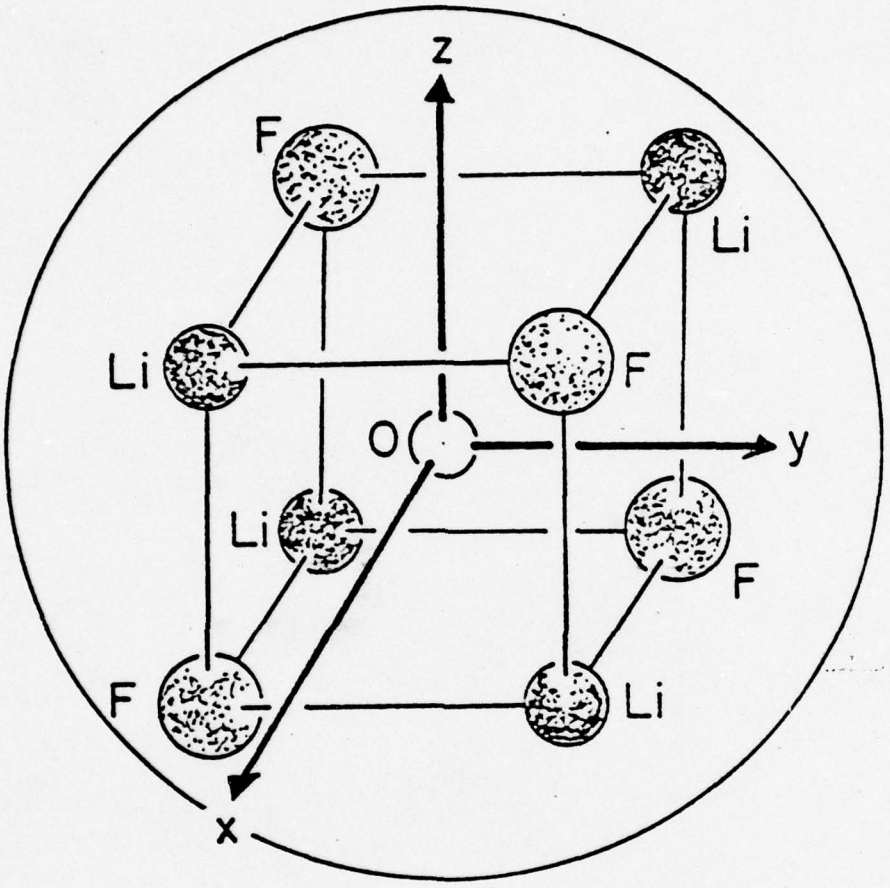

LiF

Fig. 4

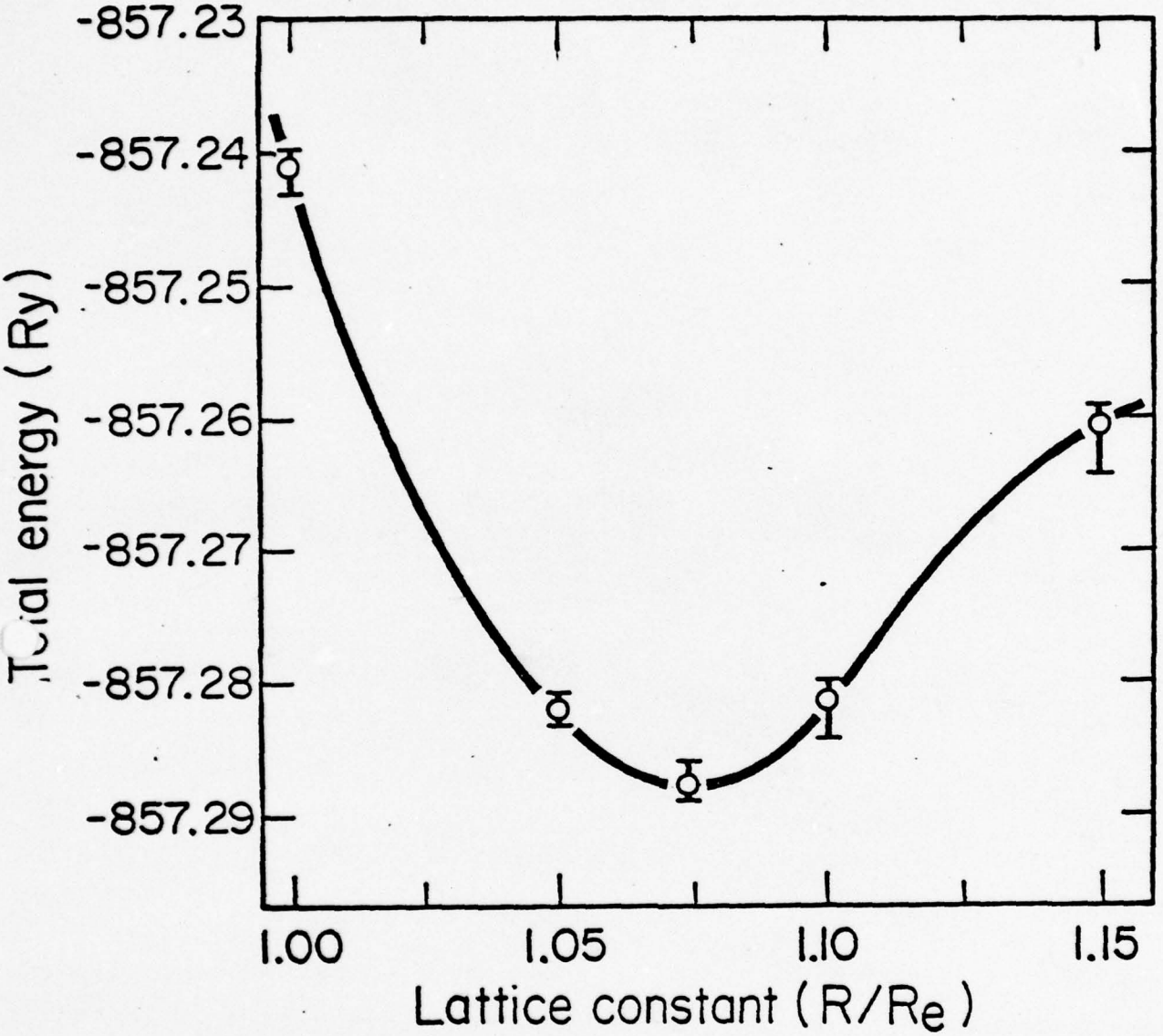
-857.23
-857.24
-857.25
-857.26
-857.27
-857.28
-857.29
Total energy (Ry)
1.00
1.05
1.10
1.15
Lattice constant (R/Re)

LiF

Fig. 5

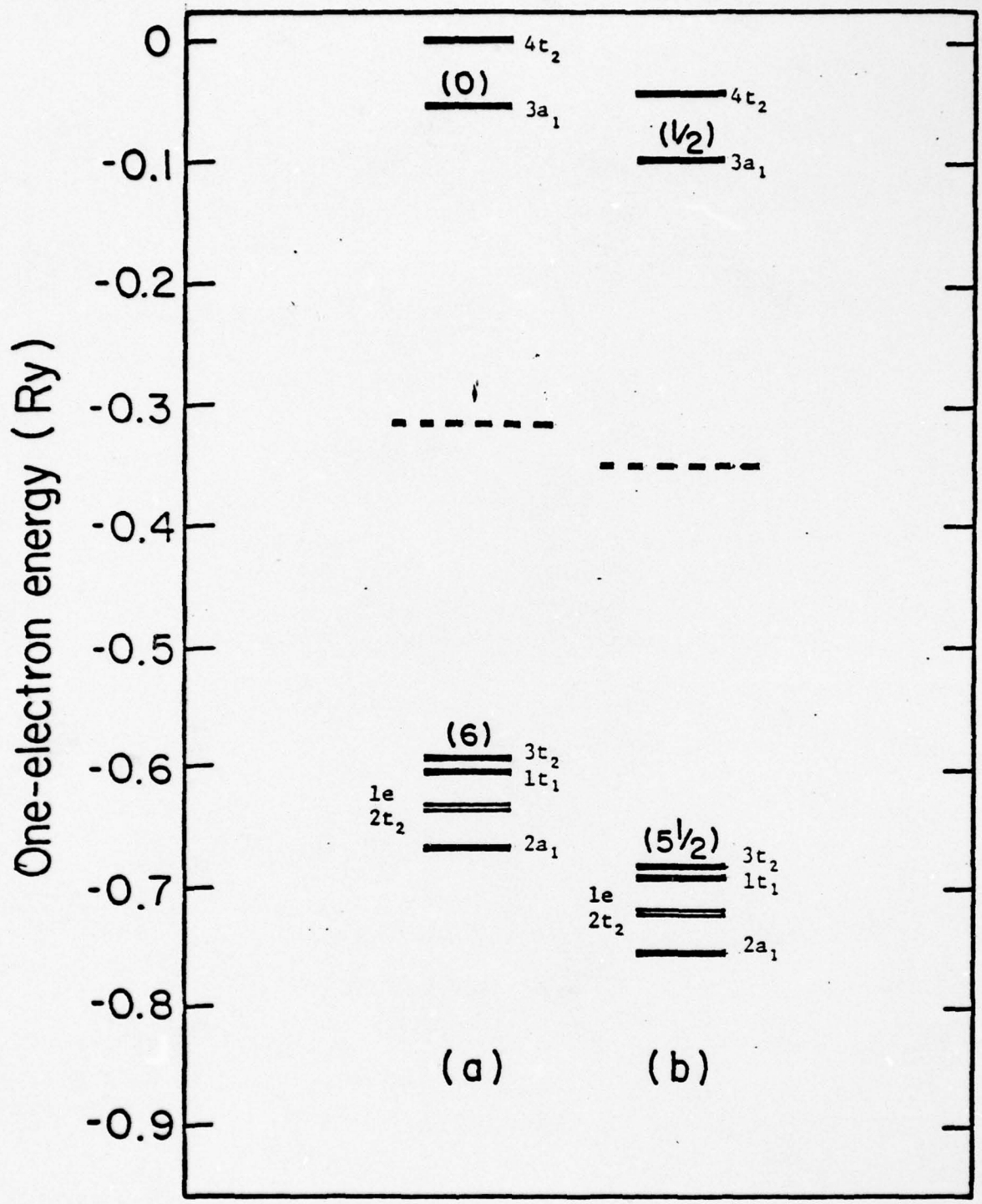
0
-0.1
-0.2
-0.3
-0.4
-0.5
-0.6
-0.7
-0.8
-0.9
One-electron energy (Ry)
4t2
(0)
3a1
4t2
(1/2)
3a1
(6)
3t2
1t1
1e
2t2
2a1
(5 1/2)
3t2
1t1
1e
2t2
2a1
(a)
(b)

LiF

Fig. 6

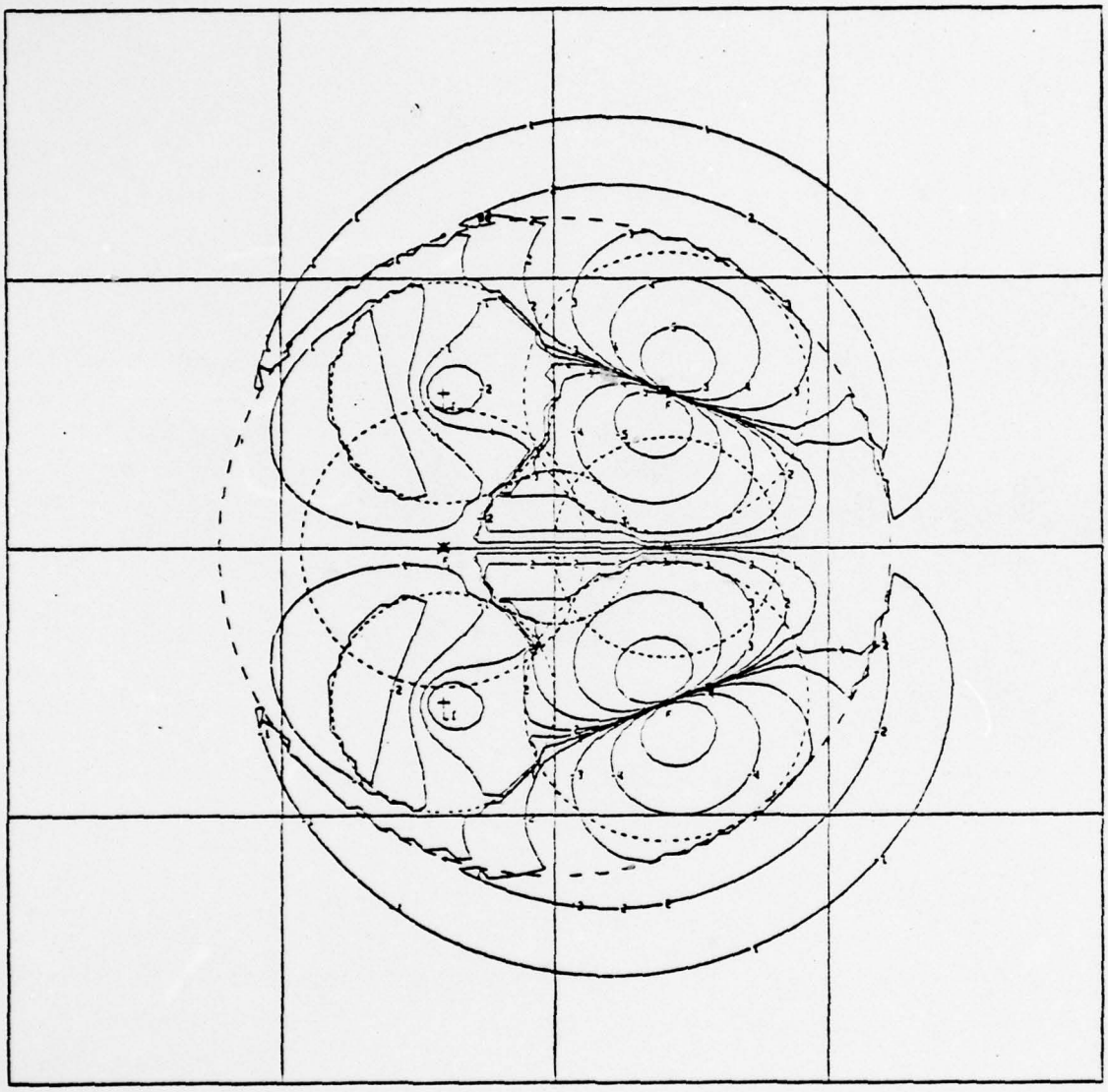

64

LiF

Fig. 7a

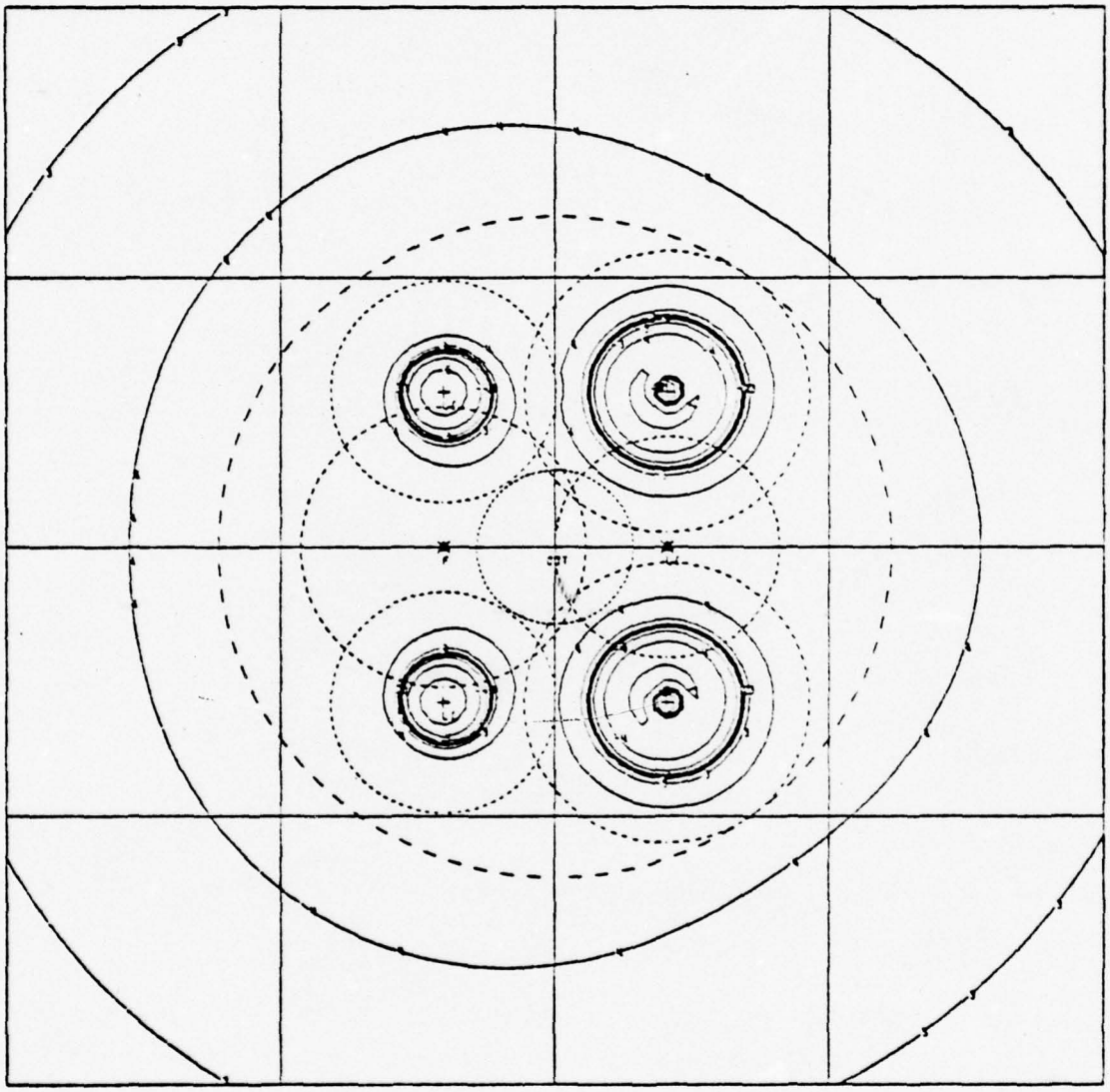

LiF

Fig. 7b

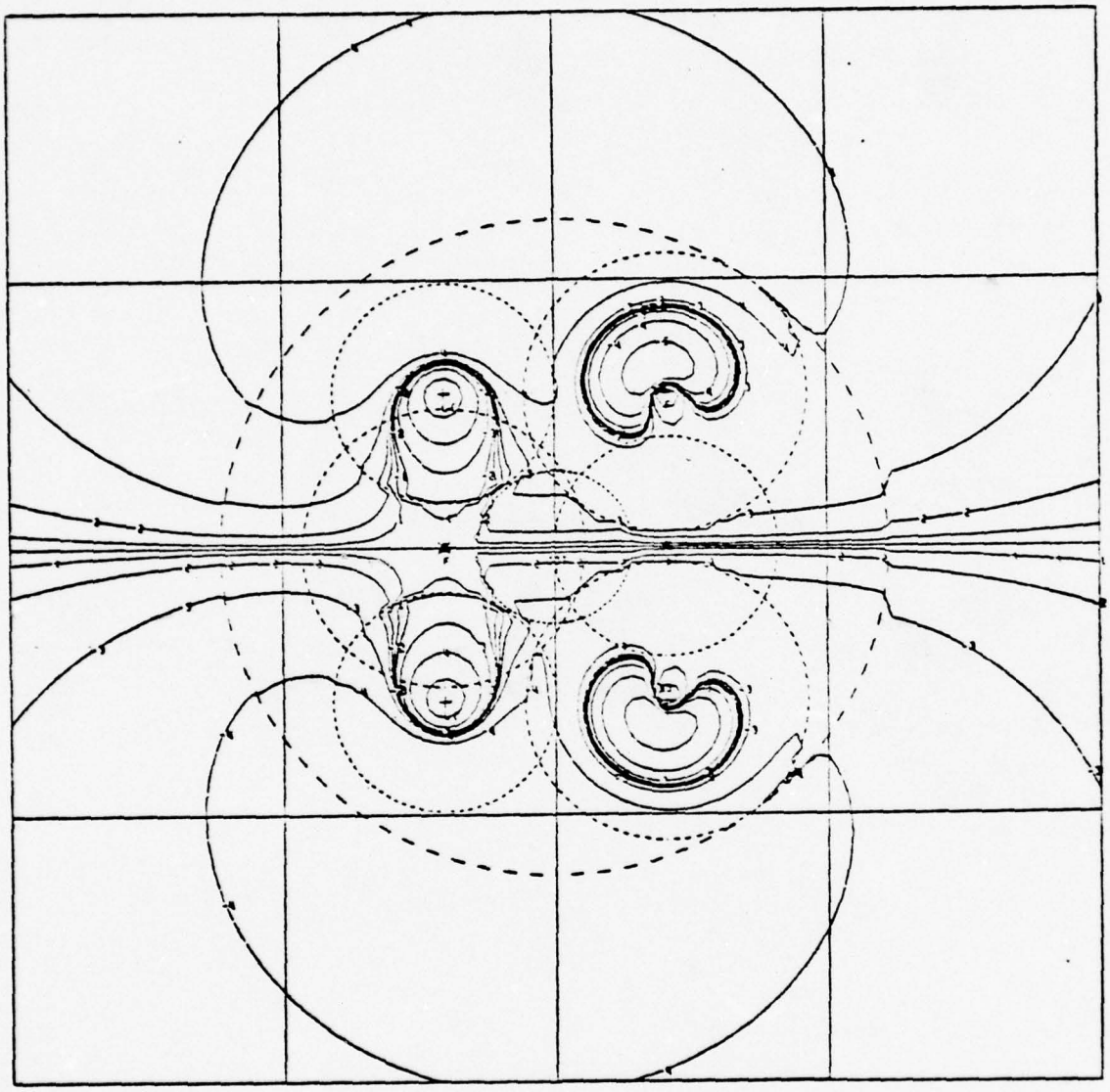

LiF

Fig. 7c

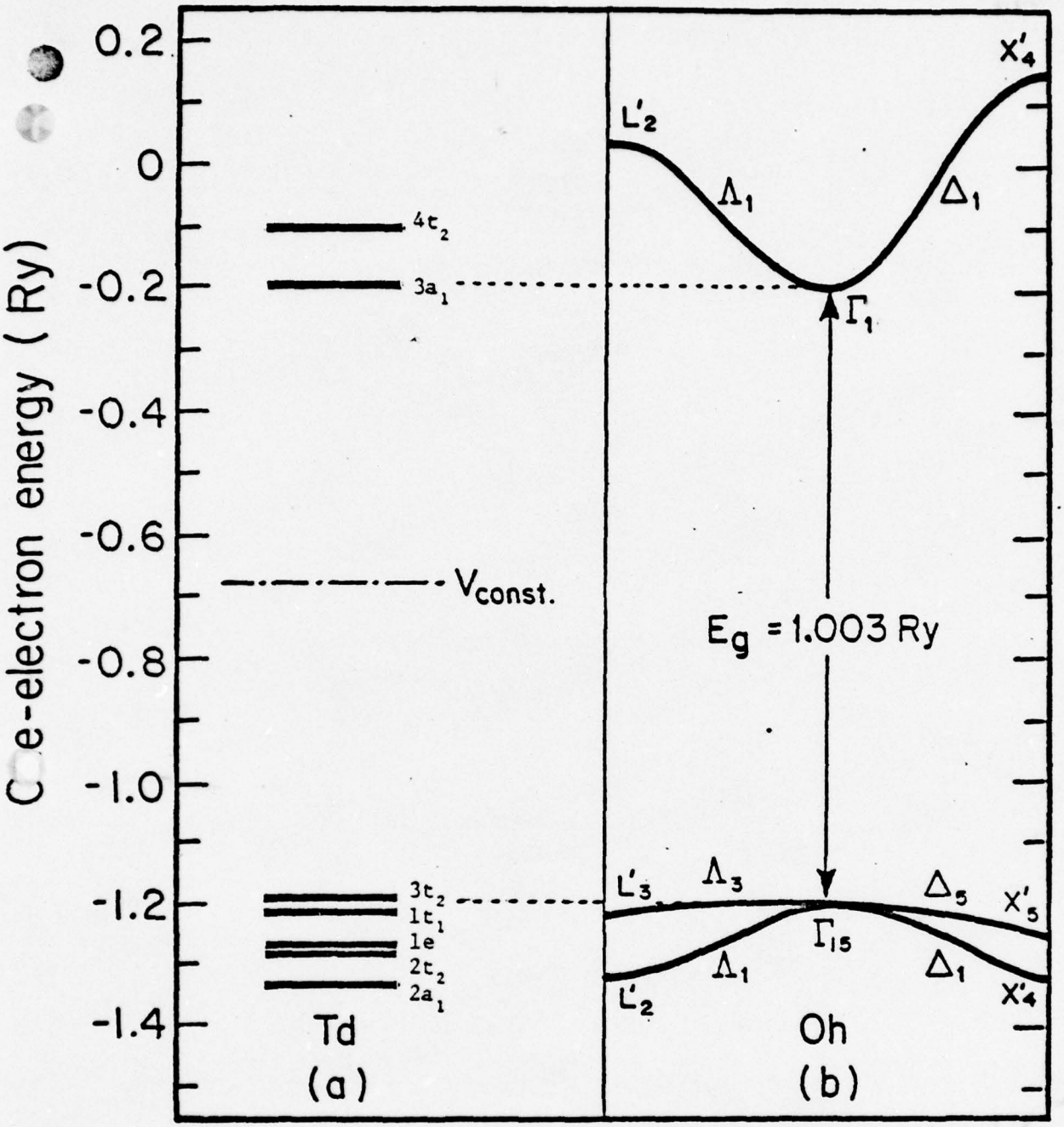
0.2
0
-0.2
-0.4
-0.6
-0.8
-1.0
-1.2
-1.4
Crystal-electron energy (Ry)
4t2
3a1
Vconst.
3t2
1t1
1e
2t2
2a1
Td
(a)
X'4
L'2
Λ1
Δ1
Γ1
Eg = 1.003 Ry
L'3
Λ3
Δ5
X'5
Γ15
Λ1
Δ1
L'2
X'4
Oh
(b)

61

LiF

Fig. 8

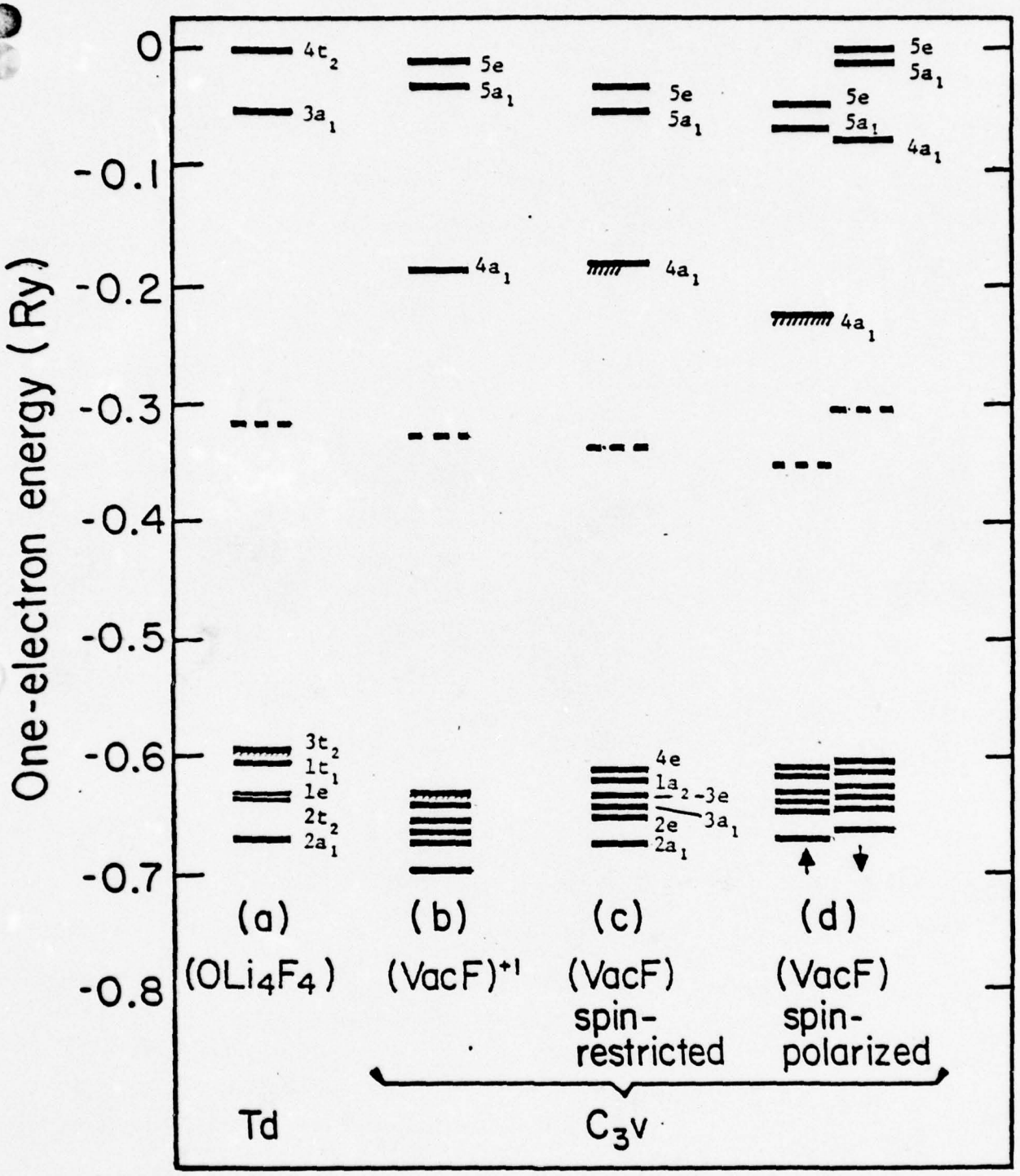
One-electron energy (Ry)
0
-0.1
-0.2
-0.3
-0.4
-0.5
-0.6
-0.7
-0.8
4t2
3a1
5e
5a1
4a1
3t2
1t1
1e
2t2
2a1
4e
1a2
3e
3a1
2e
2a1
(a)
(OLi4F4)
(b)
(VacF)+1
(c)
(VacF)
spin-restricted
(d)
(VacF)
spin-polarized
Td
C3v

LiF

Fig. 9

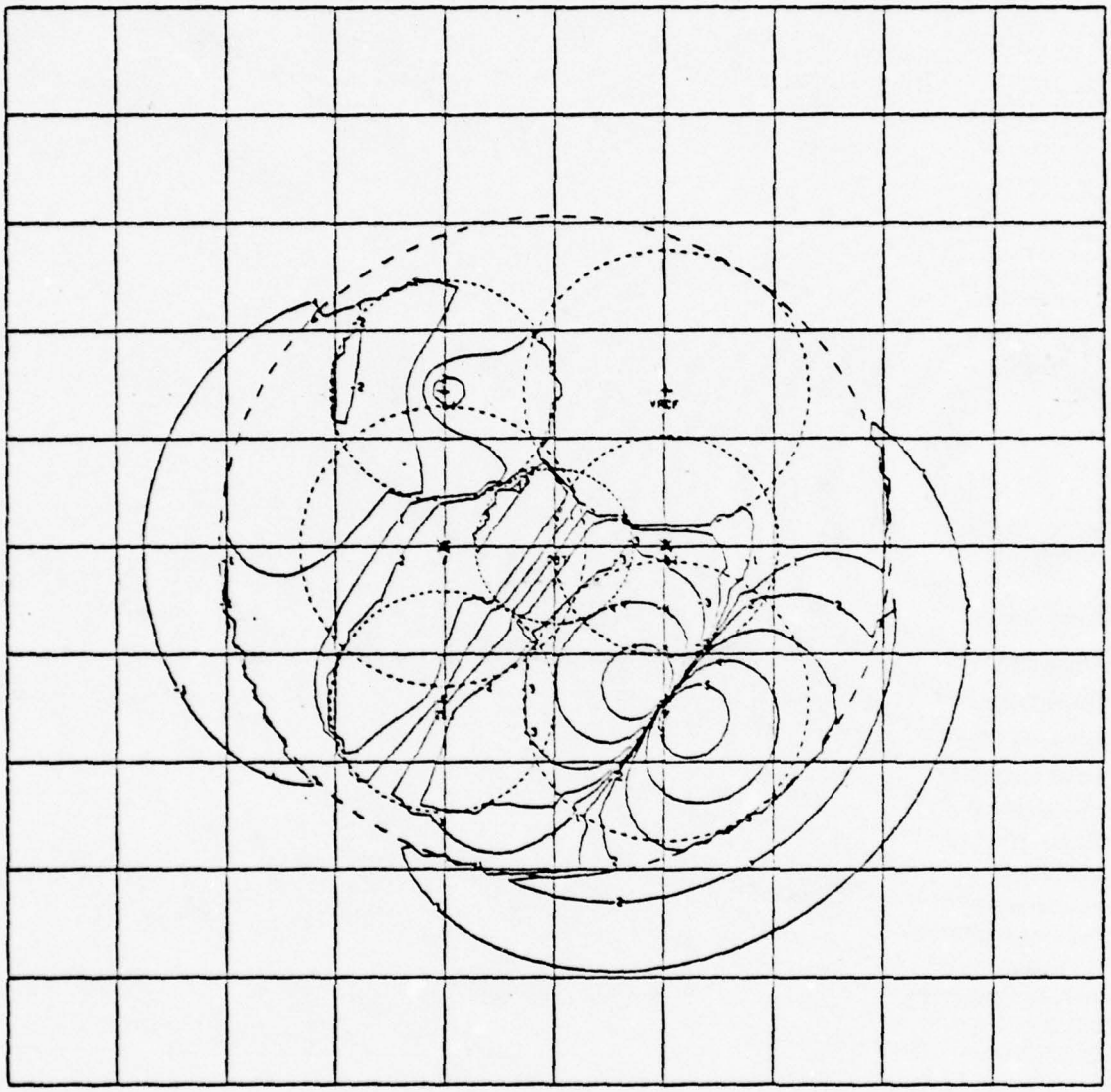

LiF

Fig. 10a,

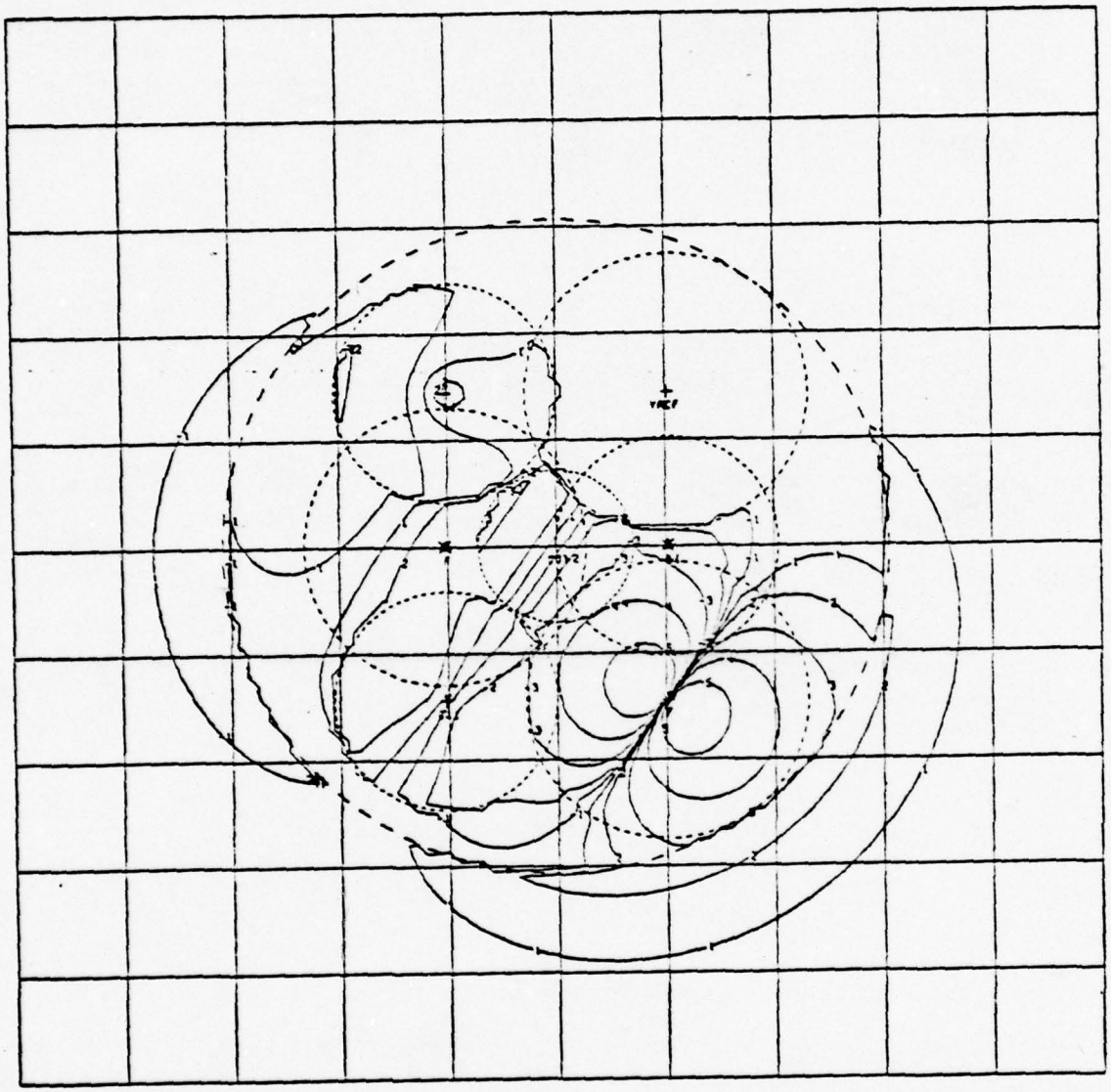

LiF

Fig. 10 a_2

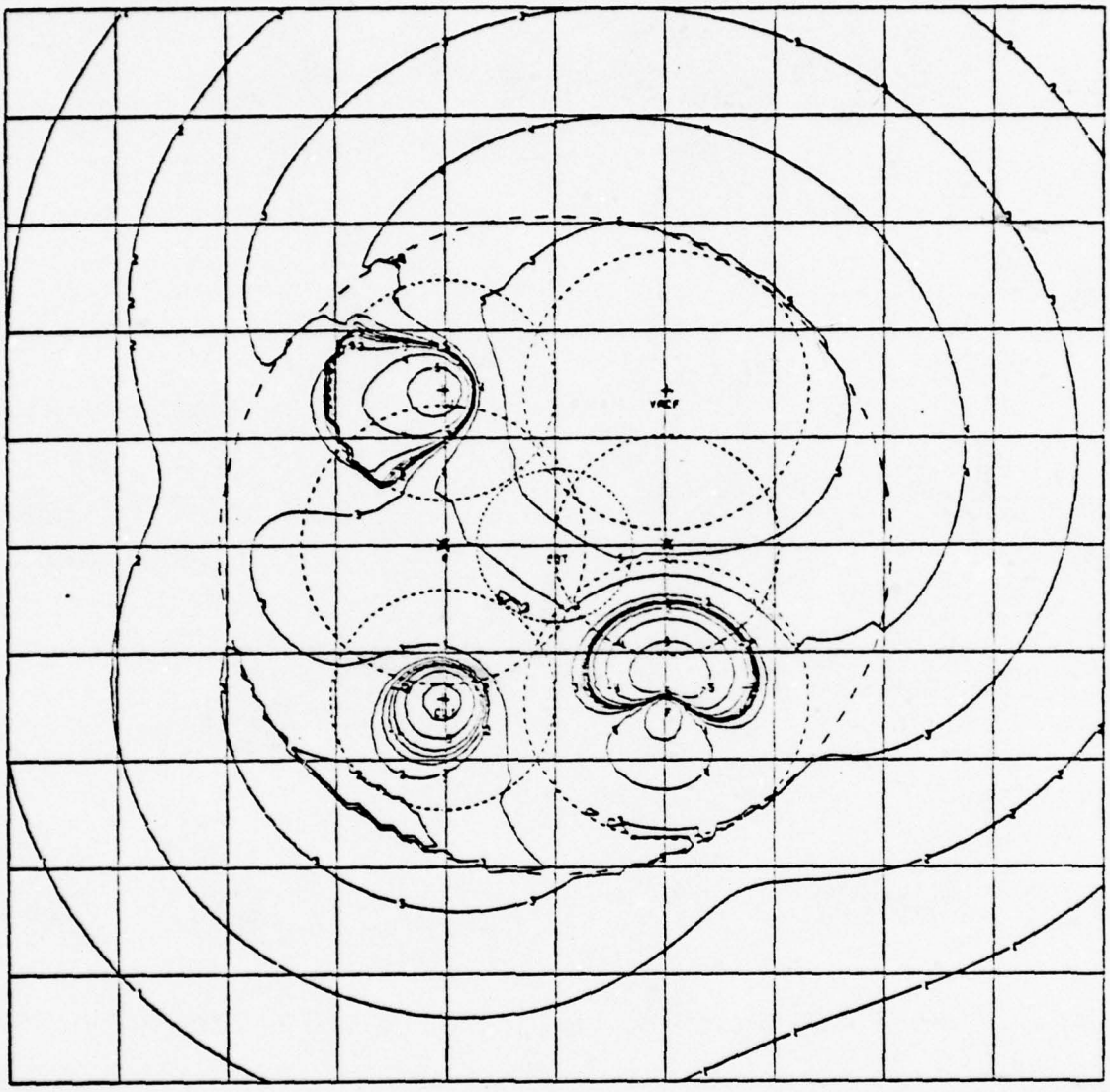

LiF

Fig. 10 b1

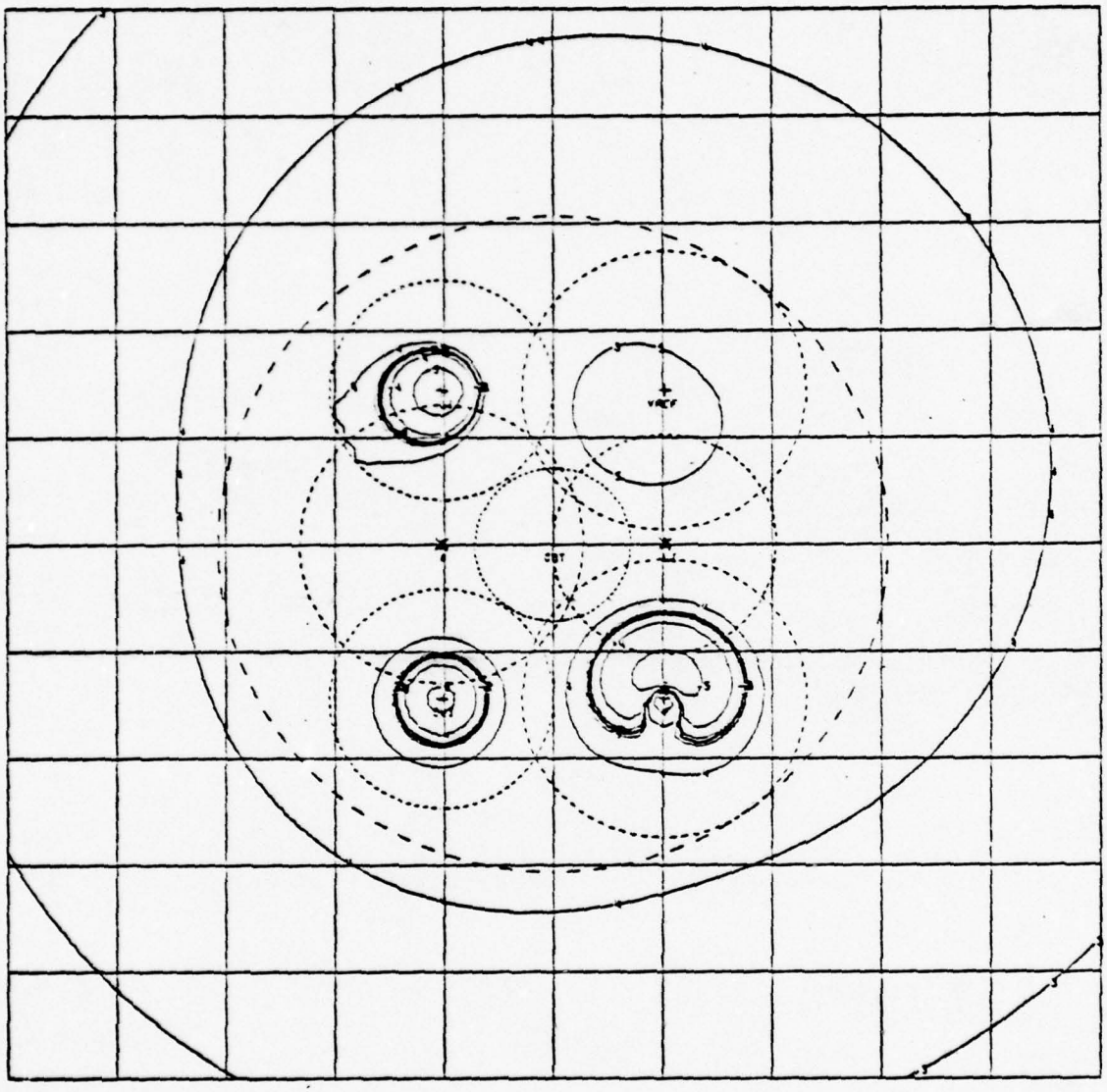

LiF

Fig. 10 b_2

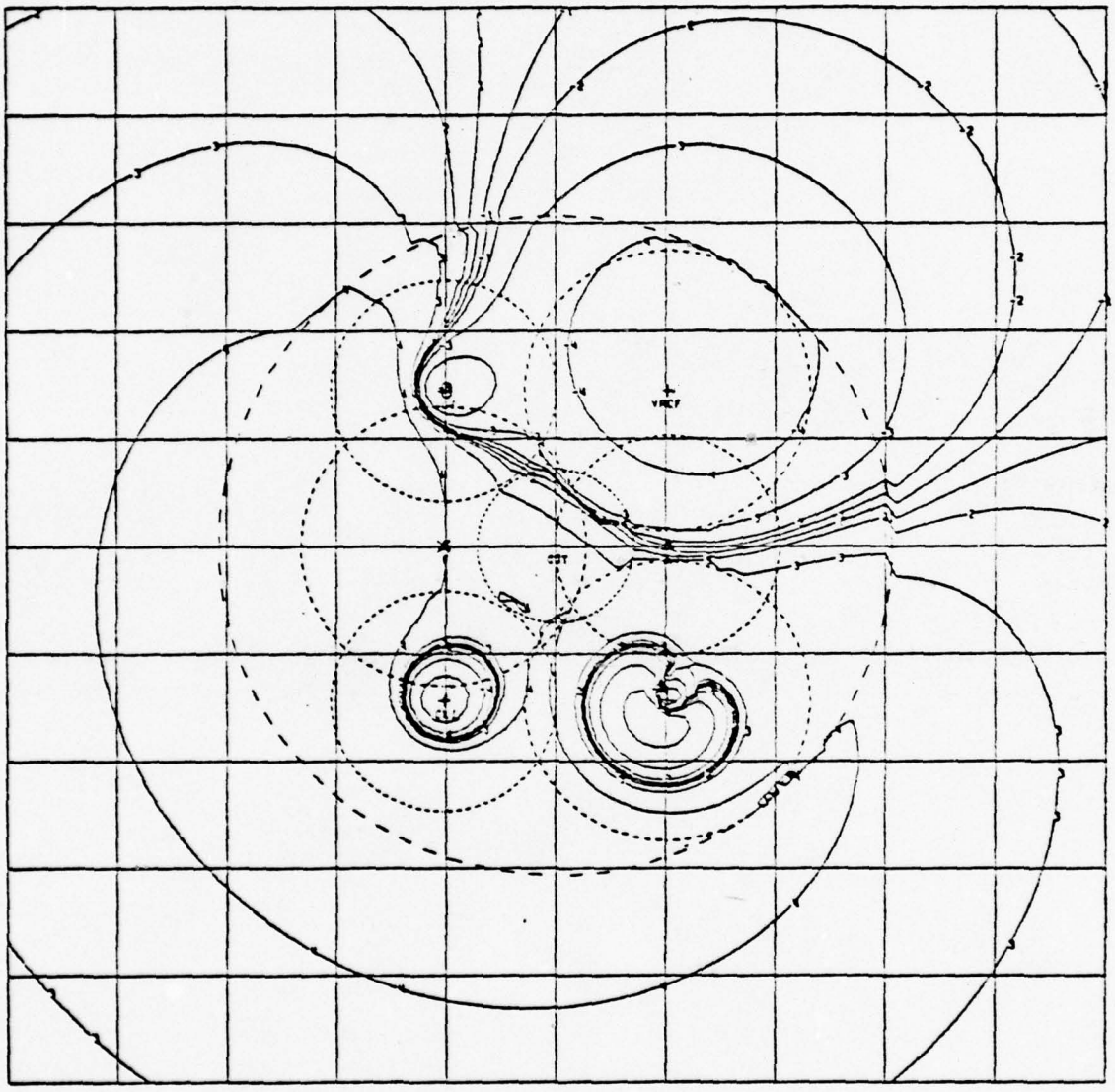

LiF

Fig. 10 C1

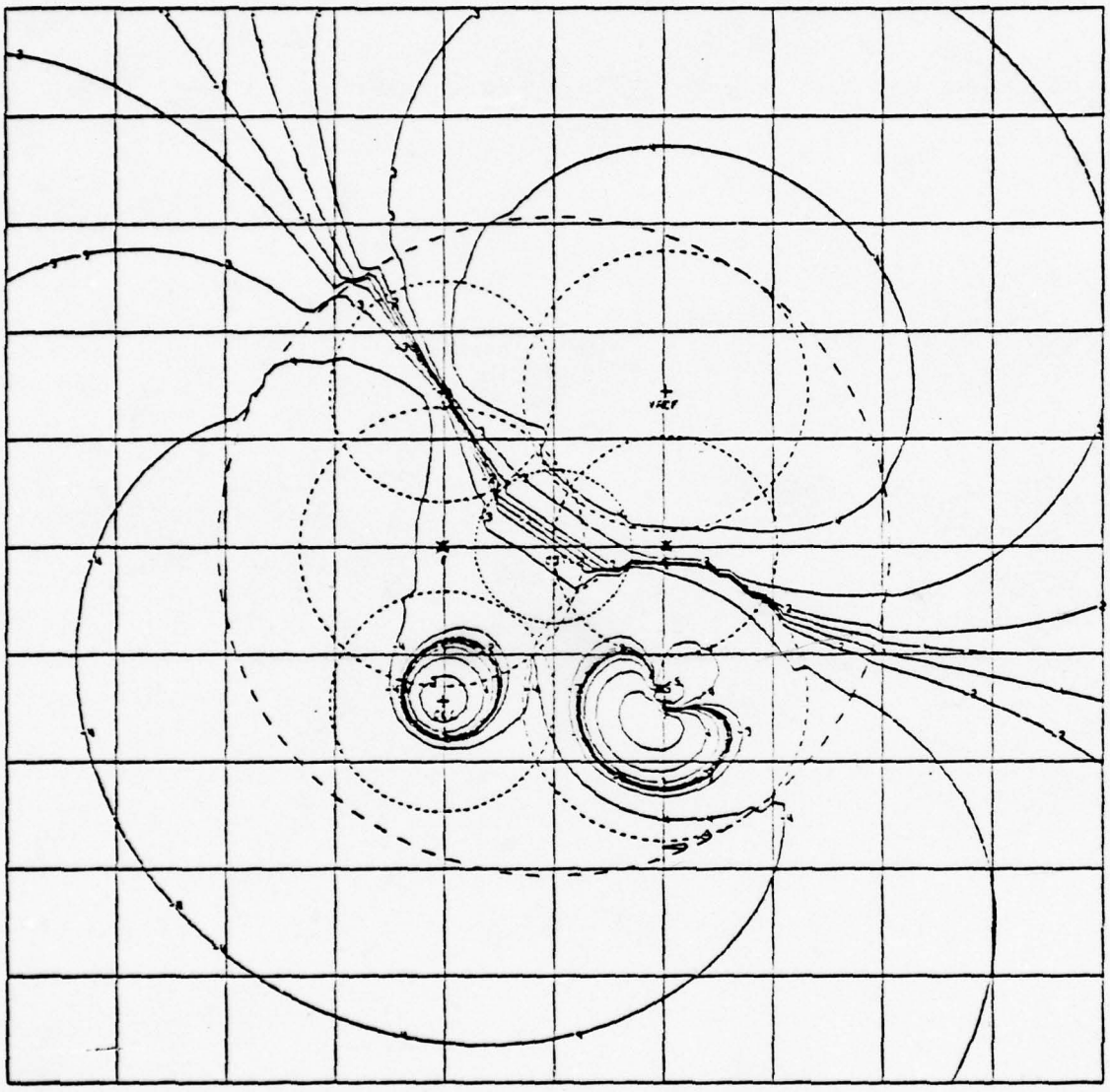

LiF

Fig. 10 C_2

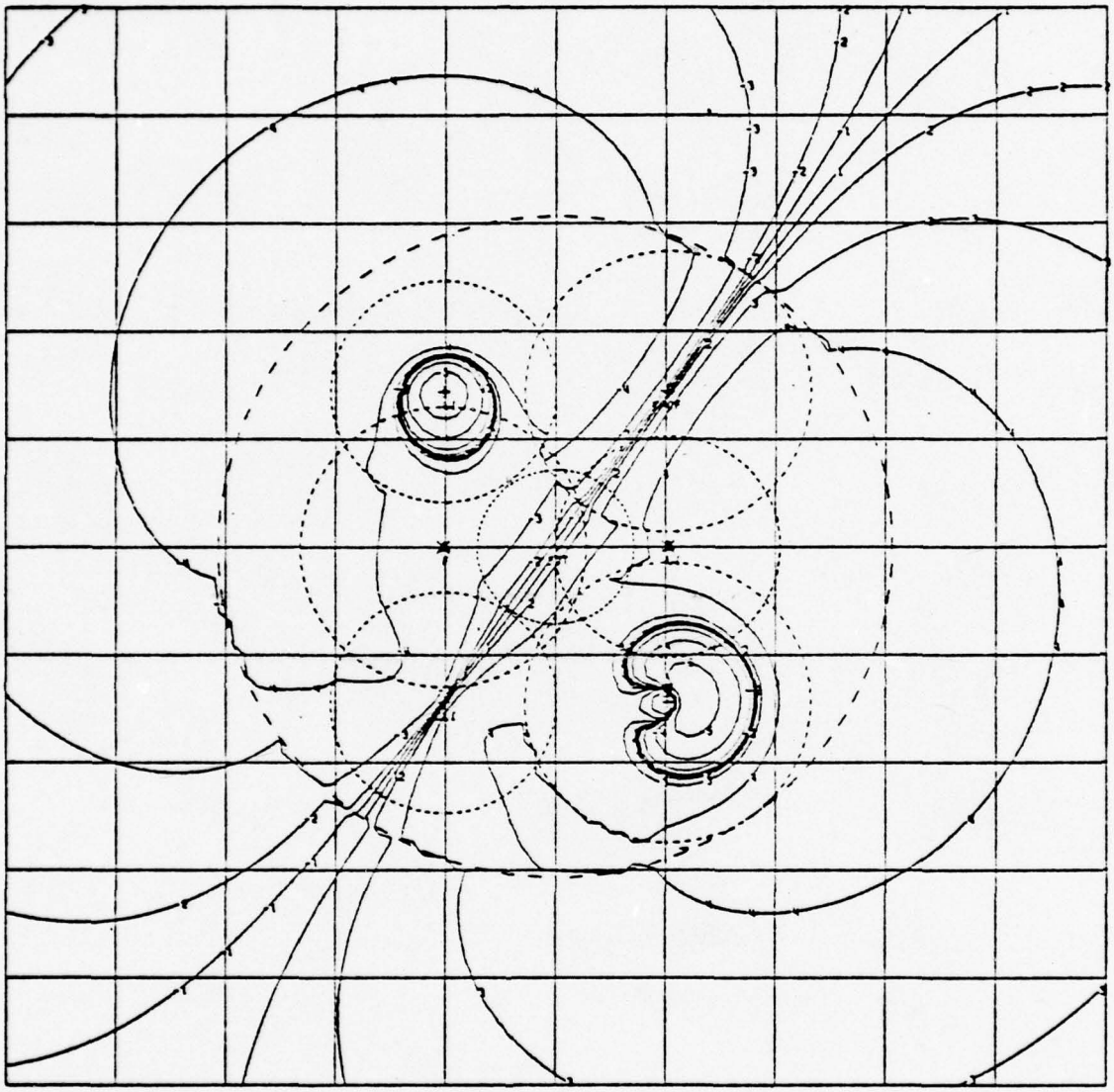

LiF

Fig. 10 d$_1$

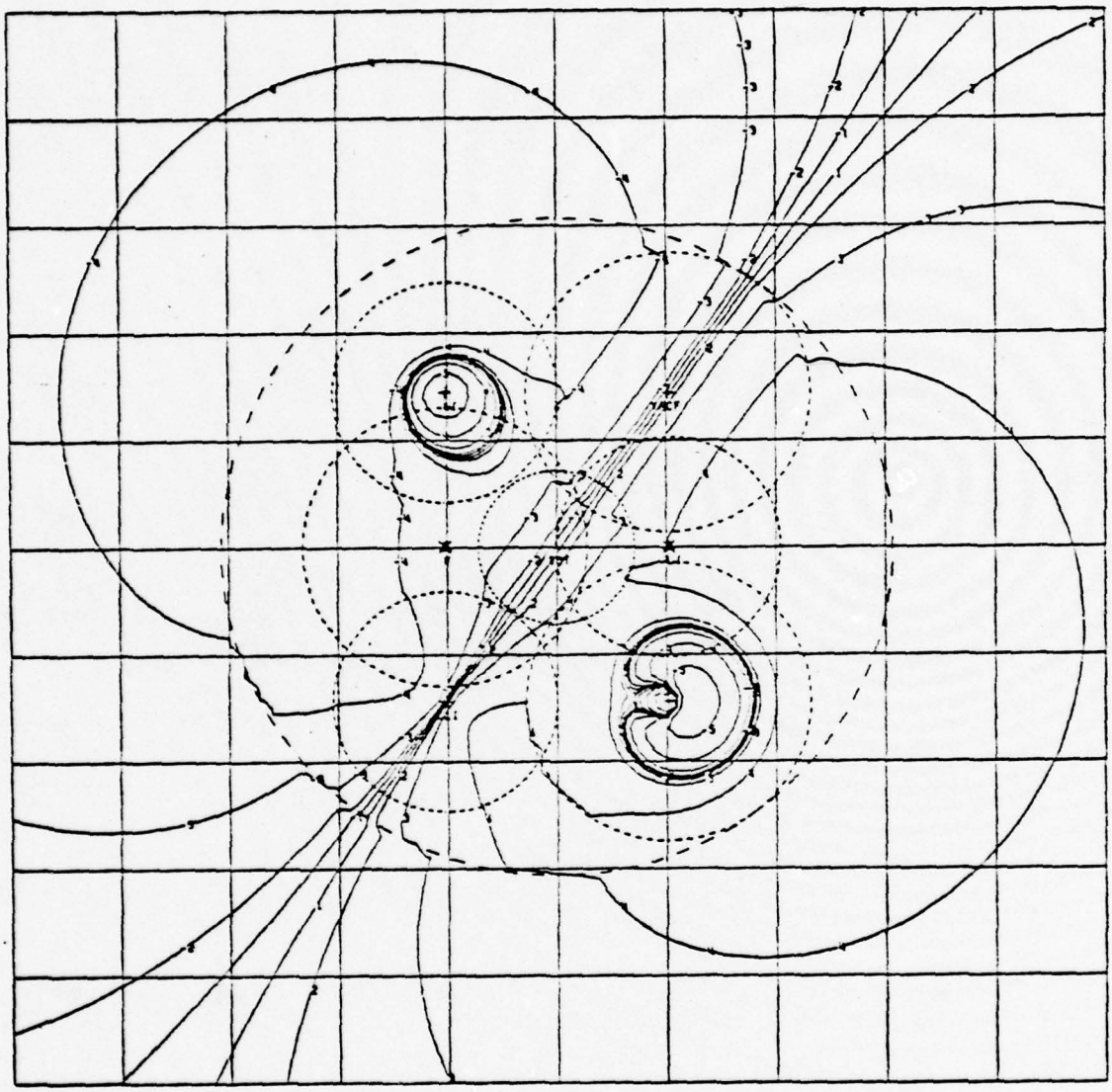

LiF

Fig. 10 d_2

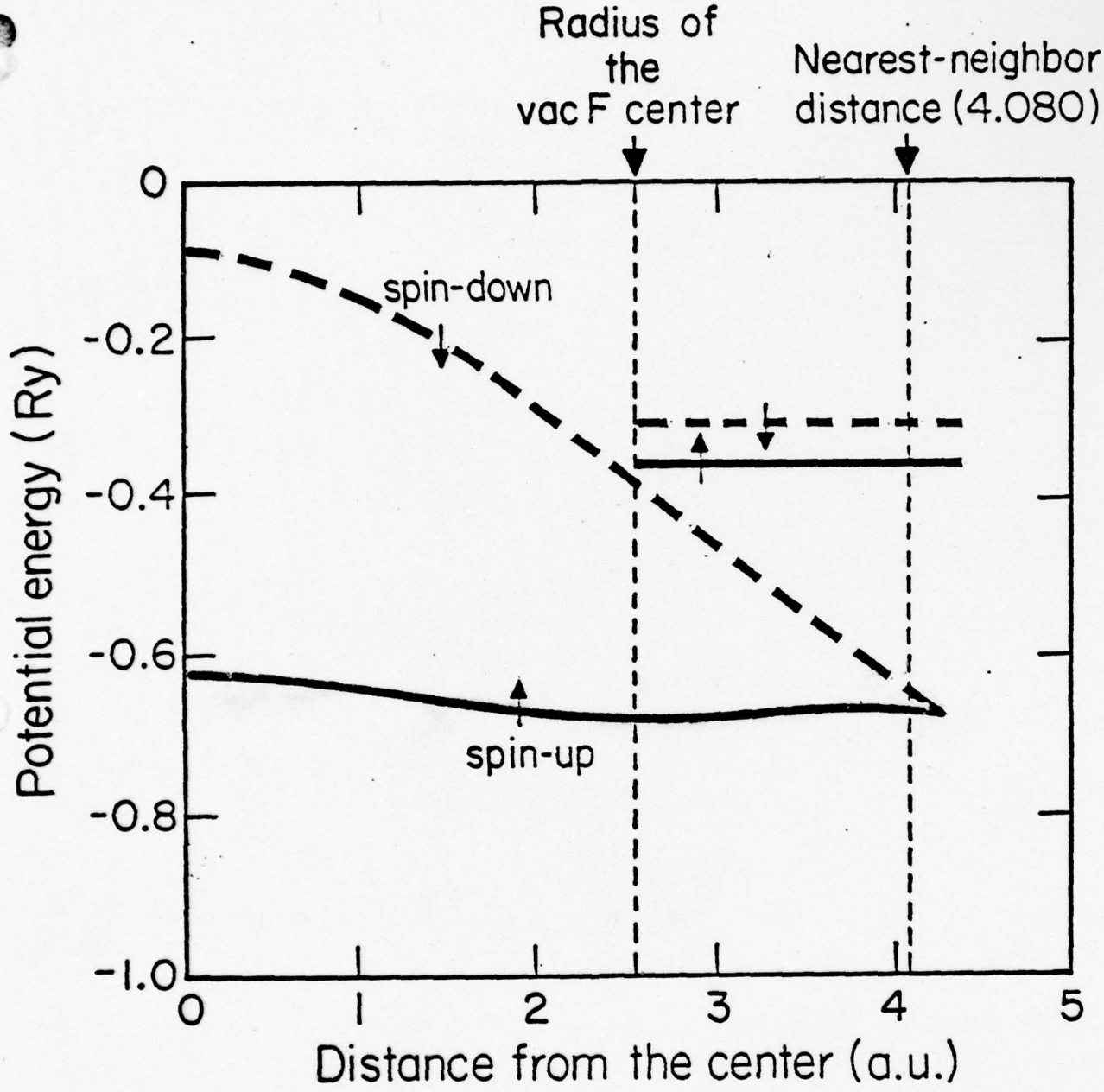
Radius of the vac F center
Nearest-neighbor distance (4.080)
spin-down
spin-up
Potential energy (Ry)
0
-0.2
-0.4
-0.6
-0.8
-1.0
0
1
2
3
4
5
Distance from the center (a.u.)

77

Li F

Fig. 11

Appendix II.

Investigation of the Effects of Intrinsic Point Defects on the Conductivity of PbTe via the SCF Xα Cluster Method*

D. Choo† and G.W. Pratt, Jr.

Department of Electrical Engineering and Computer Science, and
Center for Materials Science and Engineering
Massachusetts Institute of Technology
Cambridge, Mass. 02139

ABSTRACT

A PbTe crystal is modeled by an OPb_4Te_4 cluster, comprised of four tetrahedrally placed atoms for each of Li and F, and a central empty spherical region called O. Then vacancies, interstitials, and Frenkel defects of either Pb or Te are introduced in the cluster, resulting in defect clusters which simulate the PbTe crystals with such point defects. The various clusters are investigated by the SCF $X\alpha$ multiple-scattering method of Johnson, with the mass-velocity and Darwin relativistic corrections. The results that Pb and Te vacancies produce two free holes and two free electrons agree with Parada and Pratt's results of energy-band calculations through the Green's function method. A Pb interstitial and a Pb Frenkel defect are shown to give four and two free electrons respectively. A Te interstitial seems to generate two free holes while a Te Frenkel defect does not seem to contribute any to the conductivity. Anti-bonding mechanisms are found to play very important roles in the interstitial-containing complexes by shifting some valence electron levels of a pure crystal up into the conduction band.

I. INTRODUCTION

PbTe, PbSe, and PbS form a group a lead chalcogenides, Group IV-VI semiconductors of NaCl structure. They have been the subject of extensive investigations because of their technologically important optical and thermoelectric properties. These properties are closely related to the free carriers produced by the intrinsic point defects which are controlled by the use of high ranges of non-stoichiometry.

Experiments on the effect of an intrinsic point defect on the conductivity of lead chalcogenides lead to ambiguous conclusions since there usually are several kinds of intrinsic point defects present simultaneously in one sample. The are reviewed by Abrikosov, et al.[1], Ravich, et al.[2] and Davin.[3] In this paper it is attempted to solve the problem theoretically for vacancies, interstitials, and Frenkel defects of both Pb and Te in PbTe.

Either p-type or n-type semiconductor can be made of PbTe by adding excess tellurium or lead. In both cases the free carriers are characterized by high mobilities, and they can not be frozen out even at very low temperatures.[4,5] With such experimental evidence, it has been assumed that there are no bound states in the bandgap. Very recently, Bauer, et al.[6] showed conclusively that their measurements of the Hall effect and the magnetoresistance rule out the existance of deep impurity levels as well as of levels originating from intrinsic point defects within the bandgap in PbTe. If there were any bound states, in the bandgap, it would have been very difficult to exhibit them in calculations because the bandgap is extremely narrow. It is only 0.19 eV at 4.2°K,

increasing to 0.32 eV at 300°K.[7]

The problems of Pb and Te vacancies in PbTe were first solved by Parada and Pratt[8-10] by the Green's function method of Koster and Slater[11] in which a point defect is treated by a localized perturbing potential and the perturbed wave functions of electrons are expanded in terms of the Wannier functions of the unperturbed lattice. The calculations are quite complicated because the Bloch functions as well as the eigen-energies have to be known for all $\vec{k}$ vectors of the entire Brillouin zone in order to compute the Wannier functions. Therefore, the calculations were carried out without self-consistency using the potentials of netural atoms.

In recent years, Johnson[12] has developed the SCF $X\alpha$ multiple-scattering method for molecular clusters. The method is very efficient and accurate in comparison with the traditional methods such as the LCAO method; it has been successfully applied to many polyatomic molecules. It is also possible to treat crystals by the method once suitable cluster models are chosen for the crystals. Vacancies in PbTe were considered by Hamstreet[13] using a 27 atom cluster for the crystal. In this paper, the smallest possible neutral cluster of eight atoms and a central empty spherical region is employed in simulating the PbTe crystal, and all the intrinsic point defects are studied within the same cluster format. This cluster model is the one which was adopted for a LiF crystal in a previous paper by the present authors.[14]

In Section II, the cluster model calculation for a perfect PbTe crystal is described; and subsequently in Sections III-V, vacancies, interstitials, and Frenkel defects of Pb and Te are treated.

II. OPb_4Te_4 CLUSTER MODEL CALCULATION

The OPb_4Te_4 cluster model for a PbTe crystal is schematically shown in Fig. 1, corresponding to a cubic section of a PbTe crystal. The symmetry of the cluster now belongs to the T_d point group reduced from the O_h for the crystal. The central empty spherical region, O, is inserted so that the scattered waves from the atomic centers are more accurately described in the central region of the cluster by the use of a spherically symmetric, r-dependent, potential rather than a volume-averaged one. The importance of the O center was illustrated in the previous paper[14] for the LiF crystal in achieving an equilibrium state for the OLi_4F_4 cluster. The nearest-neighbor distance of the cluster model was taken from the experimental equilibrium value 3.226 Å of the crystal.

In the OPb_4Te_4 cluster, Pb and Te atoms are equally treated and every atom is equivalent to the other atoms of the same species as they should be in the PbTe crystal. However, each atom has three nearest-neighbors in the cluster while it has six in the crystal. Therefore, there will be some rearrangement in the covalent-bonding characteristics, but the cluster model is quite adequate in describing the ionic-bonding characteristics with the use of Madelung correction terms to the atomic potentials from the ions in the remainder of the crystal which are not represented in the cluster model (refer to Ref. 14). Due to the neutrality of the cluster all the electrons can be contained without the need of using a Watson sphere.[15]

The atomic radii of Pb and Te in compounds are 1.80 and 1.40 Å

respectively.[16] However, the atomic potentials calculated self-consistently for the Pb and Te atomic centers in the cluster model are almost the same at the midpoint between the two adjacent atoms. Therefore, both the atomic radii were set equal in the subsequent iterations.

In the case for the OLi_4F_4 cluster,[14] the overlapping-scale factor of the atomic centers was determined such that the virial coefficient[17] becomes unity. The virial coefficient calculated for the OPb_4Te_4 cluster with touching atomic centers is already very close to unity with a deviation of less than 0.01% due to the enormously deep core energy levels (for example, the eigen-energy of Pb 1s core electron state is about -6000 Ry). Because the virial coefficient hardly varies by changing the degree of the overlap for the atomic centers, the overlapping scale factor of the OP_4Te_4 cluster is set at 1.14 as we found for the OLi_4F_4 cluster.

The exchange parameter α's for Pb and Te were obtained through interpolation from the Schwarz's atomic α's.[18] For the interatomic and extramolecular regions, a weighted average α was computed with respect to the number of valence electrons of the atoms. In the OPb_4Te_4 cluster all the α values are approximately 0.7 which is close to the lower limit.

It was found that relativistic effects are important in getting the correct energy-band structure of the PbTe crystal.[19,20] Therefore, we included the mass-velocity and Darwin relativistic corrections to the SCF Xα multiple-scattering method for the OPb_4Te_4 cluster, (the formalism is illustrated in Appendix). The spin-orbit coupling term was not in-

corporated because of the symmetry restrictions. For a given potential, the relativistic corrections tend to lower the electron energy levels; however, the relativistic and non-relativistic energy-level structures become increasingly similar as self-consistent iterations proceed.

The calculated electron states of the OPb_4Te_4 cluster are listed in Table I with their eigen-energies, normalized partial-wave coefficients, and electronic charge distributions. The electron energy levels of the cluster are shown in Fig. 2(a), compared with the energy-band structure of the PbTe crystal in Fig. 2(b) which was obtained by the pseudopotential method using five parameters to fit experimental data by Lin and Kleinman.[21]

The two lowest levels of the cluster, $1a_1$ and $1t_2$, correspond to the lowest crystal energy-band of mostly Te s character; and the next two levels, $2t_2$ and $2a_1$, correspond to the second lowest crystal energy-band of mostly Pb s character. These two energy-bands will be referred to as Te s and Pb s bands for convenience.

The next five levels, $1e$ through $4t_2$, form the top valence band which is primarily made of Te p basis states but they also contain significant components of Pb p basis states. The rest of the levels from $5t_2$ and up constitute the conduction band of the crystal as they are made of mostly Pb p basis states and some Te p basis states. The conduction band states have large amounts of electronic charge in the interatomic region.

As we see from Fig. 2, each energy-band of the crystal matches well to

a set of cluster energy levels of similar characteristics. The bandgap of the cluster as the difference in eigen-energies between the $4t_2$ and $5t_2$ levels, is 0.19 Ry which is about ten times as large as the bandgap of the crystal at L point of the Brillouin zone. The bandgap of the cluster, rather, corresponds to an average of the energy gap between the conduction and the valence bands throughout the Brillouin zone.

The non-relativistic total energy of the cluster is -209,088.7 Ry self-consistently, while the sum of the RHF total energies for free atoms is -209,086.1 Ry. This gives 2.6 Ry for the cohesive energy of the cluster; however, it should be considered to give only an indication of cohesion since the total energies are too large to be accurate on the order of 0.01 Ry. The inclusion of the relativistic correction terms drastically lowers the total energy of the cluster by 4671.7 Ry from the non-relativistic value while the corresponding relativistic RHF total energies of free atoms are not available. It is impossible to determine the equilibrium state of the cluster or formation energies of defects by comparing the total energies of clusters which, for such purposes, must be calculated accurately to the order of 0.1 Ry.

The ionicty of the OPb_4Te_4 cluster indicates that about 0.75 electron is transferred from a Pb to a Te atom. It was calculated by assigning the electronic charges in the interatomic, extramolecular, and the O center regions to the atomic centers in proportion to the valence electronic charges which are already in the atomic centers

as a result of SCF calculations. Because a completely ionic picture of PbTe implies the transfer of two electrons from a Pb to a Te atom, the ionicity of the crystal may be said to be about 37% in the present cluster model.

III. Pb AND Te VACANCIES

A Pb or Te vacancy cluster was made by vacating a Pb or Te neutral atom from the OPb_4Te_4 cluster. This results in reduction of the cluster symmetry from the T_d to C_{3v} point group. (In the crystal the symmetry is reduced from the O_h to T_d point group.) The exchange α parameters are the same as the OPb_4Te_4 cluster except in the vacancy centers where the average α is used. The same Madelung correction terms were kept but now with the final ionicity found with the OPb_4Te_4 cluster.

The energy levels of the Pb and Te vacancy clusters are shown in Figs. 3(a) and 3(c) respectively, compared with the levels of the OPb_4Te_4 cluster in Fig. 3(b).

We will discuss the results of the Pb vacancy cluster first. The lowest three levels of Fig. 3(a), $1a_1$, $2a_1$, and 1e, constitute a perturbed Te s band due to the Pb vacancy. Likewise, the next two levels, 2e and $3a_1$, constitute a perturbed Pb s band. The set of the levels from 3e through 6e make up the top valence band, and the levels of $7a_1$ and up make up the conduction band of the perturbed cluster.

The topmost valence electron level is the four-fold 6e state, and it is occupied by only two electrons; therefore, the valence band has two less electrons than required if it were to be completely filled. We notice that an a_1 level is missing from the Pb s band as a Pb is removed from the OPb_4Te_4 cluster by considering the compatibility relationships for the representations between the T_d and C_{3v} point groups. In terms of a perturbative treatment, a doubly degenerate atomic Pb s

level is so much perturbed by the vacancy potential that is is driven up into the conduction band. Now the Pb vacancy cluster has two less electron states, counting degeneracy, in the valence bands and four less valence electrons due to the missing Pb atom than the OPb_4Te_4 cluster; therefore, it results in two free holes in the valence band.

The extremely narrow bandgap of PbTe is located very close to the constant potential in the interatomic region of the OPb_4Te_4 cluster as we see in Fig. 2. Figure 3 now shows that the constant potential hardly varies when the Pb vacancy (or Te vacancy for that matter) is introduced in the OPb_4Te_4 cluster, and it still indicates approximately the position of the bandgap of the crystal. The large gap between the 6e and $7a_1$ levels further assures that the crystal bandgap must be between them. From the partial-wave analysis it is seen that the 6e state is indeed a valence-band state whose characteristics are very similar to those of the top valence electron state, $4t_2$, of the OPb_4Te_4 cluster.

Now we will discuss the case for the Te vacancy. The two lowest levels, $1a_1$ and 1e, constitute a perturbed Te s band. This band is lacking one a_1 state compared with the Te s band of the OPb_4Te_4 cluster accounting for the 5s level of the missing Te atom. The next three levels, $2a_1$, 2e, and $3a_1$, constitute a perturbed Pb s band.

The set of next six levels, from 3e to $5a_1$, makes up a perturbed top valence band which now accommodates only 18 electrons while there are 24 electron states in the corresponding valence band of the OPb_4Te_4 clsuter. The effect of the perturbation by the Te vacancy is to make an a_1 and e levels missing from the top valence band. Skipping the

$6a_1$ and 6e levels for the moment, the top two levels, 7e and $7a_1$, belong to the conduction band as their wave functions have similar characteristics as the wave functions of the conduction band levels of the OPb_4Te_4 cluster.

In order to illustrate the $6a_1$ and 6e states, we list their partial-wave coefficients and electronic charge distributions in Table II. Both the states have large partial-wave coefficients for the Pb p basis functions and considerable amount of electronic charges in the inter-atomic region; such properties are characteristic of the conduction band states of PbTe. They also lie above the constant potential which is indicative of the location of the crystal bandgap. Furthermore, it is known experimentally that there are no bound electron states in the bandgap of the crystal; therefore, the two states belong to the conduction band of the PbTe crystal.

The $6a_1$ and 6e states also have significant contributions from Te vacancy basis functions. The $6a_1$ state has particularly large coefficient for a Te vacancy s basis function so that it can be said to be the electron state of the greatly perturbed Te 5s atomic orbital which was stated earlier as missing from the perturbed Te s band. On the other hand, the 6e state is the perturbed electron state which has been driven out of the top valence band of primarily Te p character. The other perturbed a_1 level, which has also been driven out of the top valence band, would be located further above the $7a_1$ level.

The $6a_1$ conduction band level is the highest filled level occupied by two electrons. The situation can be expalined by the following. Due

to a missing Te atom there are six fewer electrons and eight fewer electron levels, counting degeneracy, in the valence bands of the Te vacancy cluster. Consequently we have two extra electrons left over after all the valence band levels are filled. These two electrons go to the lowest conduction band level, $6a_1$, resulting in two free electrons in the PbTe crystal.

Our conclusions on the effects of the Pb and Te vacancies on the conductivity of PbTe are in agreement with the results of perturbative energy-band calculations of Parada and Pratt[8-10] by the Green's function method. In their calculations for the Te vacancy, the perturbed Te s level is slightly higher than the perturbed Te p levels while the present cluster-model calculations show otherwise. In any case such change of ordering does not present and change in physical meaning because they are all in the conduction band. In the Green's function method, all the Bloch states of the crystal are considered unperturbed except producing some localized defect electron states, while in the cluster method all the states are perturbed by the defect. The multiple-scattering calculations for 27-atom clusters by Hamstreet[13] also give the same results regarding to the effects of the vacancies on the conductivites of the PbTe crystal.

IV. Pb AND Te INTERSTITIALS

In PbTe the Pb interstitial is still important,[22] although the primary intrinsic defect species is the Te vacancy when the material contains excess lead.[23] It seems that the Pb interstitials can be rather easily accommodated by the crystal due to their small ionic size, but the Te ions are too large to be interstitials. However, for competeness, both the Pb and Te interstitials will be considered here.

The interstitial clusters are formed very conveniently by putting either Pb or Te atom at the place of the central O empty center of the OPb_4Te_4 cluster. The resulting interstitial clusters retain the T_d group symmetry which is correct for interstitials in the crystal. The electron energy levels of the Pb and Te interstitial clusters are shown in Fig. 4, compared with those of the OPb_4Te_4 cluster.

Let us consider the Pb interstitial case first. From the partial-wave analysis it can be shown that all the e, t_1, and t_2 states of the Pb interstitial cluster are perturbed electron states from the ones with the same denominations in the OPb_4Te_4 cluster. Their eigen-energies have been lowered by almost the same amount with the average of about 0.1 Ry. On the other hand, all the a_1 states have been affected irregularly by the Pb interstitial. In order to describe their characteristics, we show their partial-wave coefficients and electronic charge distributions in Table III (for comparison, the $5t_2$ bottom conduction band state is also included).

The $1a_1$ state represents a bonding combination of the Te 5s, IPb

AD-A053 584 MASSACHUSETTS INST OF TECH CAMBRIDGE DEPT OF ELECTRI--ETC F/G 20/12
CLUSTER MODEL INVESTIGATION OF DEFECTS IN SOLIDS.(U)
APR 78 G W PRATT N00014-75-C-0785
UNCLASSIFIED NL

2 OF 2
AD
A053584

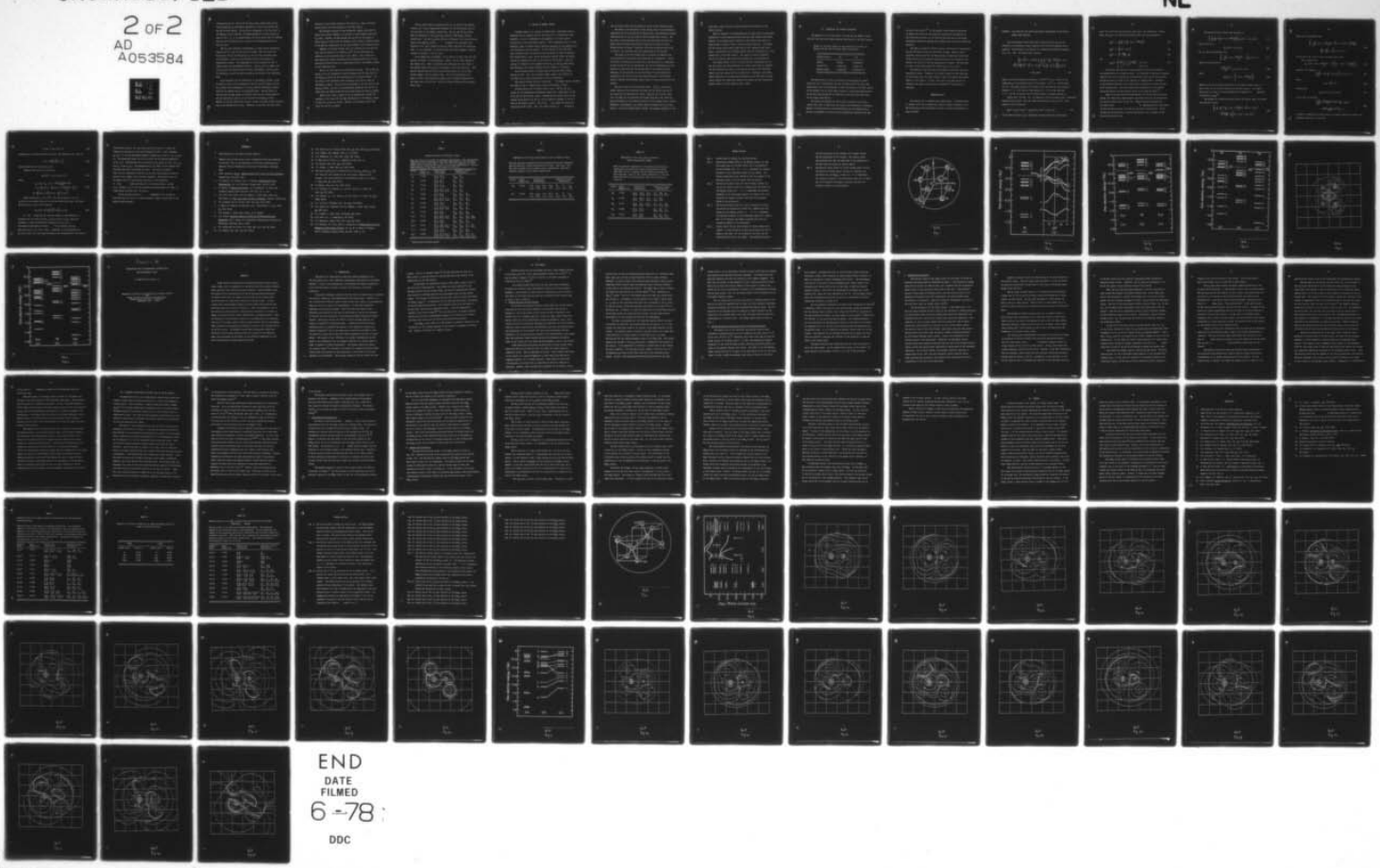

END
DATE
FILMED
6-78
DDC

(interstitial Pb) 6s, and the Pb 6s atomic basis states while the $2a_1$ state represents an antibonding combination of the Te 5s-p hybrid and the IPb 6s basis states. The $3a_1$ state corresponds to the $2a_1$ state of the OPb_4Te_4 cluster; however, its eigen-energy has not been lowered as much as the e, t_1, or t_2 states because the IPb 6s basis state is combined with the Pb 6s-p hybrid state to produce an antibonding behavior for the $3a_1$ state.

The $4a_1$ state exhibits, interestingly, a rather strong antibonding between the Te 5p and the IPb 6s basis states; thus, its level has been raised from the corresponding $3a_1$ level in the top valence band of the OPb_4Te_4 cluster to the conduction band of the present Pb interstitial cluster. The contour map of its wave function in Fig. 5 clearly shows such antibonding character. The $4a_1$ level is higher than the $5t_2$ level the electron state of which corresponds to the $5t_2$ state of the OPb_4Te_4 cluster and hence represents the bottom of the conduction band.

As we introduce the Pb interstitial in the OPb_4Te_4 cluster, we get an extra a_1 state in the combination of the $1a_1$ and $2a_1$ states and lose an a_1 state, which corresponds to the $4a_1$ state of the OPb_4Te_4 cluster, from the top valence band to the conduction band. The net result is that we have the same number of electron levels in the valence bands of the Pb interstitial cluster as in the case of the OPb_4Te_4 cluster. However, in the Pb interstitial cluster, we have four more valence electrons due to the interstitial Pb atom. Therefore, we are left with four extra

electrons in the bottom conduction band state $5t_2$. Thus a Pb interstitial gives four free electrons to the PbTe crystal.

The constant potential of the interatomic region, near which we suppose the crystal bandgap to be located, is only slightly below the $5t_2$ level. However, the gap between the $4t_2$ and the $5t_2$ levels is large enough to assure that the bandgap of the crystal is indeed located in the gap and consequently the $5t_2$ level beongs to the conduction band.

Commonly it has been thought that a Pb interstitial would give up only two free electrons by becoming a Pb^{2+} ion and depositing two electrons in the conduction band of the crystal. Such a model was made apparently without considering the antibonding effect due to the interstitial which drives up a valence band state of the perfect crystal to the conduction band.

Now let us look into the Te interstitial problem. The $1a_1$ and $2a_1$ states of the Te interstitial cluster originate from the $1a_1$ state of the OPb_4Te_4 cluster and ITe (interstitial Te) 5s atomic orbital. The $3a_1$ state is the perturbed state originating from the $2a_1$ state of the OPb_4Te_4 cluster. The $4a_1$ state corresponds to the $3a_1$ state of the OPb_4Te_4 cluster, but due to its antibonding character with the ITe 5s basis state its eigen-energy has been raised unlike the other a_1 states

Each of the e and t_1 states of the Te interstitial cluster corresponds to the state with the same denomination in the OPb_4Te_4 cluster. So does the $1t_2$ and $2t_2$ states. However, the situation is not very clear for the 3-6 t_2 states.

The $3t_2$ state seems to originate from the $3t_2$ state of the OPb_4Te_4 cluster, but it has a significant component of the Pb 6s basis state as the $2t_2$ state of the OPb_4Te_4 cluster has. The $4t_2$ and the $6t_2$ states seem to correspond to the $4t_2$ and $6t_2$ states of the OPb_4Te_4 cluster respectively. But the $5t_2$ state does not correspond to any one particular state of the OPb_4Te_4 cluster; it seems to be a perturbed combination of all the t_2 states in the top valence band and the conduction band. It is, therefore, not certain where the crystal bandgap would be located in relation to the $5t_2$ level.

If we assume that the bandgap of the crystal is still very near the constant potential in the interatomic region, the $5t_2$ level belongs to the valence band. Then a Te interstitial would give two free holes to the crystal since the $5t_2$ level is occupied by only four electrons. This picture implies that all the 5s and 5p atomic levels of the Te interstitial belong to the top valence band. If the Te interstitial ever exists in PbTe, the interstitial complex will be greatly relaxed due to the large size of the Te ion; this fact further obscures the conclusion drawn here.

V. Pb AND Te FRENKEL DEFECTS

A Frenkel defect in a crystal is formed when a constituent atom is displaced from its regular site in the lattice to an interstitial site. Therefore, it may be considered as an aggragate of a vacancy and an interstitial of the same atomic species. Such an aggragate leads to many different types of Frenkel defect complexes depending on the separation of the interstitial and the vacancy. In this section we will deal only with a Frenkel defect in which the pair are placed as close as possible. The Frenkel defect, then, can be conveniently modeled within the OPb_4Te_4 cluster by displacing an atom to the center of the cluster. This decreases the symmetry of the complex from the T_d to the C_{3v} point group and reproduces the correct symmetry of such a defect in a crystal.

The Pb Frenkel defect is another kind of important point defect species in PbTe. But, the Te Frenkel defect seems to be difficult to be formed for the same reason given to the Te interstitial.

The electron energy levels of the Pb and Te Frenkel defect clusters are shown in Fig. 6, compared with those of the OPb_4Te_4 cluster.

We will discuss the Pb Frenkel defect first. The $1a_1$ and $3a_1$ states are the bonding and antibonding combinations, repectively, of the Te 5s and the IPb 6s basis states. Between the two levels there are two closely lying levels, $2a_1$ and 1e, which originally belonged to the Te s band of the OPb_4Te_4 cluster. The 2e and $4a_1$ levels now constitute the perturbed Pb s band. Next, the levels from $5a_1$ to 6e make up

the top valence band, and the levels of 7e and up the conduction band.

One thing to be noted here is that the $8a_1$ state is an antibonding combination of the Te 5p and IPb 6s basis states, thus exhibiting similar characteristics as the $4a_1$ state of the Pb interstitial cluster. The $8a_1$ level in the conduction band is the only level which has been removed from the valence bands while no electrons are lost as the Pb Frenkel defect is formed. Therefore, the bottom conduction band state 7e carries two electrons which will become free in the crystal.

The result of the Pb Frenkel defect is exactly an algebraic sum of the results of the separate Pb vacancy and Pb interstital. In the Pb s band, the missing Pb 6s level due to the Pb vacancy is compensated by the 6s level of the Pb interstitial, but the Pb interstitial in turn loses an a_1 state from the top valence band to the conduction band. Therefore, we may say that the two free holes of the Pb vacancy are cancelled by the two out of the four free electrons of the Pb interstitial, thereby the Pb Frenkel defect leaves two free electrons for the crystal.

Now let us turn to the Te Frenkel defect. The $1a_1$, 1e, and $2a_1$ levels constitute the perturbed Te s band, and the levels from $3a_1$ to $4a_1$ constitute the perturbed Pb s band. Next, the set of levels from 3e to $7a_1$ makes up the perturbed top valence band while the levels $8a_1$ and up correspond to the conduction band of the Te Frenkel defect cluster. Therefore, the bandgap in the cluster model is between the $7a_1$ and $8a_1$ levels. In this Te Frenkel defect cluster, the constant potential in the

interatomic region does not correctly indicate the location of the crystal bandgap.

There is ambiguity in interpreting the 6e level which is a perturbed combination of some conduction band states and some valence band states. However, let us assume that it belongs to the valence band since its eigen-energy is equal to that of the top valence level $7a_1$. This makes all the valence band levels filled and all the conduction band levels empty; consequently the Te Frenkel defect does not contribute any to the conductivity of the PbTe crystal. This result is also an algebraic sum of the separate results from a Te vacancy and a Te interstitial.

The Frenkel defect of Pb or Te which we have illustrated thus far has the vacancy and the interstitial as close to each other as possible. Yet they show that the result is the same as the sum of the individual effects from the vacancy and the interstitial. Therefore, any Frenkel defect regardless of the separation between the pair will give the same result because the interaction between the vacancy and the interstitial becomes weaker as their separation gets larger.

VI. CONCLUSION AND FURTHER DISCUSSION

We summarize, in the table below, the type and the number of free carriers that each point defect species would induce in the PbTe crystal.

Effects of the point defects on the conductivity of PbTe, as deduced from the SCF Xα cluster model calculations.

Defects Species	Pb	Te
Vacancy	2 holes	2 electrons
Interstitial	4 electrons	2 holes (?)
Frenkel defect	2 electrons	No carrier (?)

The difficulties we have encountered in interpreting the energy levels for the Te interstitial and the Te Frenkel defect may have some relationship with the unlikeliness of their occurrence in the PbTe crystal. If we disregard the two point defect species, a p-type PbTe semiconductor can be made only through the Pb vacancies, as all the other kinds lead to the n-type semiconductor.

The results we obtained for the Pb and Te vacancies in the PbTe crystal were shown to agree with the results from perturbative treatments. However, the conclusions for the interstitials and the Frenkel defects are not in agreement with such strictly perturbative considerations made

by one of the authors.[24] In the present cluster model calculations, we showed that there are some electron levels which are affected by the perturbing potential in the opposite direction due to particular antibonding mechanisms although most energy levels follow the perturbing potential.

The defect clusters for the Pb vacancy, both kinds of interstitials, and the Pb Frenkel defect are open-shell systems. However, spin-polarized calculations have not been pursued, because the incompletely filled levels do not represent localized states in the bandgap of the crystal, but they fall into one energy band or another. The electrons or holes in the energy bands will become free in the crystal.

The effects of the intrinsic point defects in PbTe are very much localized in space. Therefore, such small clusters as have been used in the present paper were good enough to show the relevent short-range effects of the defects. In fact, they lead to the same results as obtained from larger cluster models by Hamstreet[13] in the case of vacancies.

ACKNOWLEDGMENTS

The authors wish to express their appreciation to Professor Keith H. Johnson of MIT for providing the original computer programs for the SCF Xα multiple-scattering method and also for helpful discussions on many occasions.

APPENDIX: MASS VELOCITY AND DARWIN RELATIVISTIC CORRECTIONS IN THE ATOMIC RADIAL WAVE EQUATION

The two-component relativistic Pauli equation for an electron is obtained by eliminating two small components from the four-component Dirac equation. Specializing to an electron in a spherically symmetric potential, V(r), one gets the radial Pauli equation,

$$\left\{\left(1 + \frac{\alpha^2}{4}\,[E - V(r)]\right)^{-1}\left(-\frac{1}{r^2}\frac{d}{dr}\,r^2\,\frac{d}{dr} + \frac{\ell(\ell+1)}{r^2} + V(r)\right.\right.$$
$$\left.\left. - \frac{\alpha^2}{4}\,\frac{1}{r}\,\frac{dV(r)}{dr}\left(1 + \frac{\alpha^2}{4}\,[E - V(r)]\right)^{-2}\left(r\,\frac{d}{dr} + \begin{bmatrix} -\ell \\ \ell+1 \end{bmatrix}\right)\right\} R_\ell(r;E)$$
$$= E\,R_\ell\,(R;E), \qquad (1)$$

where α is the fine-structure constant, $(137.037)^{-1}$ in a.u., and E is the eigen-energy of an electron less its rest energy, $2\,\alpha^{-2}$ a.u. In the above Eq. (1), the upper quantity $(-\ell)$ refers to the case when the total angular momentum $J = \ell + 1/2$, and the lower quantity $(\ell + 1)$ to the case when $J = \ell - 1/2$ for an electron in the atomic orbital of angular momentum ℓ.

Rather than solving Eq. (1) directly, we will proceed to get a simplified equation which retains only the terms of the order of unity and α^2. This equation can be written as

$$[H_o(r) + H_m(r) + H_d(r) + H_{so}(r)]\,R_\ell\,(r;E) = E\,R_\ell\,(r;E). \qquad (2)$$

In the above equation, $H_o(r)$ represents the non-relativistic Hamiltonian,

$H_m(r)$ the relativistic mass-velocity term, $H_d(r)$ the relativistic Darwin term, and $H_{so}(r)$ the spin-orbit coupling term; they are expressed by

$$H_o(r) = -\frac{1}{r^2}\frac{d}{dr}r^2\frac{d}{dr} + V(r) + \frac{\ell(\ell+1)}{r^2}, \tag{3}$$

$$H_m(r) = -\frac{\alpha^2}{4}[E - V(r)]^2, \tag{4}$$

$$H_d(r) = -\frac{\alpha^2}{4}\frac{dV(r)}{dr}\frac{d}{dr}, \tag{5}$$

and

$$H_{so}(r) = \begin{cases} -\frac{\alpha^2}{4}\begin{bmatrix} -\ell \\ \ell+1 \end{bmatrix}\frac{1}{r}\frac{dV(r)}{dr} & \text{for } \ell \geq 1, \\ 0 & \text{for } \ell = 0. \end{cases} \tag{6}$$

In crystals and molecular clusters, electron states are classified by representations of a symmetry group. The inclusion of spin-orbit coupling requires the use of double group representations while the SCF Xα multiple-scattering method is based on the symmetry of single groups. Therefore, in the present modification for relativistic corrections, we drop the spin-orbit coupling term. The fully relativistic formalism for the multiple-scattering method has been recently worked out by Yang and Rabii.[25]

Since we use the muffin-tin approximation for the multiple-scattering method, the relativistic mass-velocity and Darwin terms can be incorporated as they are shown in Eqs. (4) and (5). These terms are necessary only for heavy atoms. In implementing such corrections, we will directly solve Eq. (2) less the spin-orbit coupling term. Before we describe the procedure in solving the equation, let us briefly review the non-relativistic case.

The non-relativistic radial wave equation is

$$\left[-\frac{1}{r^2}\frac{d}{dr}r^2\frac{d}{dr}+V(r)+\frac{\ell(\ell+1)}{r^2}\right]R_\ell(r;E)=E\,R_\ell(r;E). \tag{7}$$

Now by the use of

$$P_\ell(r;E)=r\,R_\ell(r;E), \tag{8}$$

Eq. (7) can be transformed into

$$\left[-\frac{d^2}{dr^2}+V(r)+\frac{\ell(\ell+1)}{r^2}-E\right]P_\ell(r;E)=0 \tag{9}$$

which can be rewritten as

$$\frac{dP_\ell(r;E)}{dr}=g_\ell(r;E)\,P_\ell(r;E), \tag{10}$$

where

$$g_\ell(r;E)=-\left[E-V(r)-\frac{\ell(\ell+1)}{r^2}\right]. \tag{11}$$

Equation (10) can be solved numerically by the Numerov method with a r-mesh, given the two initial values $P_\ell(r_1;E)$ and $P_\ell(r_2;E)$. The Numerov method and the scheme of starting numberical integration is described by Mattheiss, et al.[26]

Now adding the relativistic mass-velocity and Darwin terms, the radial wave equation becomes

$$\left\{-\frac{1}{r^2}\frac{d}{dr}r^2\frac{d}{dr}+V(r)+\frac{\ell(\ell+1)}{r^2}-\frac{\alpha^2}{4}[E-V(r)]^2-\frac{\alpha^2}{4}\frac{dV(r)}{dr}\frac{d}{dr}\right\}R_\ell(r;E)=E\,R_\ell(r;E), \tag{12}$$

which can be transformed into

$$\left\{ -\frac{d^2}{dr^2} + V(r) + \frac{\ell(\ell+1)}{r^2} - \frac{\alpha^2}{4}\,[E - V(r)]^2 - \frac{\alpha^2}{4}\,\frac{dV(r)}{dr} - \left[\frac{1}{r} + \frac{d}{dr}\right] - E \right\} P_\ell\,(r;E) = 0\ , \tag{13}$$

by the use of Eq. (8) as in the non-relativistic case.

Let us define that

$$g_\ell\,(r;E) = V(r) + \frac{\ell(\ell+1)}{r^2} - \frac{\alpha^2}{4}\left\{[E - V(r)]^2 - \frac{1}{r}\,\frac{dV(r)}{dr}\right\} - E\ , \tag{14}$$

then Eq. (13) becomes

$$\left[\frac{d^2}{dr^2} + f(r)\,\frac{d}{dr} - g_\ell\,(r;E)\right] P_\ell\,(r;E) = 0, \tag{15}$$

where

$$f(r) = \frac{\alpha^2}{4}\,V'(r). \tag{16}$$

Substituting

$$P_\ell\,(r;E) = y(r)\,Q_\ell\,(r;E), \tag{17}$$

in Eq. (15), we now have

$$\left[\frac{d^2}{dr^2} + \frac{2y'(r) + f(r)\,y(r)}{y(r)}\,\frac{d}{dr} - g_\ell(r;E) + \frac{y''(r) + f(r)\,y'(r)}{y(r)}\right] = 0. \tag{18}$$

In order to eliminate the second term in the above equation, we choose the arbitrary function y(r) such that

$$2y'(r) + f(r)\, y(r) = 0, \tag{19}$$

assuming that $y(r)$ does not have any zeros. The solution of Eq. (19) is

$$y(r) = \exp\left[-\frac{\alpha^2}{8} V(r) \right], \tag{20}$$

which indeed does not vanish for any r.

Equation (18) can now be written as

$$Q_\ell''(r;E) = G_\ell\ (r;E)\ Q_\ell\ (r;E), \tag{21}$$

where

$$\begin{aligned} G_\ell\ (r;E) &= g_\ell\ (r;E) - \frac{y''(r) + f(r)\, y'(r)}{y(r)} \\ &= (1 + \frac{\alpha^2}{2} E)V(r) - \frac{\alpha^2}{4} [V(r)]^2 + \frac{\ell(\ell+1)}{r^2} - \frac{\alpha^2}{4} E^2 \\ &\quad -E + \frac{\alpha^2}{8} V''(r) + \frac{\alpha^2}{4} \frac{1}{r} V'(r) + \frac{\alpha^4}{64} [V'(r)]^2. \end{aligned} \tag{22}$$

After evaluating $G_\ell\ (r;E)$ of Eq. (22) and solving Eq. (21) for $Q_\ell\ (r;E)$ by the Numerov method as in the non-relativistic case, the radial wave function $R_\ell\ (r;E)$ can be found by

$$R_\ell\ (r;E) = \frac{1}{r} \exp\left[-\frac{\alpha^2}{8} V(r) \right] Q_\ell\ (r;E). \tag{23}$$

It was found that an iterative scheme is very efficient in obtaining the two initial values, $Q_\ell\ (r_1;E)$ and $Q_\ell\ (r_2;E)$, which are necessary to start the numberical integration for $Q_\ell\ (r;E)$. The scheme is explained as follows. For the several starting mesh points for $r \sim 0$, $V(r) \sim -2Z/r$. Therefore, in the expression for $G_\ell\ (r;E)$ in Eq. (22), the terms involving E are insignificant at $r \sim 0$ even for

core electron levels. We now set $Q_\ell(r_2) \equiv Q_\ell(r_2;E) = 1$, since the radial wave function $R_\ell(r;E)$ can be normalized later. First, assuming $Q_\ell(r_1) = 1$, we use the Numerov method to compute $Q_\ell(r)$ for $r = r_3$, r_4, and r_5. For these mesh points, $R_\ell(r) \equiv R_\ell(r;E)$ can be obtained immediately by Eq. (23). Extrapolation from the fixed $R_\ell(r_2)$ and $R_\ell(r)$ for $r = r_3$, r_4, and r_5, we get $R_\ell(r_1)$ and subsequently $Q_\ell(r_1)$ which is now compared with the value with which we started the cycle. The cycle is iterated until the two consecutive values for $Q_\ell(r_1)$ are close enough to make the relative error smaller than a pre-set tolerance. The relative error can be smaller than 10^{-5} very quickly only after a few iterations. In this iterative scheme for the starting values, we used $R_\ell(r)$ instead of $Q_\ell(r)$ for the extrapolation step, because the former is a more smooth function than the latter.

As the starting values are independent of E, we need to calculate them only once for a given potential energy in searching for the electron eigen-energies.

REFERENCES

* Work supported by the Office of Naval Research.

† Based in part on this author's Ph.D. dissertation which was submitted in the Fall, 1975, to the Department of Electrical Engineering and Computer Science, Massachusetts Institute of Technology, Cambridge, Mass.

1. N.Kh. Abrikosov, et al., Semiconducting II-VI, IV-VI, and V-VI Compounds, Plenum Press, New York, 1969.
2. Y.I. Ravich, B.A. Efimova, and I.A. Smirnov, Semiconducting Lead Chalcogenides, ed. L.S. Stillbans, Plenum Press, New York, 1970.
3. R. Dalvin, in Solid State Physics, ed. H Ehrenreich, F. Seitz, and Turnbull, Academic Press, New York, 1973, Vol. 28, p. 179.
4. K.F. Cuff, M.R. Ellett, and C.D. Kuglin, J. Appl. Phys. Suppl. 32, 2179 (1961); in Proc. Int. Conf. on Phys. of Semicond. (Exeter, 1962),p.316.
5. R.S. Allgaier and W.W. Scalon, Phys. Rev. 111, 1029 (1958).
6. G. Bauer, H. Burkhard, H. Heinrich, and A. Lopez-Optero, J. Appl. Phys. 47, 1721 (1976).
7. W.W. Scanlon, J. Phys. Chem. Solids 8, 423 (1959).
8. N.J. Parada, Localized Defects in PbTe via a $\vec{k}\cdot\vec{\pi}$-APW Energy Band Calculation (Ph.D. Thesis, E.E. Department, Massachusetts Institute of Technology, Cambridge, Mass., 1968).
9. N.J. Parada and G.W. Pratt, Jr., Phys. Rev. Lett. 22, 180 (1969).
10. N.J. Parada, Phys. Rev. B 3, 2042 (1971).

11. G.F. Koster and J.C. Slater, Phys. Rev. 95, 1167 (1954); 96, 1208 (1954).

12. K.H. Johnson, Adv. Quantum. Chem. 7, 147 (1973).

13. L.A. Hemstreet, Jr., Phys. Rev. B 12, 1212 (1975).

14. D. Choo and G.W. Pratt, Jr., submitted to Phys. Rev. B.

15. R.E. Watson, Phys. Rev. 111, 1108 (1958).

16. J.C. Slater, J. Chem. Phys. 41, 3199 (1964).

17. The virial coefficient is defined here as $-K.E./E_{tot}$, where E_{tot} and K.E. mean the total energy and the total kinetic energy of the cluster. For virial theorems in the Xα method, refer to J.C. Slater J. Chem. Phys. 57, 2389 (1972).

18. K. Schwarz, Phys. Rev. B 5, 2466 (1972).

19. L.E. Johnson, J.B. Conklin, Jr., and G.W. Pratt, Jr., Phys. Rev. Lett. 11, 538 (1963).

20. J.B. Conklin, Jr., L.E. Johnson, and G.W. Pratt, Jr., Phys. Rev. 137, A1282 (1965).

21. P.J. Lin and L. Kleinman, Phys. Rev. 142, 478 (1966).

22. M.P. Gomez, D.A. Stevenson, and R.A. Huggins, J. Phys. Chem. Solids 32, 335 (1971).

23. A.J. Crocker, J. Phys. Chem. Solids 28, 1903 (1967).

24. G.W. Pratt, Jr., J. Nonmetals 1, 103 (1973).

25. C.Y. Yang and S. Rabii, Phys. Rev. A 12, 362 (1975).

26. L.F. Matheiss, J.H. Wood, and A.C. Switendick, in Energy Bands of Solids, Methods in Computational Physics, Vol. 8, ed. B. Adler, S. Ferback and M. Rotenberg, Academic Press, New York, 1968, p. 63.

TABLE I

Electron states of the OPb_4Te_4 cluster.

They are listed in the order of increasing eigen-energy. Only the important components of the normalized partial-wave coefficients and the electronic charge distributions are shown. (The "In" and "Out" represent the interatomic and the extramolecular region of the cluster respectively.) The constant potential in the interatomic region is -0.335 Ry.

States	Eigen-energy (Ry)	Partial-wave coefficients			Electronic Charge distribution			
$1a_1$	-1.095	Te s	Pb s		Te	Pb		
		0.89	-0.35		0.80	0.15		
$1t_2$	-1.050	Te s	Pb s		Te	Pb		
		0.95	0.14		0.91	0.04		
$2t_2$	-0.766	Pb s	Te p		Pb	Te		
		0.87	-0.30		0.77	0.15		
$2a_1$	-0.737	Pb s	Te s	Te p	Pb	Te		
		0.78	0.40	0.39	0.61	0.31		
1e	-0.519	Te p	Pb p		Te	Pb	In	
		0.77	0.48		0.60	0.23	0.16	
$3a_1$	-0.502	Te p	Pb p	Pb s	Te	Pb	In	
		-0.63	-0.50	0.38	0.40	0.40	0.09	
$1t_1$	-0.462	Te p	Pb p		Te	Pb	In	
		0.83	-0.42		0.69	0.17	0.12	
$3t_2$	-0.450	Te p	Pb p	Te p	Te	Pb	In	
		0.72	-0.40	0.38	0.65	0.20	0.14	
$4t_2$	-0.401	Te p	Pb p		Te	Pb	In	
		0.77	0.29		0.68	0.20	0.08	
$5t_2$*	-0.211	Pb p	Out p	Te p	Pb	In	Te	Out
		0.70	0.27	-0.20	0.51	0.32	0.08	0.08
$2t_1$*	-0.155	Pb p	Te p		Pb	In	Te	
		0.73	0.39		0.53	0.30	0.15	
$6t_2$*	-0.147	Pb p	Te p	Out d	Pb	Te	In	Out
		0.65	0.38	0.36	0.50	0.18	0.17	0.14
2e *	-0.106	Pb p	Te p		Pb	Te	In	
		0.66	-0.51		0.43	0.26	0.28	
$4a_1$*	-0.098	Pb p	Te p	Out f	Pb	Te	Out	In
		0.60	-0.51	0.38	0.39	0.34	0.15	0.09

* Excited empty electron states.

TABLE II

Description of the $6a_1$ and 6e states of the Te vacancy cluster.

Only the important components of the normalized partial-wave components and the electronic charge distributions are shown. (The "V_{Te}", "In", and "Out" represent the Te vacancy center, ineteratomic, and extra-molecular regions of the cluster respectively.)

States	Eigen-energy (Ry)	Partial-wave coefficients				Electronic charge distribution		
$6a_1$	-0.323	Pb p	V_{Te}s	Te p	V_{Te}p	Pb	In	V_{Te}
		0.70	-0.39	-0.22	0.13	0.50	0.23	0.17
6e	-0.245	Pb p	V_{Te}p	Te p	Out d	Pb	In	V_{Te}
		0.77	-0.23	0.16	-0.09	0.60	0.28	0.05

TABLE III

Description of the $1\text{-}4a_1$ and $5t_2$ states of the Pb interstitial cluster.

Only the important components of the normalized partial-wave coefficients and electronic charge distributions are shown. (The "IPb" and "In" represent the Pb interstitial center and the interatomic region of the cluster respectively.) The constant potential in the interatomic region of the cluster is -0.351 Ry.

States	Eigen-engergy (Ry)	Partial-wave coefficients			Electronic charge distribution		
$1a_1$	-1.361	Te s 0.66	IPb s -0.53	Pb s -0.40	Te 0.50	IPb 0.26	Pb 0.24
$2a_1$	-1.013	Te s 0.72	IPb S 0.45	Te p -0.39	Te 0.67	IPb 0.20	
$3a_1$	-0.777	Pb s 0.83	Pb p 0.31	IPb s -0.29	Pb 0.79	In 0.09	IPb 0.09
$4a_1$	-0.333	Te p 0.79	IPb s 0.40		Te 0.66	IPb 0.16	In 0.14
$5t_2$	-0.345	Pb p 0.74	Te p 0.28		Pb 0.56	In 0.23	Te 0.13

FIGURE CAPTIONS

Fig. 1 Cluster model of OPb_4Te_4 for the PbTe crystal.

Fig. 2 One-electron energy levels of the OPb_4Te_4 cluster (a), and the energy bands of the PbTe crystal (b) as calculated by Lin and Kleinman (ref. 21). —·—·— represents the constant potential in the interatomic region of the cluster. The crystal energy bands were shifted so that the centers of the band gaps match in the two energy level structures.

Fig. 3 One-electron energy levels for the Pb vacancy cluster (a) and the Te vacancy cluster (c), compared with the levels for the OPb_4Te_4 cluster (b). —·—·— represents the constant potential in the interatomic region of a cluster, and ∿∿∿ indicates the highest occupied level with its occupation number in the parenthesis.

Fig. 4 One-electron energy levels for the Pb interstitial cluster (a) and the Te interstitial cluster (b), compared with the levels for the OPb_4Te_4 cluster (c). —·—·— represents the constant potential in the interatomic region of a cluster, and ∿∿∿ indicates the highest occupied level with its occupation numbuer in the parenthesis.

Fig. 5 Contour map of the $4a_1$ wave function of the Pb interstitial cluster. It was plotted in a plane which bisects the two Te atoms at the right, the two Pb atoms at the left, and the interstitial Pb atom at the center. The broken-line circles

are the projections of the spheres of the atomic centers and the outersphere of the cluster. The contour curves were selected such that the logarithms of the magnitudes of the wave function values are equally spaced.

Fig. 6 One-electron energy levels for the Pb Frenkel defect cluster (a) and the Te Frenkel defect cluster (b), compared with the levels for the OPb_4Te_4 cluster (c). —·—·— respresents the constant potential in the interatomic region of a cluster, and ∿∿∿ indicates the highest occupied level with its occupation number in the parenthesis.

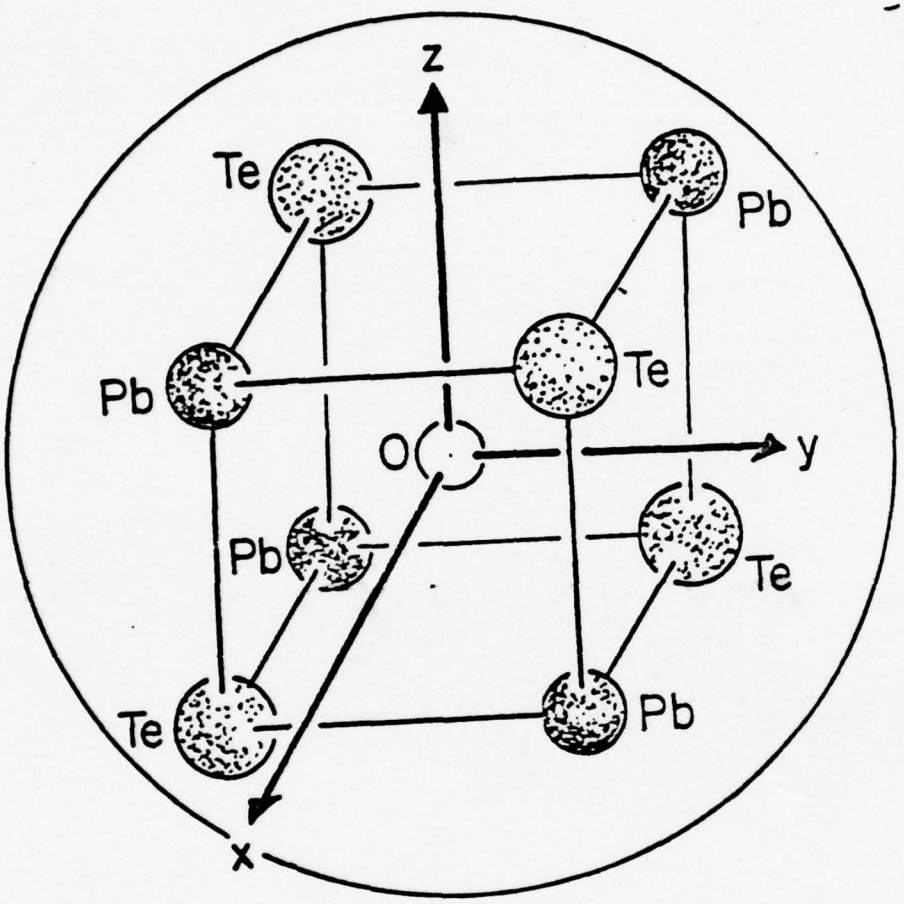

Pb Te

Fig. 1

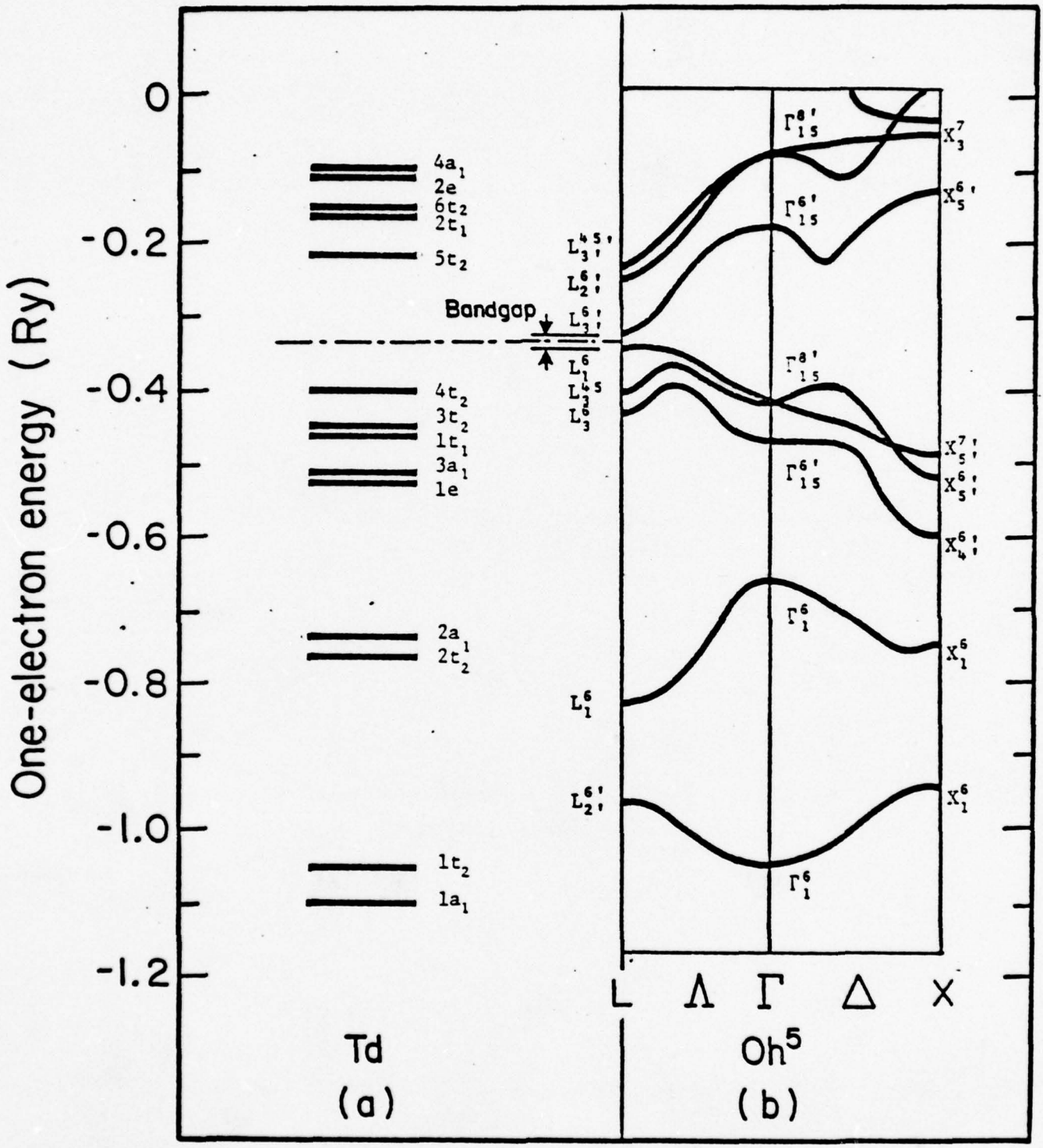
One-electron energy (Ry)
0
-0.2
-0.4
-0.6
-0.8
-1.0
-1.2
4a1
2e
6t2
2t1
5t2
Bandgap
4t2
3t2
1t1
3a1
1e
2a1
2t2
1t2
1a1
L3 4 5 '
L2 6 '
L3 6 '
L1 6
L3 4 5
L3 6
L1 6
L2 6 '
Γ15 8 '
Γ15 6 '
Γ15 8 '
Γ15 6 '
Γ1 6
Γ1 6
X3 7
X5 6 '
X5 7 '
X5 6 '
X4 6 '
X1 6
X1 6
L Λ Γ Δ X
Td
(a)
Oh5
(b)

PbTe

Fig. 2

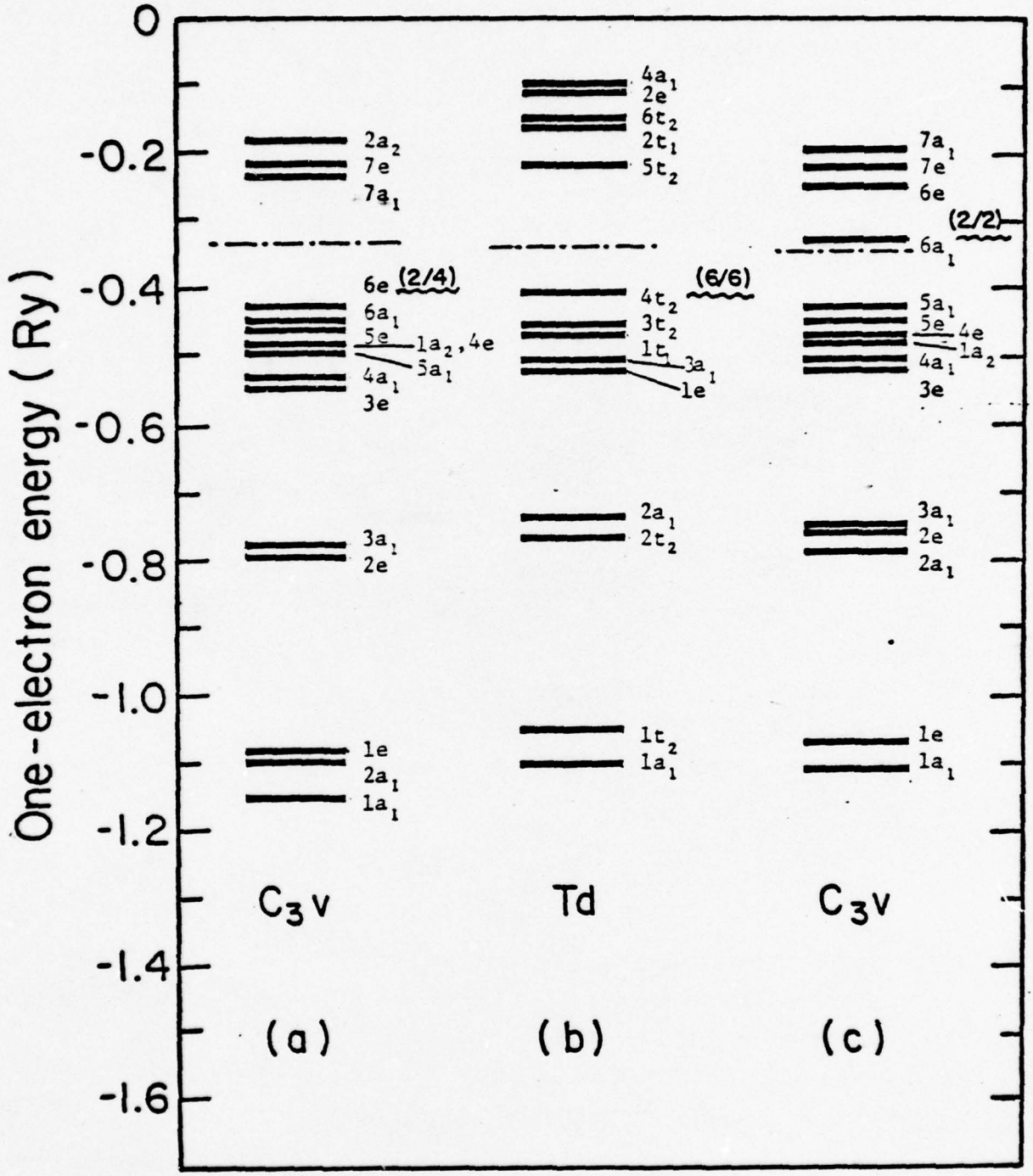
0
-0.2
-0.4
-0.6
-0.8
-1.0
-1.2
-1.4
-1.6
One-electron energy (Ry)
2a2
7e
7a1
6e (2/4)
6a1
5e
1a2, 4e
5a1
4a1
3e
3a1
2e
1e
2a1
1a1
C3v
(a)
4a1
2e
6t2
2t1
5t2
4t2 (6/6)
3t2
1t1
3a1
1e
2a1
2t2
1t2
1a1
Td
(b)
7a1
7e
6e
(2/2)
6a1
5a1
5e
4e
1a2
4a1
3e
3a1
2e
2a1
1e
1a1
C3v
(c)

37

Pb Te

Fig. 3

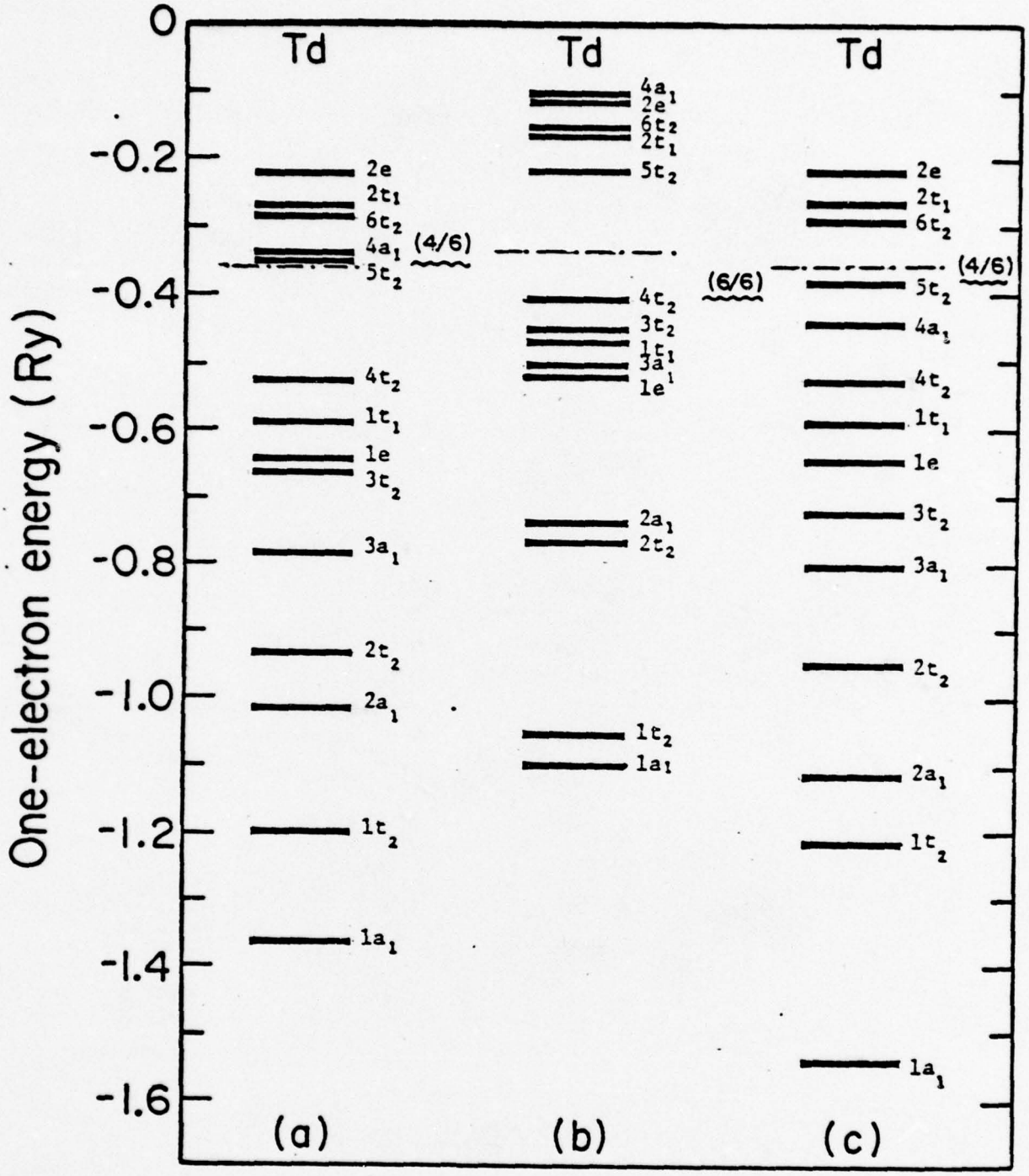
One-electron energy (Ry)
0
-0.2
-0.4
-0.6
-0.8
-1.0
-1.2
-1.4
-1.6
Td
Td
Td
2e
2t1
6t2
4a1
5t2
(4/6)
4t2
1t1
1e
3t2
3a1
2t2
2a1
1t2
1a1
4a1
2e
6t2
2t1
5t2
4t2
3t2
1t1
3a1
1e
2a1
2t2
1t2
1a1
(6/6)
2e
2t1
6t2
(4/6)
5t2
4a1
4t2
1t1
1e
3t2
3a1
2t2
2a1
1t2
1a1
(a)
(b)
(c)

PbTe

Fig. 4

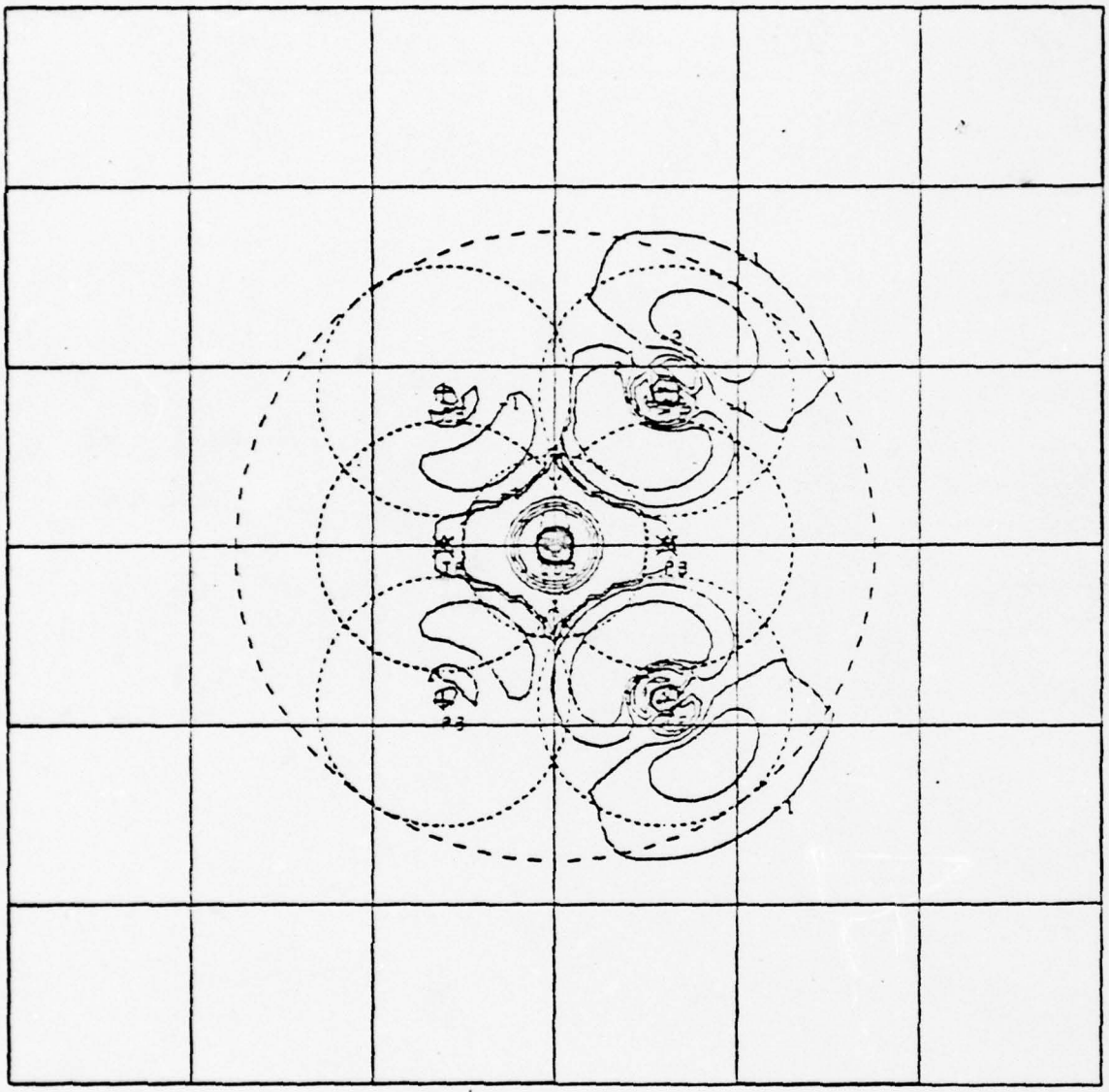

39

PbTe

Fig. 5

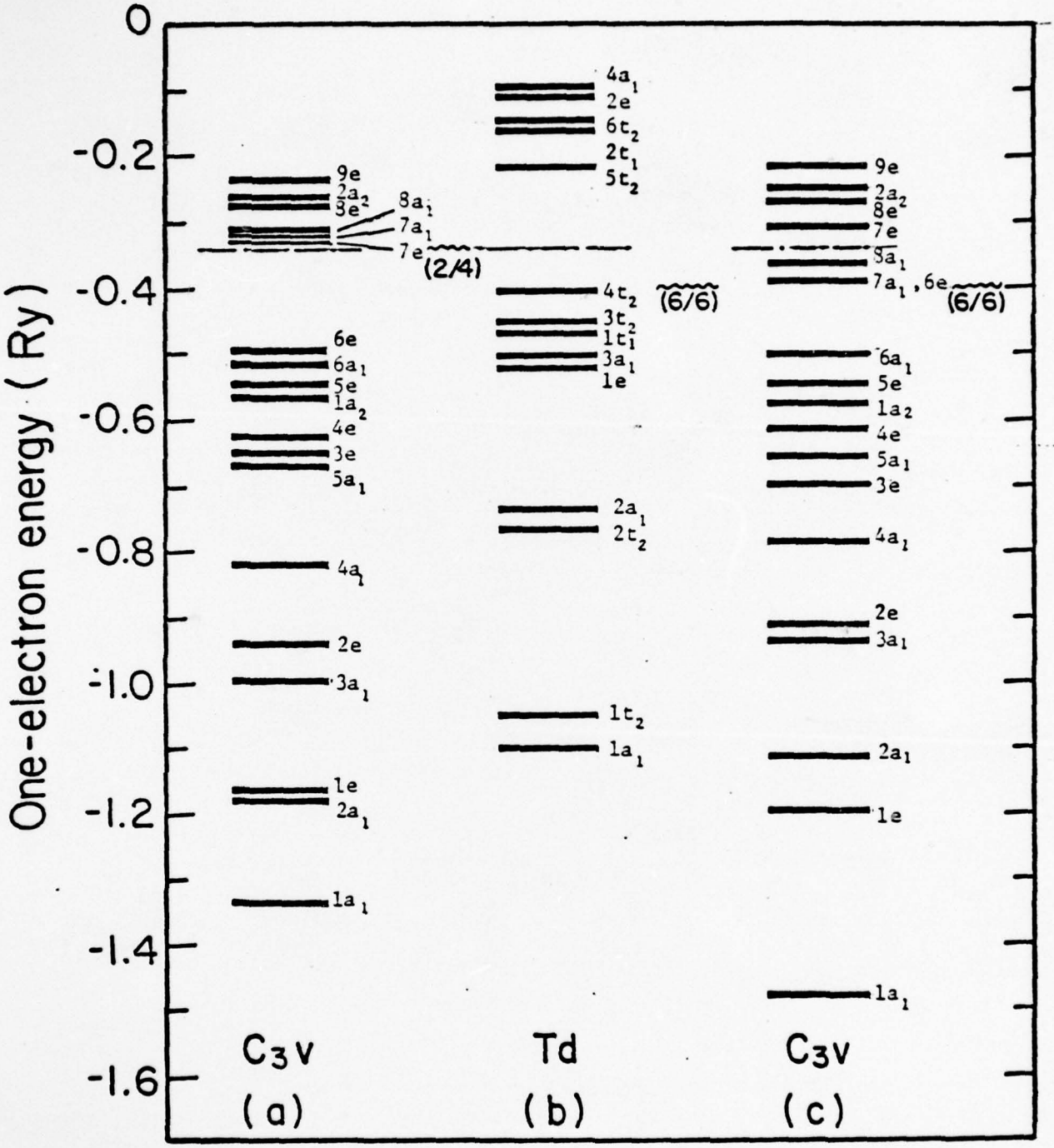
0
-0.2
-0.4
-0.6
-0.8
-1.0
-1.2
-1.4
-1.6
One-electron energy (Ry)
9e
2a2
8e
8a1
7a1
7e
(2/4)
6e
6a1
5e
1a2
4e
3e
5a1
4a1
2e
3a1
1e
2a1
1a1
4a1
2e
6t2
2t1
5t2
4t2
(6/6)
3t2
1t1
3a1
1e
2a1
2t2
1t2
1a1
9e
2a2
8e
7e
8a1
7a1, 6e
(6/6)
6a1
5e
1a2
4e
5a1
3e
4a1
2e
3a1
2a1
1e
1a1
C3v
(a)
Td
(b)
C3v
(c)

PbTe

Fig. 6

Appendix III.

CALCULATIONS FOR AN ISOELECTRONIC ELECTRON TRAP DUE TO NITROGEN IN GaP*

D. Choo† and G.W. Pratt, Jr.

Department of Electrical Engineering and Computer Science
and
Center for Materials Science and Engineering
Massachusetts Institute of Technology
Cambridge, Mass. 02139

ABSTRACT

A GaP crystal was simulated by the smallest-possible neutral cluster model, $GaPH_6$, which is comprised of a GaP molecule and six boundary hydrogen atoms replacing three gallium and three phosphorus nearest-neighbor atoms. The results of the calculation by the SCF $X\alpha$ multiple-scattering method of Johnson showed that the energy-level structure of the cluster fairly well duplicates the energy-band structure of the GaP crystal. In this cluster model some hydrogenic surface electron states were found and they were made unoccupied in the SCF iterations. Next, the phosphorus atom of the cluster was substituted by a nitrogen atom, resulting in a cluster of $GaNH_6$, to simulate the GaP crystal embedded with a nitrogen impurity. Careful analysis of the electronic structure of the $GaNH_6$ cluster in comparison with that of the $GaPH_6$ cluster reveals a bound electron state in the bandgap which represents the isoelectronic electron trap due to the nitrogen impurity in the GaP crystal. The present cluster model calculations showed that the bound electron state originates from the Γ_1 state of the conduction band, thus explaining the occurrence of the efficient luminescence A line due to isoelectronic nitrogen impurities in GaP.

I. INTRODUCTION

The Group III-V semiconductors have been studied extensively over the last decade due to their important technological implications in electronic devices.[1] In most of the applications, the materials are doped by impurities or by intrinsic defects in order to control the electrical and optical properties.

The shallow hydrogenic impurity electron states in semiconductors in general are now well understood, both experimentally and theoretically. However, for the localized bound electron states caused by some point defects in semiconductors there are still a lot more to be comprehended. In this area theoretical knowledge is particularly lacking; there have been only several first-principles calculations for the kind of point defects, such as the vacancies in silicon[2] and lead telluride[3] by the energy-band method through the Green's function formalism of Koster and Slater[4], and the nitrogen impurity and vacancy in diamond[5] by the LCAO-MO method. Recently the SCF $X\alpha$ multiple-scattering method of Johnson[6] was applied to the vacancies in lead chalcogenides by Hamstreet[7] and to the impurities in silicon by Cartling[8] to find the electronic structures of the point defect complexes by the use of cluster models. This method is very efficient, but careful consideration must be given to the configuration and the boundary condition of a cluster model in order to simulate a crystal successfully. The authors applied the method, in a previous paper,[9] to simulate a LiF crystal by a smallest-possible neutral cluster model and obtained the bulk properties of the crystal in very good agreement with experiments. The F-center problem of the LiF crystal was also

studied. Then in a subsequent paper,[10] the same formalism was used for a PbTe crystal to find the effects of various intrinsic point defects to the conductivity of the PbTe crystal.

In this paper, we extended our study to GaP crystal, which is one of the Group III-V semiconductors. The crystal was first simulated by the smallest-possible neutral cluster model, and then the isoelectronic electron trap caused by a nitrogen impurity was investigated with the same cluster format. The nitrogen isoelectronic electron trap, which was first discovered by Thomas, et al.,[11] is responsible for the efficient green-light luminescence in the GaP light-emitting diode. This problem, as far as we are aware of, has not been treated by any theoretical means. Since the materials we studied in the previous papers[9,10] are very much ionic, the highly covalent GaP here will provide a complementary example in the treatment of crystals and their point defects by the SCF $X\alpha$ multiple-scattering method.

The $GaPH_6$ cluster model for a GaP crystal is treated in Section II, and the effects of the nitrogen impurity in the cluster is explained in Section III. Finally, in Section IV a summary is given.

II. GaP CRYSTAL

The GaP crystal has the zinc-blende structure, whose symmetry belongs to the space group Td^2, with a nearest-neighbor distance of 2.36 Å.[12] It has an indirect bandgap of 0.172 Ry (2.34 eV) at 0°K which decreases to 0.166 Ry (2.26 eV) at 300°K.[13]

In a simple valence-bond picture of GaP, each atom is described as having four covalent bonds tetrahedrally directed to its four nearest neighbors. Once electron of each P atom is transferred to each Ga atom in this model so that every atom may have four equivalent hyrid orbitals made of atomic s and p functions.

A. Cluster Model for the GaP Crystal

If we choose the smallest-possible cluster model for the GaP crystal, retaining the full point group symmetry of the crystal while having a phosphorus atom at the center of the cluster so that it provides a convenient site for a nitrogen impurity, it will be a PGa_4 cluster where four gallium atoms are placed tetrahedrally around the phosphorus atom. This cluster is very much unbalanced regarding the composition of the GaP crystal; since the cluster contains only one phosphorus atom with four gallium atoms, the energy-bands of the cluster[14] will have less contribution from the phosphorus than the gallium atoms compared to the energy-bands of the crystal. Also, the electronic charge transfer between the phosphorus and gallium atoms in the cluster will not render the same meaning as that in the crystal.

A SCF $X\alpha$ multiple-scattering calculation for the PGa_4 cluster model shows that there is one electron left over after the valence bands are completely filled. This is explained as follows. The top valence band level of the cluster is a six-fold degenerate t_2 level whose wave function is composed primarily of P 3p atomic orbitals. Since there are only three P 3p electrons, the rest of the t_2 level must be filled by three Ga 4p electrons. However, there are four Ga 4p electrons in the cluster, one for

each Ga atom, and the one remaining electron goes over to a conduction band level whose wave function is made primarily of Ga 4p atomic orbitals. Therefore, we have to remove this conduction band electron so that we have completely filled valence bands and completely empty conduction bands, as in the case for the perfect GaP crystal. This means that we have to freeze the conduction band electron on a Watson sphere,[15] thus resulting in a $(PGa_4)^+$ cluster. The use of the Watson sphere will make the cluster model more artifical. Furthermore, the calculation of the $(PGa_4)^+$ cluster shows no a_1 state in the conduction band which would correspond to the Γ_1 state of the GaP crystal, the buttom conduction band state at the center of the Brillouin zone. Therefore, no detailed comparison of the band-edge structure can be made between the cluster and the crystal, and this makes further investigation of the isoelectronic electron trap meaningless.

In order to accommodate all the electrons equally without the need of freezing any electrons, the cluster model must be neutral, i.e. it must contain the constituent atoms of the crystal in the same proportion as the crystal. The smallest neutral cluster for the GaP crystal, but larger than a mere molecule, is a Ga_4P_4 cluster in which each atom of an inner GaP molecule has four nearest-neighbor atoms of the other kind. The cluster symmetry now belongs to the C_{3v} point group, a subgroup of the Td group of the crystal. It is impossible to formulate a cluster which is both neutral and fully symmetric. For the Ga_4P_4 cluster, however, there will be a lot of dangling bonds from the six outer atoms due to the covalent-bonding nature. In fact, a SCF Xα multiple-scattering calculation for the Ga_4P_4

cluster shows a set of practically continuous energy levels near the bandgap, thus obscuring the band-edge structure completely. The energy levels are much more numerous than what the reduction of the symmetry suggests. The fact that the cluster is less symmetric is not a serious problem by itself since we can relate the electron states of the cluster to those of the crystal by the use of compatibility relations of the representations between the two point groups. But, for any cluster model, this is possible only for the highest symmetric states.

Now, we replace all of the six outer atoms by hydrogen atoms so that they do not have any dangling bonds of their own, while properly containing the bonds originated from the inner phosphorus and gallium atoms. The six electrons of the hydrogen atoms are expected to behave similarly as the electrons of the replaced atoms which fill the bonds directed toward the inner phosphorus or gallium atoms. This $GaPH_6$ cluster model is shown in Fig. 1.

B. SCF Xα Multiple-Scattering Calculation for the $GaPH_6$ Cluster

The sphere radii of the phosphorus and gallium atoms in their tetrahedral configurations are not much different from each other (1.26 Å for Ga and 1.10 Å for P).[16] Therefore, equal radii were used for both the atomic centers of the $GaPH_6$ cluster. In fact, the spherically averaged potentials of the P and Ga atomic centers calculated self-consistently are equal at the midpoint between their nuclei. The radii of all the hydrogen atomic centers were set to be equal to the same radius of the P or Ga atomic center in order to make the hydrogen atoms closely related to the atoms

they replaced. By making the sizes of all the atomic centers equal, the interatomic region, where potential is least accurate being a constant, is kept at a minimum for a given overlapping scale factor. The overlapping scale factor is the ratio of the overlapping atomic sphere radii to the touching atomic sphere radii which, in this case, is half the nearest-neighbor distance. This factor was determined by satisfying the virial theorem (this scheme was fully explained in ref. 9). For the $GaPH_6$ cluster model the overlapping scale factor was set at 1.3 with which the virial theorem was satisfied to within 0.1%.

For the exchange α parameters the atomic values determined by Schwarz,[17] 0.72620 and 0.70690, were used for the P and Ga atomic centers respectively. For the hydrogen atomic centers, the α value of 0.77725[18] as calculated by the spin-polarized $X\alpha$ method was used instead of the Schwarz's 0.97804 which was obtained by the spin-restricted $X\alpha$ method. The exchange parameter α for the interatomic and extramolecular regions of the cluster was obtained by averaging the α's of all the valence electrons from the phosphorus and the gallium atoms; it is 0.71896 for any neutral cluster model for the GaP crystal. The electrons of the hydrogen atoms were not accounted for since they are supposed to simulate the electrons of the phosphorus or gallium atoms in the cluster model.

The basis functions were constructed from the s and p functions of the P, Ga, and H atoms. In the extramolecular region of the cluster, the basis functions were extended to have s, p, d, and f type functions.

C. Results and Discussions

The electron states of the $GaPH_6$ cluster as calculated by the SCF Xα multiple-scattering method are described in Table I. The one-electron energy levels of the cluster are shown in Fig. 2(b), compared with the one-electron energy levels of the constituent free atoms in Fig. 2(a). The hydrogen's electron levels makeup the Rydberg series, and the electron levels of the phosphorus and gallium atoms were determined by the SCF Xα method using the Schwarz's α parameters. Figure 2(c) shows the energy-band structure of the GaP crystal near its bandgap (after Dean[13]).

In the calculation for the $GaPH_6$ cluster it was found that, if we fill the lowest possible electron levels by the available 14 valence electrons, all the electron states of the top valence band which have significant contributions from the P 3p and Ga 4p atomic basis states are unoccupied. This resulted in a lack of proper bonding behavior around the P and Ga atomic centers and over-population of electrons in the Ga and H atomic centers. The reason is that in the lower valence band region there are some surface electron states which have their electronic charges distributed primarily in the boundary hydrogen atomic centers. They do not correspond to any electron states of the GaP crystal. Therefore, the hydrogenic surface electron states were carefully discerned from the rest of the valence electron states so that they could be made unoccupied by any electrons in the subsequent iterations. The 1e and 2e states, whose energy levels are indicated by dashed lines in Fig. 2(b), are such hydrogenic surface electron states. After they were made unoccupied, they retained their characteristics self-consistently in the rest of the iterations.

Figures 3a through 3k show the contour maps of the wave functions of the electron states. With the contour maps and Table I, we now illustrate the electron states below in some detail in the order of increasing eigenenergy (refer Fig 2(b)).

The $1a_1$ state is mainly made of a P 3s basis state which exhibits σ bonds with the Ga 4s and H-P (H atomic centers surrounding the P atomic center) 1s basis states. The $2a_1$ state represents a σ bond between the H-Ga 1s and Ga 4s basis states. There is also a σ bond between the P 3s and H-P 1s basis states, but its contribution to the $2a_1$ state is relatively small.

The hydrogenic surface electron state, 1e, is almost entirely a H-Ga 1s basis state containing a weak σ bond with the Ga 4p basis state. There is also a very weak σ bond between the Ga 4p and P 3p basis states. The other hydrogenic surface electron state, 2e, is mostly a H-P 1s basis state showing weak σ bonds between the H-P 1s and P 3p basis states and between the P 3p and Ga 4p basis states.

For the $3a_1$ state, approximately two thirds of the electronic charge is attributed to the H-P 1s basis state which has antibonding behavior with the nearby basis states. It carries a moderate amount of a σ bond between the Ga 4s and P 3s basis states. The $3a_1$ state looks like another hydrogenic surface electron state. However, it has less contribution from the hydrogenic basis states than the previously determined hydrogenic surface electron states, 1e and 2e. Furthermore, it was necessary to fill the $3a_1$ level in order to reproduce the features of the band-edge structure

of the GaP crystal with any physically reasonable charge distribution among the atomic centers. Therefore, the $3a_1$ state was considered to be one of the regular valence electron states of the cluster.

Next, the $4a_1$ state has large components of the Ga 4s and H-Ga 1s basis states which exhibit an antibond between them. On the other hand, the 3e state represents a strong σ bond between the P 3p and Ga 4p basis states, and the $5a_1$ state represents a strong π-bond between the same basis states. This set of the three highest valence electron levels, $4a_1$, 3e, and $5a_1$, of the $GaPH_6$ cluster corresponds to the top valence band of the GaP crystal. They all have a considerable amount of their electronic charges in the interatomic region of the cluster. Particularly, the top valence electron state, $5a_1$, has more than one third of its electronic charge in the interatomic region.

At the top of the valence band of the GaP crystal there is a Γ_{15} (or t_2) state, expressed in terms of a T_d single group representation, which decomposes into an a_1 and an e states in the C_{3v} subgroup symmetry. Therefore, the $5a_1$ state of the cluster has the correct symmetry as the top of the valence band. It also shows the correct characteristics of a valence band electron state, having the largest contribution from the P 3p basis state with a little of the Ga 4p and forming a strong bond between them.

Now across the bandgap there are several excited states. The first excited state, 4e, has a relatively large component of the extramolecular p basis state. It puts about two thirds of its electronic charge in the interatomic region, and has more or less a uniform electronic charge dis-

tribution over the entire space of the cluster. The 4e state shows a weak σ bond between the Ga 4p and H-Ga 2p basis states.

The $6a_1$ state shows similar electronic change distribution as the 4e state while exhibiting a σ bond between the Ga 4p and P 3p basis states. The $6a_1$ state has the same symmetry as the Γ_1 state, the electron state of the crystal at the bottom of the conduction band at the center of the Brillouin zone. Like the 4e state, it has the largest contribution from the Ga 4p basis state. This characteristic is the same as shown by the conduction band electron states of the GaP crystal. Although the $6a_1$ state has a higher eigen-energy than the 4e state, it is more localized in the inner P and Ga atomic centers. The $6a_1$ state of the $GaPH_6$ cluster represents the Γ_1 state of the GaP crystal, and the 4e state of the cluster corresponds to a state near the x_1 state, the electron state of the crystal at the absolute bottom of the conduction band.

Finally, the $7a_1$ state, having more than two thirds of its electronic charge in the extramolecular region, shows a very strong extramolecular s character. This state has also some contributions from the H-P 2s, and H-Ga 2s basis states, and shows a very weak bonding for all the atoms. The $7a_1$ state is a true surface electron state of the cluster.

The excited states have their wave functions more concentrated in the interatomic and extramolecular regions than the valence band states, corresponding to the similar characteristics in the crystal. For any cluster model, in general, the higher the energy level of a state is, the

more electronic charge it has in the interatomic and extramolecular regions.

Now we align the top valence electron level, $5a_1$, of the cluster to the top of the valence band of the crystal and linearly expand all the other levels with respect to this by the factor of 1.4 so that the lowest excited level, 4e, of the cluster is also aligned to the bottom of the conduction band. The contraction of the electron energy-level structure of the cluster in comparison to that of the crystal is due to the fact that there are only limited number of atoms in the cluster.[9] The linearly expanded energy-level structure of the cluster is shown in Fig. 2(d). We immediately see in the Figs. 2(c) and 2(d) that the width of the top valence band of the crystal is now matched very closely by the corresponding band-width of the cluster as a consequence. At the same time the $6a_1$ level of the cluster also fairly well matches the Γ_1 level of the crystal. These correspondences of the levels between the cluster and the crystal are the ones that we asserted earlier when we described each electron state of the cluster.

Because the hydrogen atoms in the $GaPH_6$ cluster represent either phophorus or gallium atoms of the GaP crystal, one could use the exchange parameter α of the phosphorus or gallium atoms for the hydrogen atomic centers. This change of the α parameters shifts upward, in the average by 0.025 Ry, the energy levels of only the deep valence band states, $2a_1$ through $4a_1$, which have significant components of the hydrogenic basis states. Since the electron states near the bandgap do not draw any significant contributions from such hydrogenic basis states, they are hardly affected by the change of the α values in the hydrogen atomic centers. Consequently the interpretation

of the physical phenomena associate with the band-edge structure will be the same.

The total energy of the $GaPH_6$ cluster is about 1.74 Ry higher than the sum of the total energies of the constituent free atoms. This indicates that the cluster as a molecule is unstable. In fact, 5% uniform expansion of the $GaPH_6$ cluster decreases the total energy by about 0.2 Ry (in magnitude) and it tends to be monotonically decreased as it is further expanded. The unstableness of the $GaPH_6$ cluster is not due to the empty hydrogenic surface electron states; the total energy of the cluster with filled hydrogenic surface electron states is not much different from that with empty hydrogenic surface electron states.

The ionicities of the atomic centers shown in Table II were obtained by redistributing, for each valence electron state, the electronic charge in the interatomic and extramolecular regions to the atomic centers in proportion to the valence electronic charges which are already in the atomic centers as a result of SCF calculation. Note that all the hydrogen atomic centers have practically the same ionicity. If we make the hydrogens neutral by drawing extra electronic charges from the neighboring P or Ga atomic center, the ionicity of GaP becomes 0.519 in units of electronic charge, making the gallium a cation and the phosphorus an anion. Since all three valence electrons of the gallium atom will be transferred to the phosphorus atom in a completely ionic model of GaP, the ionic character of the GaP crystal may be said to be about 17% in the present cluster model calculation.

III. NITROGEN ISOELECTRONIC ELECTRON TRAP IN THE GaP CRYSTAL

An isoelectronic trap is an isoelectronic substitutional atom which induces a bound state for either an electron or a hole in the bandgap of a host crystal. Such an electron trap was first discovered by Thomas et al.[11] for nitrogen substituents at phosphorus sites in the GaP crystal. Nitrogen impurities in the GaP crystal are one of the simplest kinds of isoelectronic traps. Yet, they are very important technologically for the efficient luminescence as evidenced by the green light-emitting diode made of such nitrogen-doped GaP crystal.

The effect of the nitorgen electron trap in the GaP crystal can be explained qualitatively as follows. A nitrogen atom attracts an electron more strongly than the phosphorus atom because its nucleus is less screened. This is reflected in the high electronegativity of the nitrogen atom which is 3.0 compared to 2.1 for the phosphorus atom in Pauling's scale. Thus, the nitrogen impurity produces a bound electron state which is highly localized. Once an electron is trapped in the state, this in turn gives rise to a Coulomb attractive field for a weakly bound hole whose wave function is hydrogenic. This electron-hole pair constitutes a bound excition. Since the bound electron state is highly localized in real space, its $\vec{k}$-vector components are widely spread in the Brillouin zone. On the other hand, the hydrogenic hole state is very much localized near the center of the Brillouin zone where the top of the valence band of the crystal is located. Therefore, once the bound exciton is formed due to the nitrogen impurity, the electron and hole can directly recombined, emitting a strong photon radiation

in the green part of the spectrum. This was shown in an optical absorption and fluorescence experiment as A line which is about 0.0015 Ry (0.02 eV) below the bandgap energy.[19]

GaN is a direct-gap semiconductor which crystallizes in the wurtzite structure. As in the zinc-blende structure of GaP, each atom in GaN is surrounded by four tetrahedrally located nearest neighbors with the distance of 1.94 Å,[12] about 18% smaller than that of GaP. It is interesting to note here that the bandgap of GaN is considerably larger (0.255 Ry at 0°K) than that of GaP (0.166 Ry at 0°K), and yet a substituted nitrogen atom causes a bound electron state in the bandgap of GaP.

A heavier isoelectronic atom of smaller electronegativity than that of the phosphorus atom could produce a localized bound state for a hole which then attracts an hydrogenic electron by Coulomb interaction. In fact, this kind of exciton was found in bismuth-doped GaP.[20,21] In this case, however, the isoelectronic impurity does not lead to any efficient radiative recombination since the localized state of the bound hole does not have any significant $\vec{k}$-vector components near the X point of the Brillouin zone where the hydrogenic electron state has primary $\vec{k}$-vector components. Between phosphorus and bismuth in the same isoelectronic column of the periodic table, there are arsenic and antimony neither of which has been found to produce any bound states for electrons or holes when substituted at phosphorus site in the GaP crystal.[21] However, their electronegativities are almost equal to that of the bismuth atom. Therefore, the size of the substitutional atom must be another important factor for producing a bound state

in the crystal.

If nitrogen atoms are heavily doped in GaP, one nitrogen tends to interact with another. Depending on the spacing between the nitrogens, the pairs form sharp optical peaks, called NN_1, NN_2, etc., while the A line caused by isolated nitrogens is subsequently weakened. The deepest line, NN_1, of the series was seen at 0.0112 Ry (0.152 eV) below the bandgap energy.[19]

A. Calculational Considerations

In order to study the nitrogen electron trap in GaP we replace the phosphorus atom of the GaP_6 cluster by a nitrogen atom. This makes the cluster model for a nitrogen-doped GaP crystal a $GaNH_6$ cluster. In tetrehedtral covalent bonds the radius of the nitrogen atom (0.70 Å) is considerably smaller than the radius of the phosphorus atom (1.10 Å).[16] However, we maintain the same radii for all the atomic centers in the $GaNH_6$ cluster so as to be consistent with the $GaPH_6$ cluster model for the GaP crystal. The potential of the N atomic center is deeper than the potential of the Ga atomic center at the midpoint between them. Therefore, if we had used the scheme of determining the sizes of the atomic centers by first matching the potentials at the point of contact, the size of the N atomic center would have been even larger than the size of the Ga atomic center.

The exchange parameter α used for the N atomic center is 0.75197 as calculated by Schwarz.[17] But the average α for the interatomic and extramolecular regions of the $GaPH_6$ cluster is kept for the corresponding regions

of the $GaNH_6$ cluster since the $GaNH_6$ cluster is still supposed to simulate the GaP crystal even though it now contains an impurity.

It is a little more ambiguous to distinguish the hydrogenic surface electron states from the regular velance electron states for the $GaNH_6$ cluster than for the $GaPH_6$ cluster. However, two e states of the $GaNH_6$ cluster are largely the same in their wave function characteristics as the two e hydrogenic surface electron states of the $GaPH_6$ cluster, though their eigen-energies are quite different. Since the wave functions of the hydrogenic surface electron states would not be modified significantly by the presence of an impurity near the center of the cluster, we identify the two e states as the hydrogenic surface electron states of the $GaNH_6$ cluster. Such close relationships maintained between the $GaNH_6$ cluster and the $GaPH_6$ cluster in the electronic structure as well as in the geometric configuration and the choice of exchange parameters α's will differentiate the $GaNH_6$ cluster from a possible cluster model for a GaN crystal.

B. Results and Discussions

The one-electron energy levels of the $GaNH_6$ cluster are shown in Fig. 4(b), compared with those of the constituent free atoms of the cluster in Fig. 4(a). The one-electron energy levels of the $GaPH_6$ cluster are shown again in Fig. 4(c) for convenience. The electron states of the $GaNH_6$ cluster are described in Table III, and the contour maps of their wave functions are shown in Figs. 5a through 5k. In the following we will study the electron states, in the order of increasing eigen-energy, while establishing correspondence relationships between them and the electron states of the $GaPH_6$ cluster.

The $1a_1$ state is almost entirely an N 2s basis state which exhibits weak σ bonds with the Ga 4s, H-N 1s, and H-Ga 1s basis states. This state corresponds to the $1a_1$ state of the $GaPH_6$ cluster.

The $2a_1$ state has most of its electronic charge in the H-Ga and Ga atomic centers, thereby making a strong σ bond between the H-Ga 1s and Ga 4s basis states. There is also a weak σ bond between the N 2s and H-N 1s basis states. This $2a_1$ state corresponds to the $2a_1$ state of the $GaPH_6$ cluster.

The 1e state is almost entirely a H-Ga 1s basis state containing weak σ bonds between the H-Ga 1s and Ga 4p basis states and between the Ga 4p and N 2p basis states. Corresponding to the 1e state of the $GaPH_6$ cluster, it is a hydrogenic surface electron state of the $GaNH_6$ cluster. Therefore, this state was made unoccupied.

The $3a_1$ state is, in a large part, an antibonding combination of the Ga 4s and H-Ga 1s basis states. It corresponds to the $4a_1$ state of the $GaPH_6$ cluster.

The 2e state has a strong σ bond between the N 2p and Ga 4p basis states, and a moderate amount of σ bond between the N 2p and H-N 1s basis states. It also exhibits a weak π-bond between the Ga 4p and H-Ga 2p basis states. This 2e state corresponds to the 3e state of the $GaPH_6$ cluster. However, it has more contribution from the H-N 1s basis state than the 3e state of the $GaPH_6$ cluster does from the corresponding H-P 1s basis state. Consequently the contribution from the Ga 4p basis state is reduced in the case of the $GaNH_6$ cluster.

The $4a_1$ state is mostly a H-N 1s basis state. Therefore, it could

have been regarded as a hydrogenic surface electron state. It is instead treated as a regular valence electron state because it corresponds to the $3a_1$ state of the $GaPH_6$ cluster. However, the contribution of the N atomic center for the $4a_1$ state comes from a hybrid of s and p functions unlike the mainly phosphorus p function for the $3a_1$ state of the $GaPH_6$ cluster.

Next, the 3e state is mostly a H-N 1s basis state which shows a bonding behavior with the N 2p basis state. This state corresponds to the 2e hydrogenic surface electron state of the $GaPH_6$ cluster; it is the other of the two hydrogenic surface electron states of the $GaNH_6$ cluster. Unlike the 2e state of the $GaPH_6$ cluster, however, the 3e state of the $GaNH_6$ cluster shows a rather strong bond between the N 2p and Ga 4p basis states, and the portion of the N 2p basis function which is responsible for the bond with the H-N 1s basis function is the inner lobe, i.e. the lobe of the p function directed toward the Ga atomic center.

The top valence state $5a_1$ corresponds to the top valence state, which is also $5a_1$, of the $GaPH_6$ cluster. As such, it has a moderate-to-strong π bond between the N 2p and Ga 4p basis states. The contribution of the N 2p basis state to the $5a_1$ state of the $GaNH_6$ cluster is larger than the contribution of the corresponding P 3p basis state to the $5a_1$ state of the $GaPH_6$ cluster.

Now across the bandgap, the $6a_1$ state represents a strong σ bond between the Ga 4p and N 2p basis states, corresponding to the $6a_1$ state of the $GaPH_6$ cluster. The former is, however, more localized than the latter inside the outersphere. It can be argued that most of the electronic charge

in the extramolecular region and some in the P atomic center of the $GaPH_6$ cluster are transferred to the Ga atomic center when the phosphorus atom is replaced by a nitrogen. This $6a_1$ state is very important in explaining the isoelectronic electron trap due to nitrogen in GaP as illustrated later.

The 4e excited state of the $GaNH_6$ cluster corresponds to the lowest excited state 4e of the $GaPH_6$ cluster. It is a little more localized in the $GaNH_6$ cluster than in the $GaPH_6$ cluster similarly to the $6a_1$ state. This 4e state of the $GaNH_6$ cluster does not show any significant bonding behavior except for a weak π bond between the Ga 4p and H-Ga 2p basis states.

Lastly, the $7a_1$ excited state is mostly an extramolecular p state with some s character. This $7a_1$ state of the $GaNH_6$ cluster will correspond to a state of the $GaPH_6$ cluster whose energy level is slightly higher than the extramolecular s type $7a_1$ level of the $GaPH_6$ cluster. The $7a_1$ states are true surface states for both clusters.

The correspondence relationships of the electron states between the $GaNH_6$ cluster and the $GaPH_6$ cluster are indicated by the interconnections between Figs. 4(b) and 4(c). In the figures the electron levels of the empty hydrogenic surface states are shown as dashed lines for both clusters. When a nitrogen atom replaces the phosphorus atom in the $GaPH_6$ cluster, the energy levels are in general shifted down because the potential of the nigtrogen is deeper than the potential of the phosphorus in the outer region of the atomic center. However, two energy levels, $4a_1$ and 3e, of the $GaNH_6$ cluster are higher than the corresponding levels, $3a_1$ and 2e respectively, of the $GaPH_6$ cluster. These two electron states of the $GaNH_6$ clusters are

the ones which have large partial-wave components of the H-N 1s basis states. The increase of the eigen-energies results from a larger Coulomb repulsive interaction in the H-N atomic centers of the $GaNH_6$ cluster than in the corresponding H-P atomic centers of the $GaPH_6$ cluster. In fact, the calculated ionicities of the atomic centers, shown in Table II, indicate a large increase of the electronic charge in the atomic center when the nitrogen atom replaces the phophorus atom of the $GaPH_6$ cluster.

The most interesting effect of the nitrogen substitutional impurity is to shift down the $6a_1$ level below the 4e level, hence into the bandgap region. In terms of the energy-bands of the crystal it can be explained by the following. A bound electron level (the $6a_1$ level of the $GaNH_6$ cluster) is formed a little below the bottom of the conduction band (the 4e level of the $GaPH_6$ cluster). The bound electron state originates from the Γ_1 state (the $6a_1$ state of the $GaPH_6$ cluster), i.e. the bottom conduction band state at the center of the Brillouin zone. Unlike the usual hydrogenic electron states due to donor impurities, the bound electron state due to the nitrogen impurity is not occupied in the ground state, therefore, it will serve as an electron trap.

As discussed earlier, the bound electron state ($6a_1$ of $GaNH_6$) is more localized than the original state ($6a_1$ of $GaPH_6$); it has about half of its electronic charge in the N atomic center. We also see from Table II that the Ga atomic center loses 0.763 electron mainly to H-N atomic centers due to the presence of the nitrogen impurity. This indicates that the Ga atomic center will be the primary site for an extra electron which can be

trapped by the nitrogen impurity. In fact, the $6a_1$ state of the $GaNH_6$ cluster has the largest normalized partial-wave coefficient, 0.67, of a Ga 4p basis state among all the electron states of both clusters.

Once an electron is trapped, a hole will be attracted by the negatively charged nitrogen impurity complex, thereby making a bound exciton which is responsible for the A line in optical absorption and fluorescence in a nitrogen-doped GaP crystal.

IV. SUMMARY

We first simulated a GaP crystal by a $GaPH_6$ cluster model. The SCF Xα multiple-scattering calculation showed that the electron energy-level structure of the cluster reproduces the essential features of the energy-band structure of the crystal. The electron energy-level structure of the $GaPH_6$ cluster was expanded linearly to fit the band-edges of the GaP crystal in order to compensate the lack of atomic interaction due to the limited number of atoms in the cluster. It is remarkable that we could, at least qualitatively, describe the crystal by using such a small cluster model (in fact, it is the smallest-possible neutral cluster model). The possible dangling bonds of the cluster were eliminated by using the hydrogen atoms instead of three phosphorus and three gallium boundary atoms. There exist some hydrogenic surface electron states in this cluster, and it is very important to make them unoccupied since they do not represent any electron states of the crystal. When one wants to work with a larger cluster model to improve quantitative results, the use of boundary hydrogen atoms while discerning the hydrogenic surface electron states carefully will still be essential in order to get correct band-structure of the crystal. In fact, this scheme should be used for cluster models for any covalent crystal.

The isoelectronic electron trap due to a nitrogen impurity in the GaP crystal was studied by replacing the phosphorus atom of the $GaPH_6$ cluster by a nitrogen atom, thus producing a $GaNH_6$ cluster, and comparing the results of the SCF Xα multiple-scattering calculations for the two clusters. In the $GaNH_6$ cluster a bound electron state is formed in the bandgap, about 0.05 Ry

below the bottom of the conduction band. It is obviously impossible in the cluster model calculation to obtain the trap level with such an accuracy as can be found in an experiment which suggests the level is about 0.0015 Ry below the bottom of the conduction band. Because the bound electron state is unoccupied, it acts as an electron trap. Once an electron is trapped, the nitrogen impurity complex will attract a hole by Coulomb interaction. This electron-hole pair is the bound exciton which causes the efficient luminescence of green light in a nitrogen-doped GaP crystal, as indicated by the A line in optical absorption and fluorescence experiments.

It was also shown that the bound electron state originates from the state which corresponds to the Γ_1 state of the crystal. In the crystal the bound electron state has larger $\vec{k}$-vector components near X point than near the Γ point in the Brillouin zone. However, the Γ point contribution of the bound electron state is the one responsible for the radiative recombination of the bound exciton. In this sense, the cluster model successfully explained the luminescence phenomena of the nitrogen impurity in the GaP crystal.

The $GaNH_6$ cluster model is different from a possible cluster model for a GaN crystal in its geometric configuration, particularly in the lattice constant, and in the choice of the exchange parameter α's. Also, the $GaNH_6$ cluster was closely related to the $GaPH_6$ cluster in determining the hydrogenic surface electron states. However, it seems that the direct bandgap nature of the GaN crystal is responsible for the formation of the bound electron state due to the nitrogen impurity in the GaP crystal.

REFERENCES

* Work supported by the Office of Naval Research.

† Based in part on this author's Ph.D. dissertation submitted in the Fall, 1975, to the Department of Electrical Engineering and Computer Science, Massachusetts Institute of Technology, Cambridge, Mass.

1. For review see, for example, Semiconductors and Semimetals, ed. R.K. Willardson and A.C. Bear, Academic Press, New York, Vol. 1 (1966) - Present.
2. J. Callaway and A.J. Hughes, Phys. Rev. 156, 860 ; 164, 1043 (1967).
3. N.J. Parada and G.W. Pratt, Jr., Phys. Rev. Lett. 22, 180 (1969). See also N.J. Parada, Phys. Rev. B 3, 2042 (1971).
4. G.F. Koster and J. C. Slater, Phys. Rev. 95, 1167; 96, 1208 (1954).
5. R.P. Messmer and G.D. Watkins, Phys. Rev. B 7, 2568 (1973).
6. K.H. Johnson, Adv. Quantum Chem. 7, 147 (1973).
7. L.A. Hamstreet, Phys. Rev. B 11, 2260; 12, 1212 (1975).
8. B.G. Cartling, J. Phys. C: Solid State Phys., to be published.
9. D. Choo and G.W. Pratt, Jr., "SCF Xα Cluster Model Calculations for LiF Molecule, LiF Crystal, and Its F-Center", submitted to Phys. Rev. B.
10. D. Choo adn G.W. Pratt, Jr., "Investigation of the Effects of Intrinsic Point Defects on the Conductivity of PbTe via the SCF Xα Cluster Method", submitted to Phys. Rev. B.
11. D.G. Thomas, J.J. Hopfield, and C.J. Frosch, Phys. Rev. Lett. 15, 857 (1965).
12. R.W.G. Wyckoff, Crystal Structures, Second ed., Vol. 1, Interscience Publ., New York, 1963.

13. P.J. Dean, J. Luminesc., 1,2, 398 (1970).

14. In the cluster model there are only finite number of electron levels. However, several levels are closely related in their characteristics of wave functions to the energy levels of a valence band or a conduction band of the crystal which the cluster model is for. Therefore, such a set of levels is referred here as an energy-band of the cluster.

15. R.E. Watson, Phys. Rev. 111, 1108 (1958).

16. L. Pauling, The Nature of the Chemical Bond, Third ed., Cornell University Press, Ithaca, New York, 1960, p. 246.

17. K. Schwarz, Phys. Rev. B 5, 2466 (1972).

18. Private communication with K.H. Johnson.

19. D.G. Thomas and J.J. Hopfield, Phys. Rev. 150, 680 (1966).

20. J.J. Hopfield, D.G. Thomas, and R.T. Lynch, Phys. Rev. Lett. 17, 312 (1966).

21. F.A. Trumbore, M. Gershenzon, and D.G. Thomas, Appl. Phys. Lett. 9, 4 (1966).

TABLE I

Electron states of the $GaPH_6$ cluster as calculated by the SCF Xα multiple-scattering method.

They are listed in the order of increasing eigen-energy. The occupation numbers of the levels are shown in the parentheses. Only the important components of the normalized partial-wave coefficients and electronic charge distributions are shown. (The "In" and "Out" represent the interatomic and extra-molecular regions of the cluster respectively.) The constant potential in the interatomic region is -0.219 Ry.

Electron state	Eigen-energy (Ry)	Partial-wave coefficients	Electronic charge distribution
$1a_1(2)$	-0.879	P 3s H-P 1s Ga 4s 0.81 0.39 -0.36	P H-P Ga 0.65 0.17 0.13
$2a_1(2)$	-0.703	H-Ga 1s Ga 4s 0.79 -0.42	H-Ga Ga 0.63 0.18
1e (0)	-0.622	H-Ga 1s 0.96	H-Ga 0.92
2e (0)	-0.572	H-P 1s 0.95	H-P 0.90
$3a_1(2)$	-0.511	H-P 1s P 3s 0.81 -0.33	H-P P 0.67 0.12
$4a_1(2)$	-0.351	Ga 4s H-Ga 1s P 3s 0.65 0.45 0.30	Ga H-Ga P In 0.43 0.24 0.15 0.12
3e (4)	-0.303	P 3p Ga 4p 0.75 -0.24	P Ga In 0.57 0.24 0.15
$5a_1(2)$	-0.226	P 3p Ga 4p 0.68 0.32	P In Ga 0.46 0.37 0.09
4e (0)	-0.103	Out p Ga 4p 0.38 0.32	In Out Ga 0.67 0.15 0.10
$6a_1(0)$	-0.066	Ga 4p P 3p Out p 0.51 0.41 0.32	In Ga P Out 0.43 0.26 0.17 0.11
$7a_1(0)$	-0.015	Out s H-P 2s H-Ga 2s 0.83 -0.16 -0.12	Out In H-P H-Ga 0.71 0.25 0.024 0.015

TABLE II

Ionicity of the atomic centers of the $GaPH_6$ and $GaNH_6$ clusters in units of electronic charge.

$GaPH_6$		$GaNH_6$	
Atomic center	Ionicity	Atomic center	Ionicity
P	-1.170	N	-0.972
Ga	-0.136	Ga	0.627
H-P	0.217	H-N	-0.139
H-Ga	0.218	H-Ga	0.254

TABLE III

Electron states of the $GaNH_6$ cluster calculated by the SCF Xα multiple-scattering method.

The are listed in the order of increasing eigen-energy. The occupation numbers of the levels are shown in the parentheses. Only the important components of the normalized partial-wave coefficients and electronic charge distributions are shown. (The "In" and "Out" represent the interatomic and extra-molecular regions of the cluster respectively.) The constant potential in the interatomic region is -0.190 Ry.

Electron state	Eigen-energy (Ry)	Partial-wave coefficients	Electronic charge distribution
$1a_1(2)$	-1.094	N 2s 0.96	N 0.92
$2a_1(2)$	-0.844	H-Ga 1s Ga 4s 0.80 -0.54	H-Ga Ga 0.65 0.29
1e (0)	-0.736	H-Ga 1s 0.97	H-Ga 0.94
$3a_1(2)$	-0.513	Ga 4s H-Ga 1s 0.71 0.57	Ga H-Ga 0.50 0.39
2e (4)	-0.361	N 2p H-N 1s Ga 4p 0.70 -0.56 -0.34	N Ga H-N 0.49 0.12 0.11
$4a_1(2)$	-0.336	H-N 1s N 2p N 3s 0.87 0.20 0.18	H-N In N 0.77 0.15 0.07
3e (0)	-0.315	H-N 1s N 2p Ga 4p 0.72 0.48 -0.32	H-N N In Ga 0.53 0.23 0.14 0.10
$5a_1(2)$	-0.276	N 2p Ga 4p H-N 2s 0.85 0.21 -0.19	N In Ga H-N 0.72 0.17 0.05 0.05
$6a_1(0)$	-0.142	Ga 4p N 2p 0.67 -0.31	Ga In N 0.45 0.40 0.10
4e (0)	-0.121	Ga 4p N 2p Out p H-Ga 2p 0.43 0.32 0.27 0.21	In Ga N Out 0.57 0.19 0.10 0.08
$7a_1(0)$	-0.011	Out p Out s Ga 5p H-Ga 2p 0.71 -0.37 -0.23 0.17	Out In Ga H-Ga 0.65 0.24 0.05 0.04

FIGURE CAPTIONS

Fig. 1. The cluster model of $GaPH_6$ for a GaP crystal. The small spheres are the atomic centers, and the large sphere is the outersphere outside of which the extramolecular region exists. They are not shown in scale. The H-P and H-Ga indicate the hydrogen atomic centers which surround the P and Ga atomic centers respectively.

Fig. 2. One-electron energy levels of the $GaPH_6$ cluster (a), compared with the one-electron energy levels of the constituent free atoms of the cluster (b) and of the GaP crystal (after Dean, ref. 13) (c). The linearly expanded energy levels of the $GaPH_6$ cluster to fit the band-edges of the GaP crystal are shown in (d). The hydrogenic surface electron levels of the cluster are shown as dashed lines. —·—·— represents the constant potential of the interatomic region of the cluster.

Fig. 3a. Contour map of the $1a_1$ wave function of the $GaPH_6$ cluster. It is plotted in a plane which bisects the Ga (middle left), the P (middle right), a H-Ga (upper left), and a H-P (lower right) atomic centers. The dashed circles are the projections of the atomic centers and the outersphere of the cluster. The contour curves were selected such that the logarithm of the magnitude of the wave function value is equally spaced for the consecutive curves. The maximum wave function is indicated by the label of +5 or -5 depending on the sign of the wave function value, and the node is indicated by the label of either +1 or -1.

Fig. 3b. Contour map of the $2a_1$ wave function of the $GaPH_6$ cluster.

Fig. 3c. Contour map of the 1e wave function of the $GaPH_6$ cluster.

Fig. 3d. Contour map of the 2e wave function of the $GaPH_6$ cluster.

Fig. 3e. Contour map of the $3a_1$ wave function of the $GaPH_6$ cluster.

Fig. 3f. Contour map of the $4a_1$ wave function of the $GaPH_6$ cluster.

Fig. 3g. Contour map of the 3e wave function of the $GaPH_6$ cluster.

Fig. 3h. Contour map of the $5a_1$ wave function of the $GaPH_6$ cluster.

Fig. 3i. Contour map of the 4e wave function of the $GaPH_6$ cluster.

Fig. 3j. Contour map of the $6a_1$ wave function of the $GaPH_6$ cluster.

Fig. 3k. Contour map of the $7a_1$ wave function of the $GaPH_6$ cluster.

Fig. 4. One-electron energy levels of the $GaNH_6$ cluster (b), compared with the one-electron energy levels of the constituent free atoms of the cluster (a) and of the $GaPH_6$ cluster (c). The hydrogenic surface electron levels are indicated by dashed lines. —·—·— represents the constant potential in the interatomic region of the cluster. The correspondence relationships of the electron states between the $GaNH_6$ cluster and the $GaPH_6$ cluster are indicated by the interconnections between Figs. (b) and (c).

Fig. 5a. Contour map of the $1a_1$ wave function of the $GaNH_6$ cluster. It is plotted in the same way as shown in Fig. 3a except that the N atomic center now replaces the P atomic center.

Fig. 5b. Contour map of the $2a_1$ wave function of the $GaNH_6$ cluster.

Fig. 5c. Contour map of the 1e wave function of the $GaNH_6$ cluster.

Fig. 5d. Contour map of the $3a_1$ wave function of the $GaNH_6$ cluster.

Fig. 5e. Contour map of the 2e wave function of the $GaNH_6$ cluster.

Fig. 5f. Contour map of the $4a_1$ wave function of the $GaNH_6$ cluster.

Fig. 5g. Contour map of the 3e wave function of the $GaNH_6$ cluster.

Fig. 5h. Contour map of the $5a_1$ wave function of the $GaNH_6$ cluster.

Fig. 5i. Contour map of the $6a_1$ wave function of the $GaNH_6$ cluster.

Fig. 5j. Contour map of the 4e wave function of the $GaNH_6$ cluster.

Fig. 5k. Contour map of the $7a_1$ wave function of the $GaNH_6$ cluster.

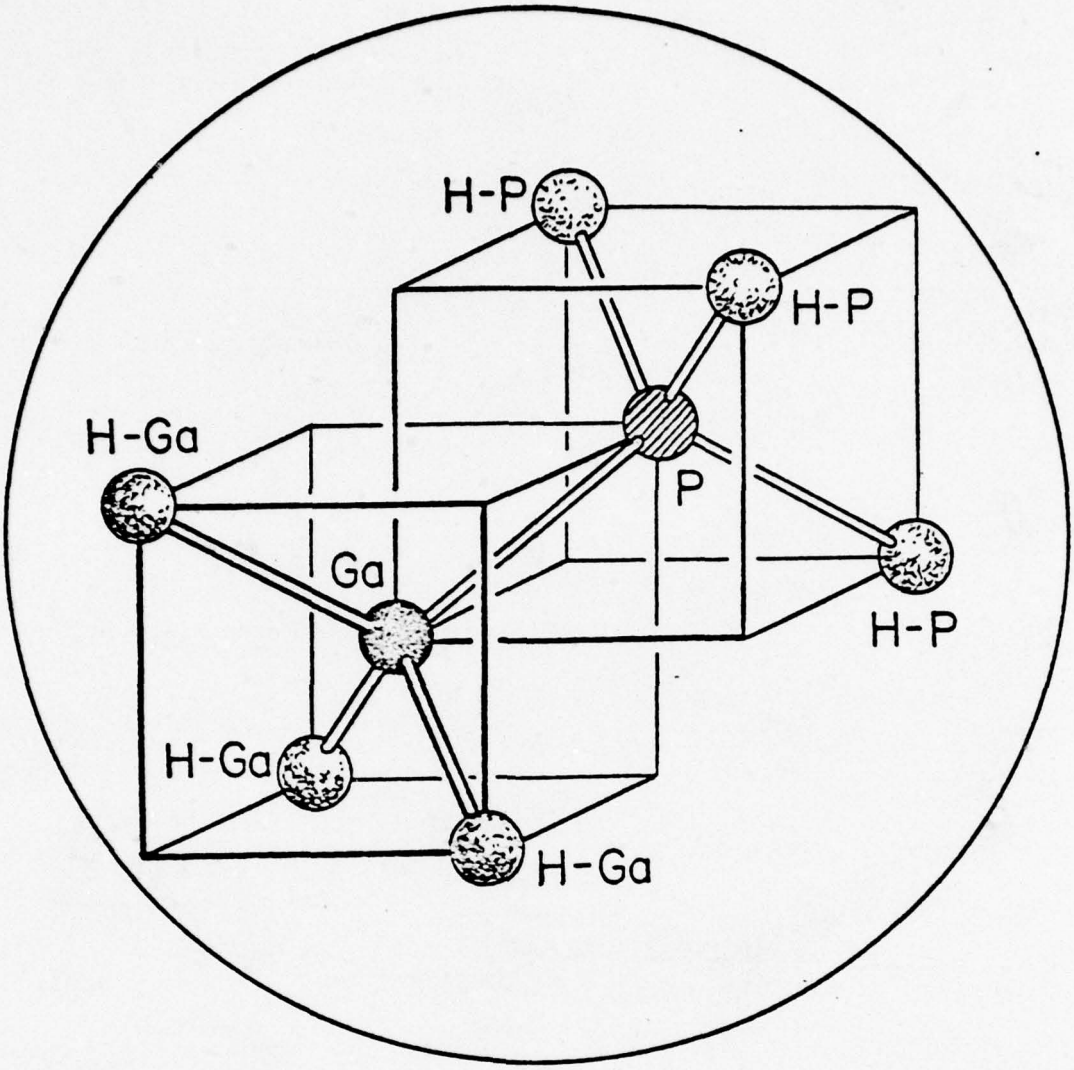

GaP

Fig. 1

One-electron energy (Ry)
0
-0.2
-0.4
-0.6
-0.8
-1.0
-1.2
(a)
(b)
(c)
(d)
H 3s,p,d
Ca 4p
H 2s,p
P 3p
Ga 4s
P 3s
H 1s
7a1
6a1
4e
5a1
3e
4a1
3a1
2e
1e
2a1
1a1
Conduction band
Valence band
X3
X1
0.212
0.172
Γ1
Γ8
Γ7
X5
L
Γ
X

GaP

Fig. 2

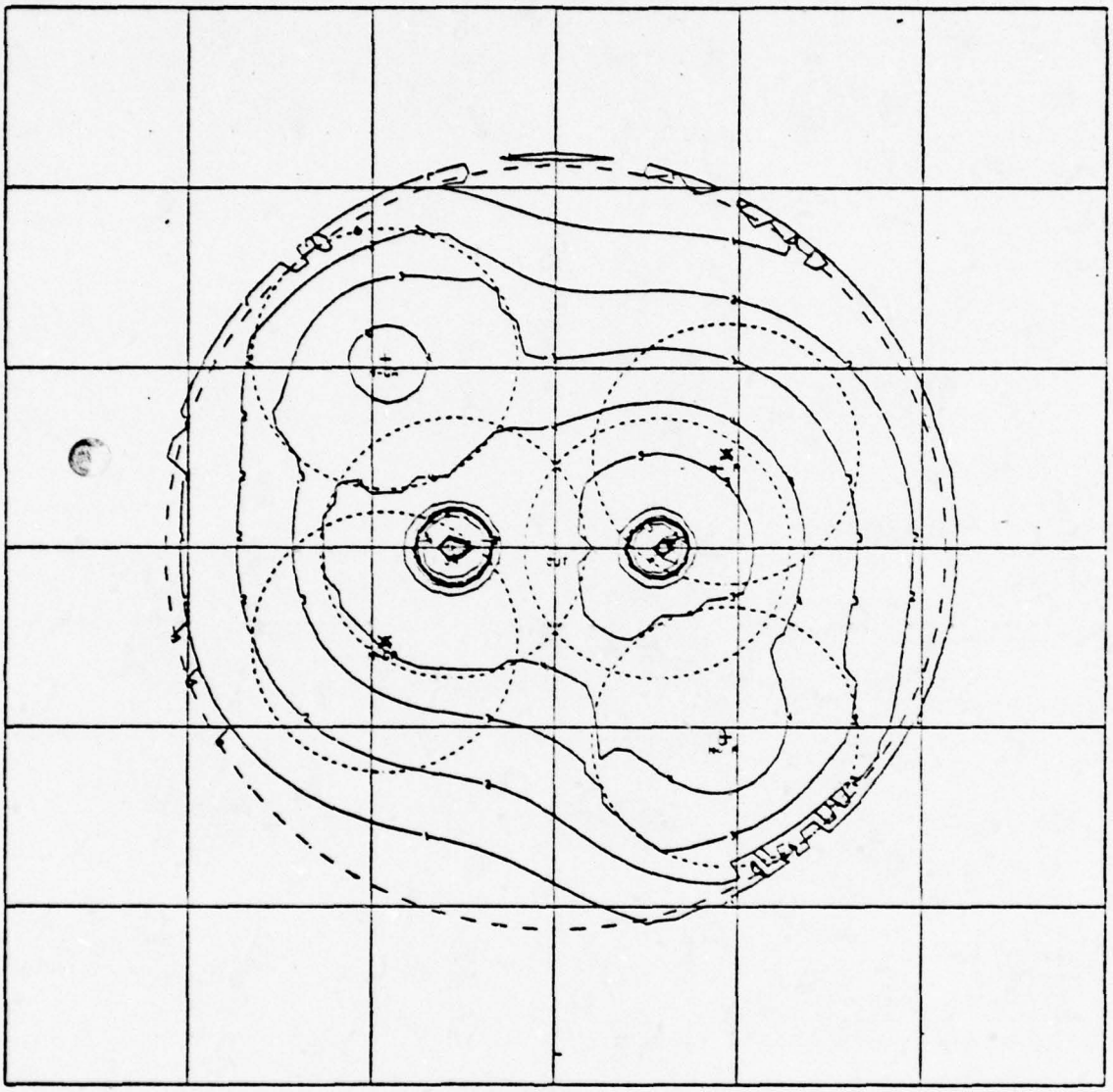

GaP

Fig. 3a

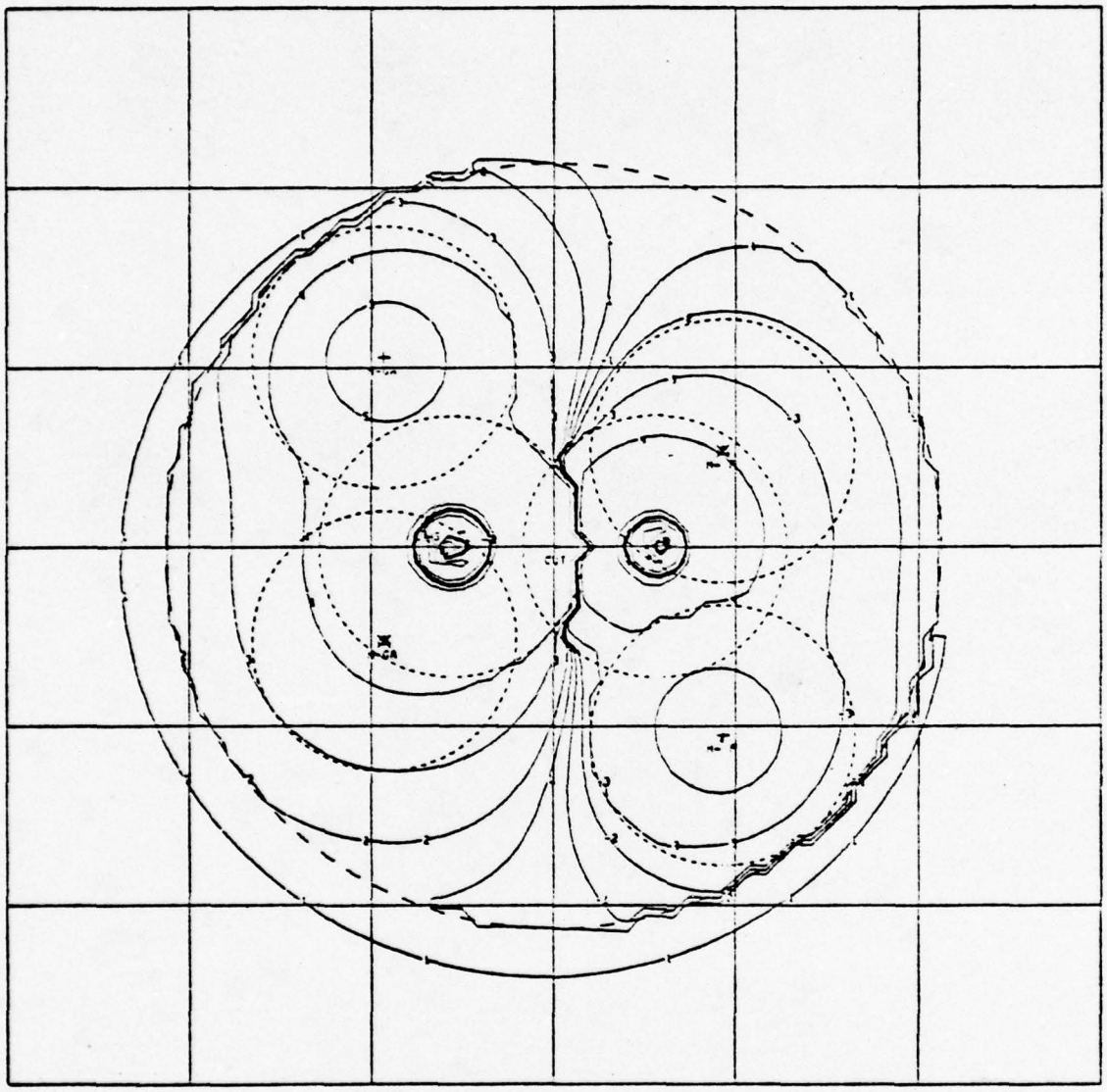

GaP

Fig. 3b

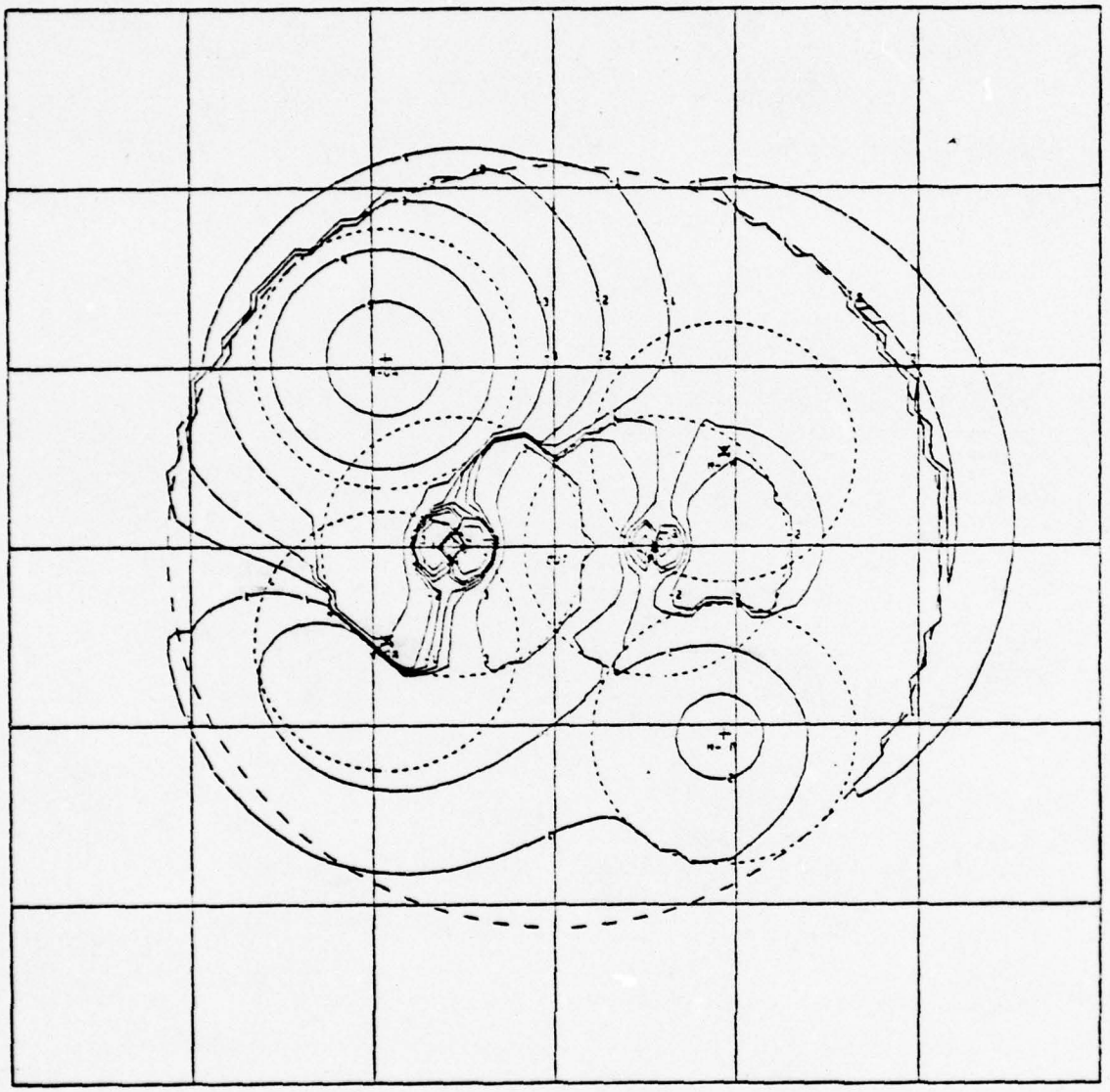

GaP

Fig. 3c

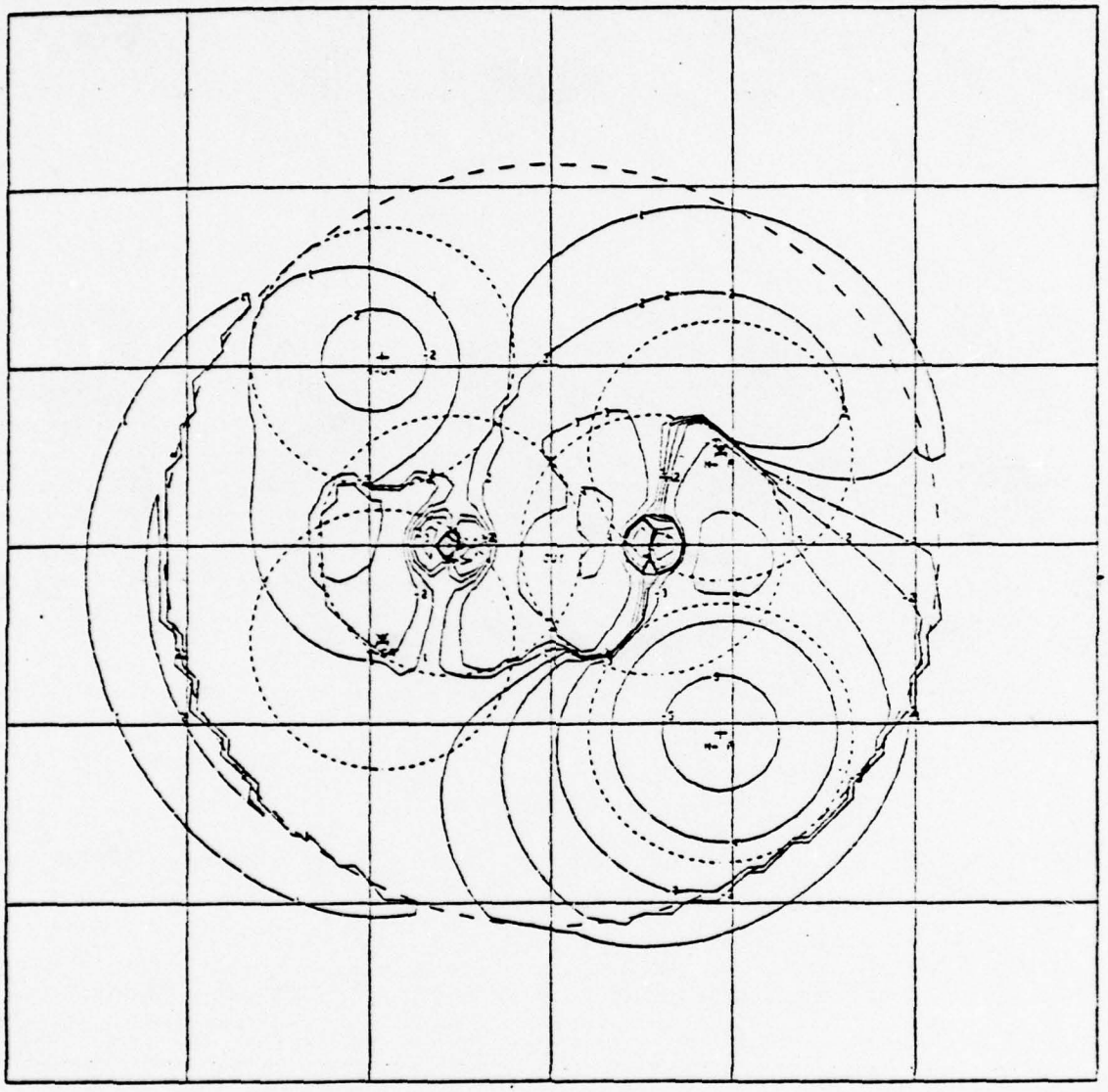

GaP

Fig. 3d

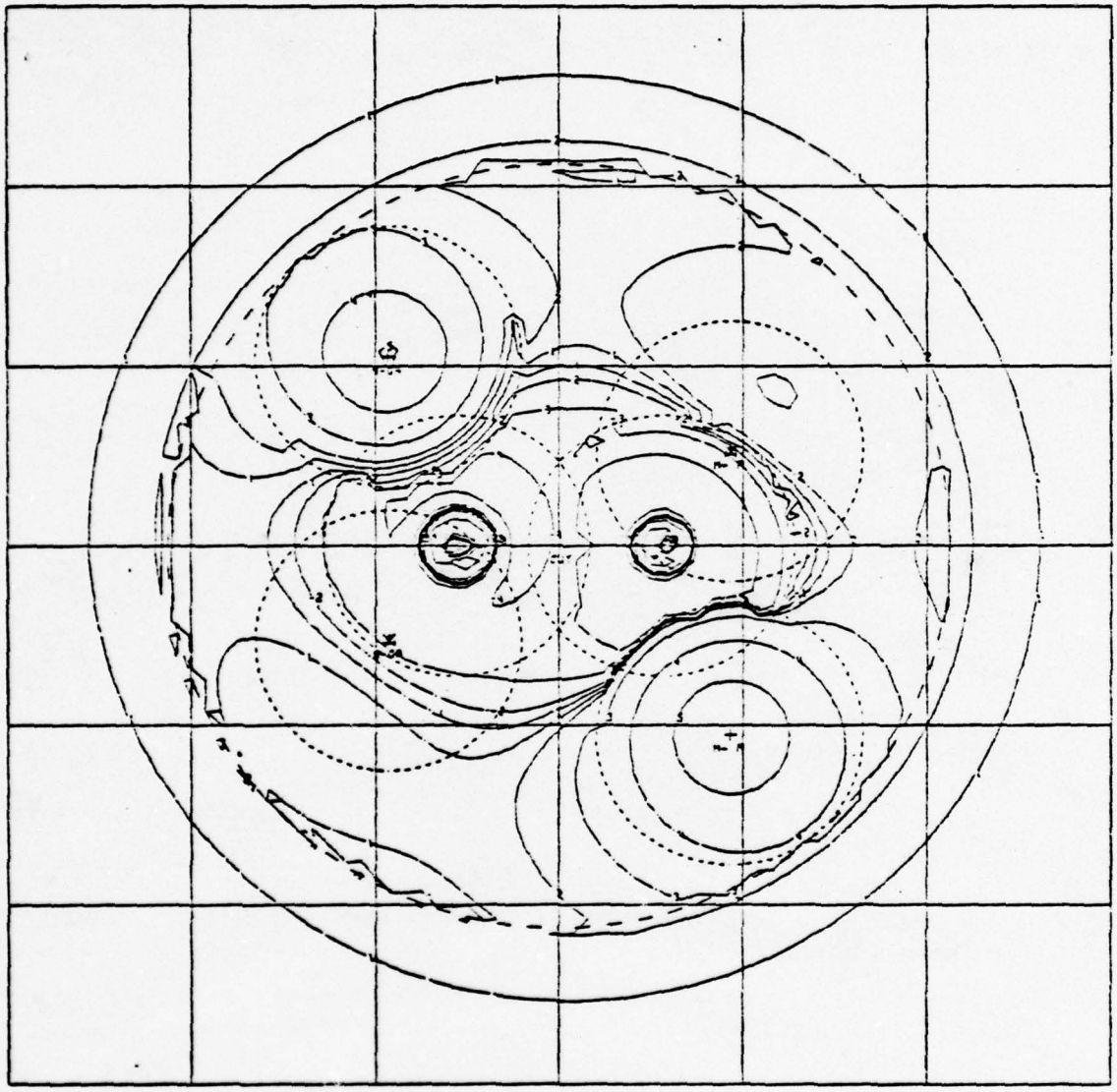

GaP

Fig. 3e

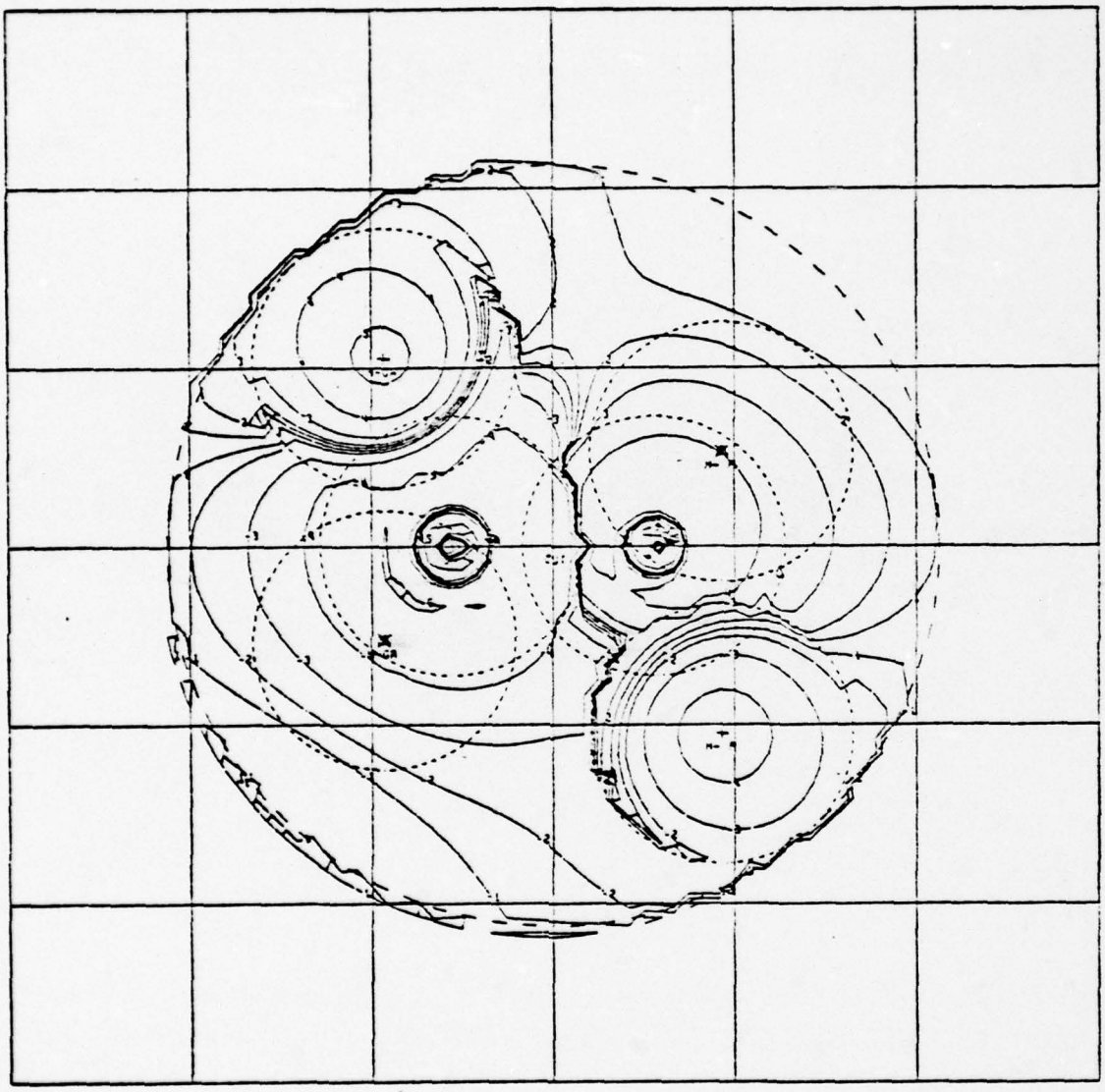

GaP

Fig. 3f

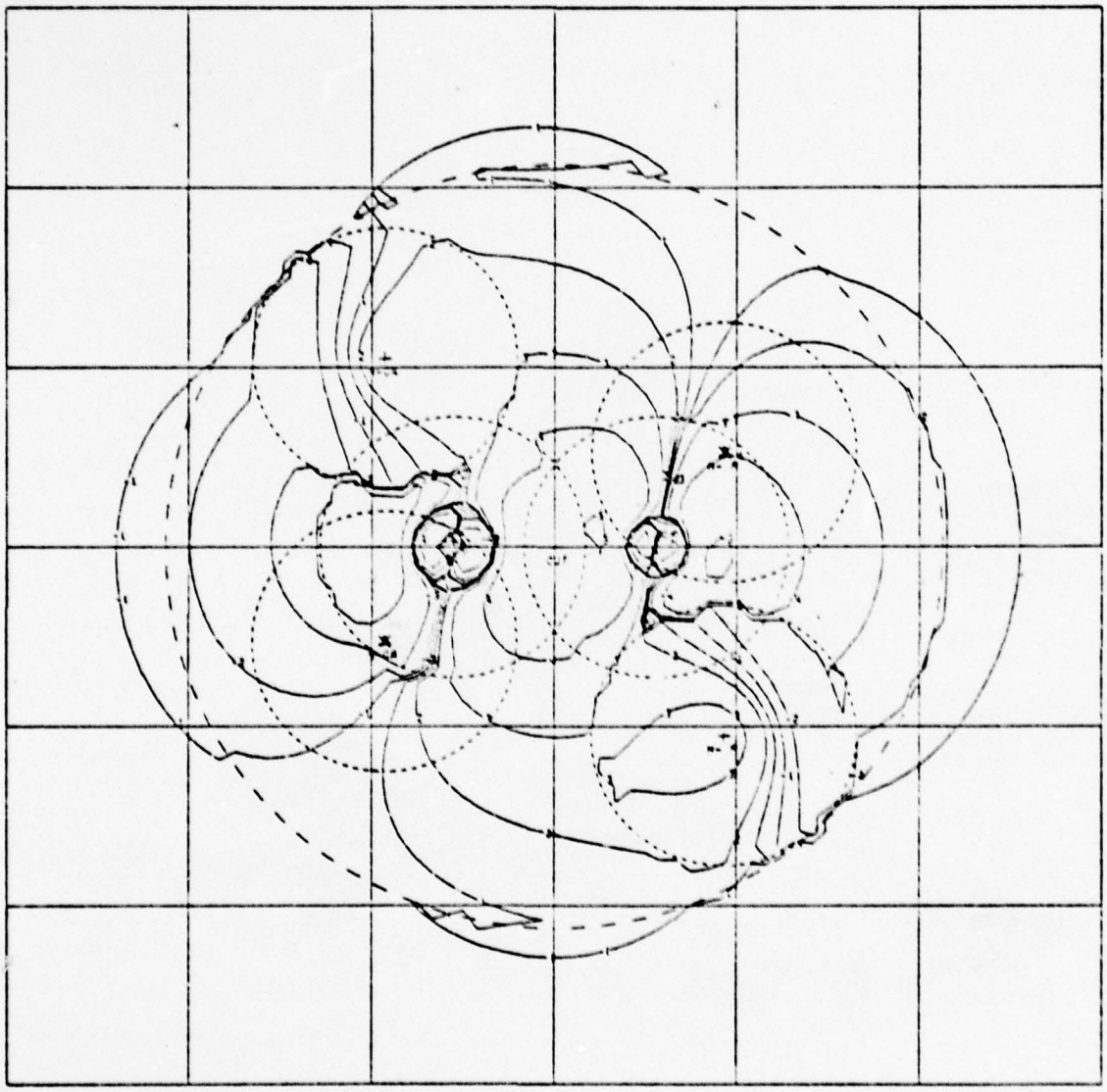

GaP

Fig. 3g

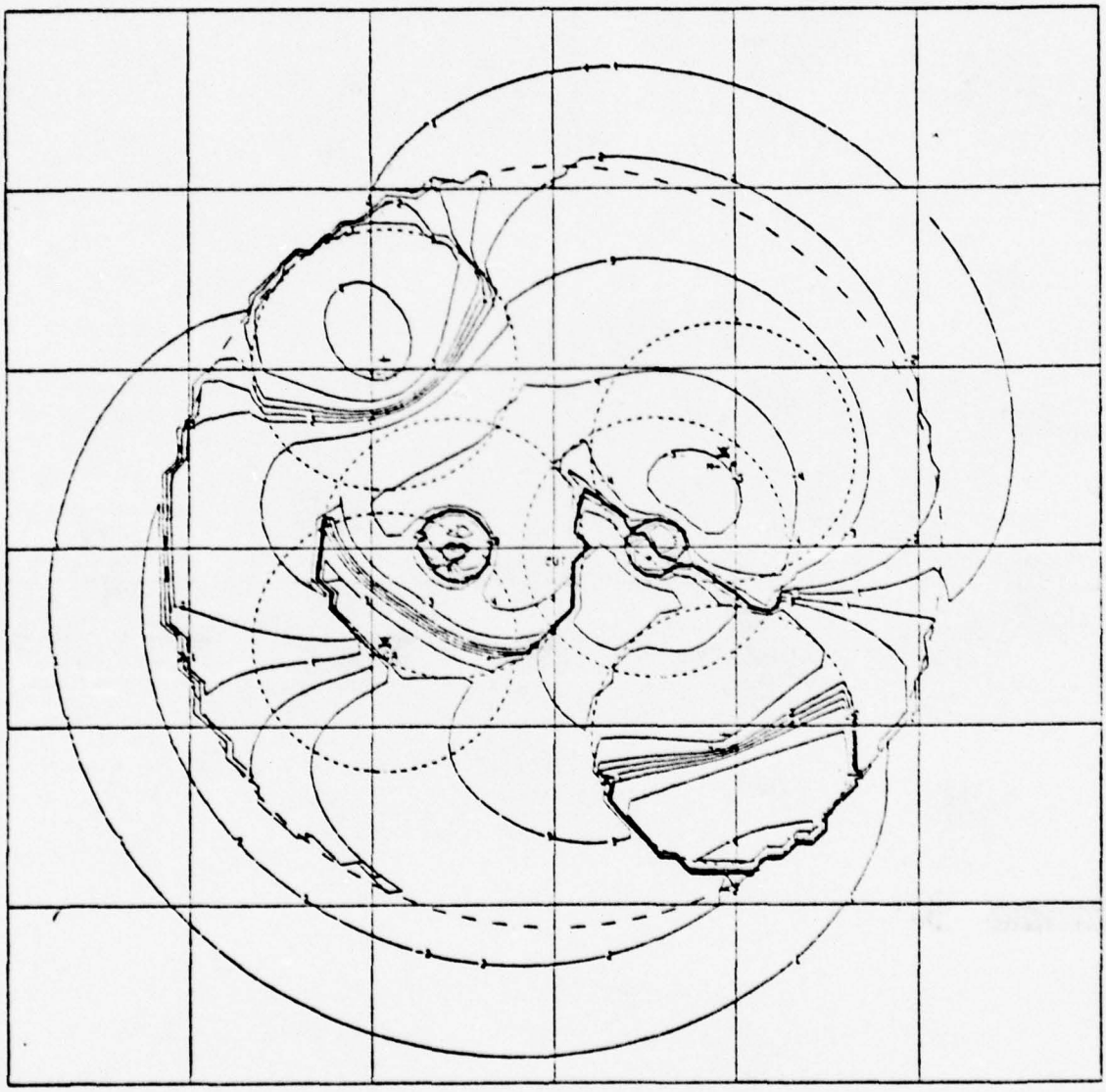

GaP

Fig. 3h

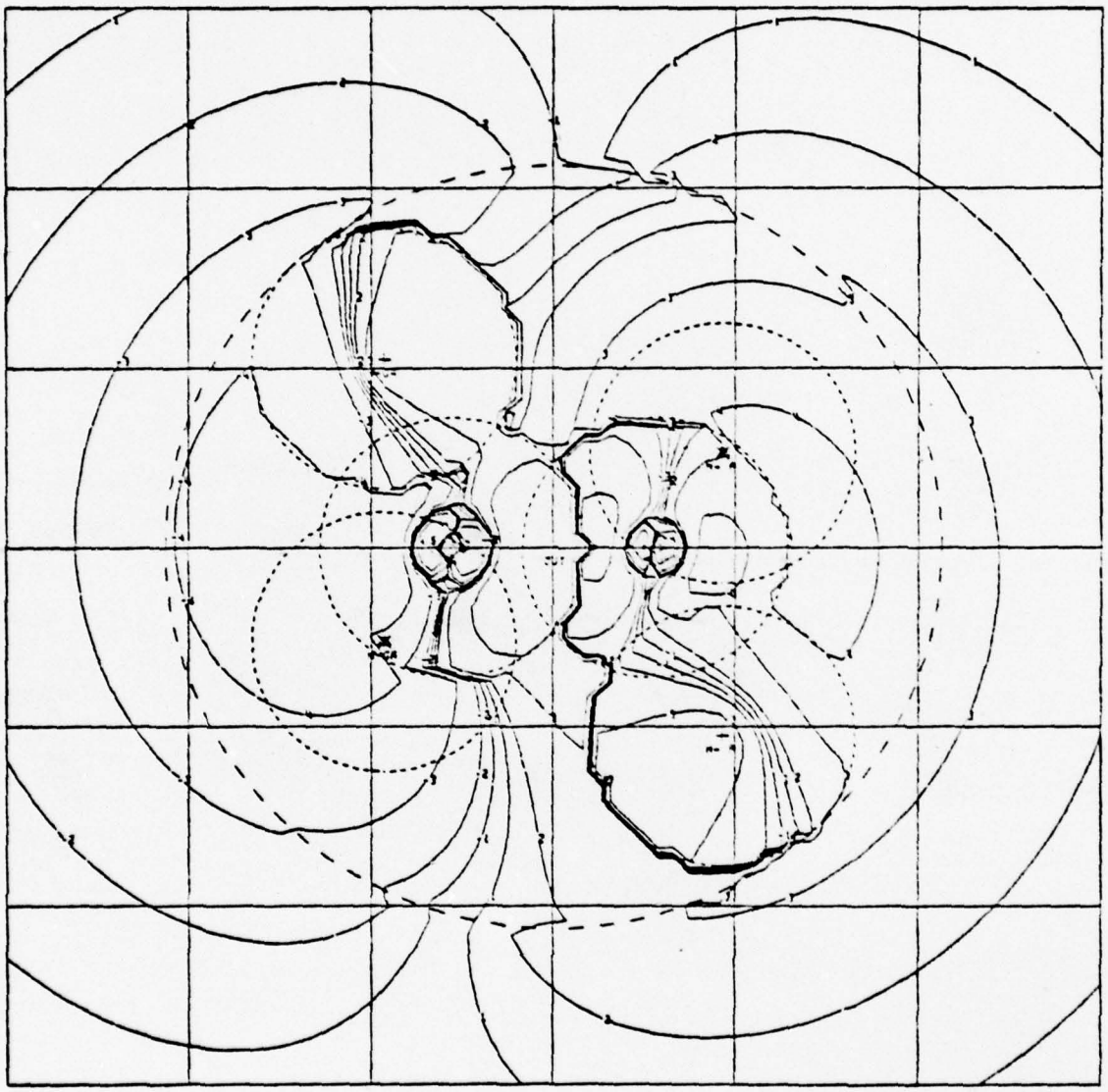

GaP

Fig. 3i

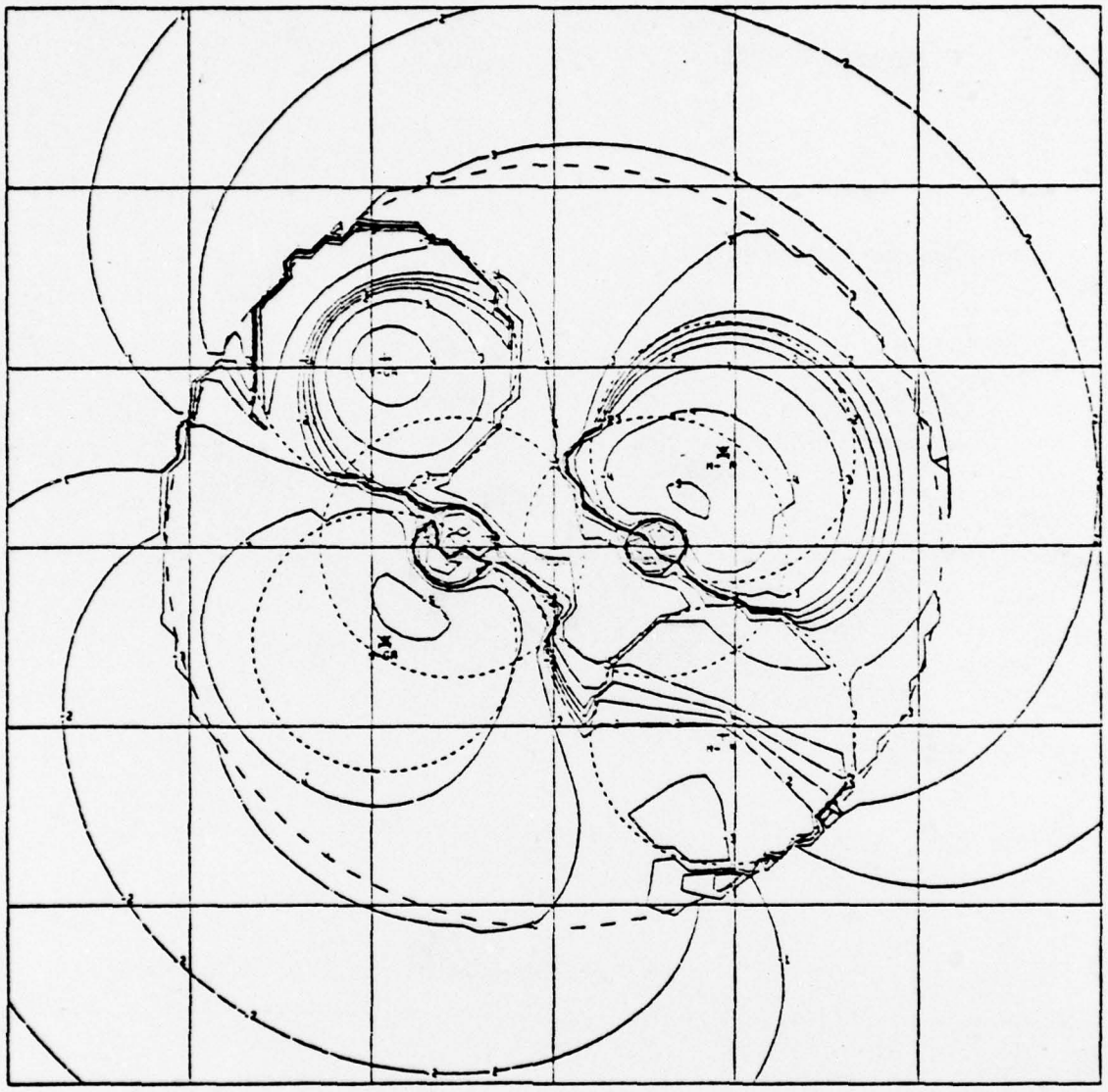

GaP

Fig. 3j

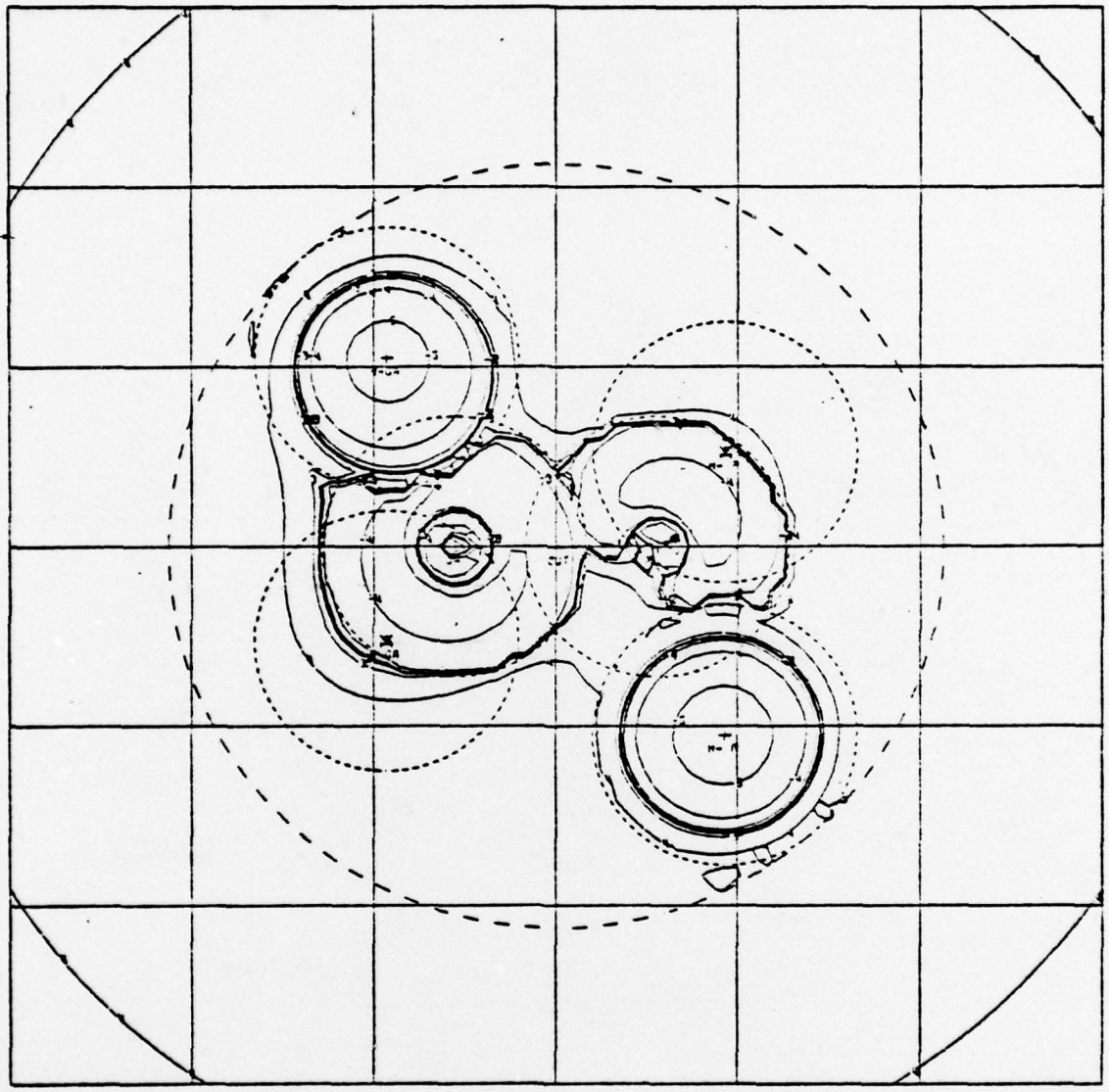

GaP

Fig. 3k

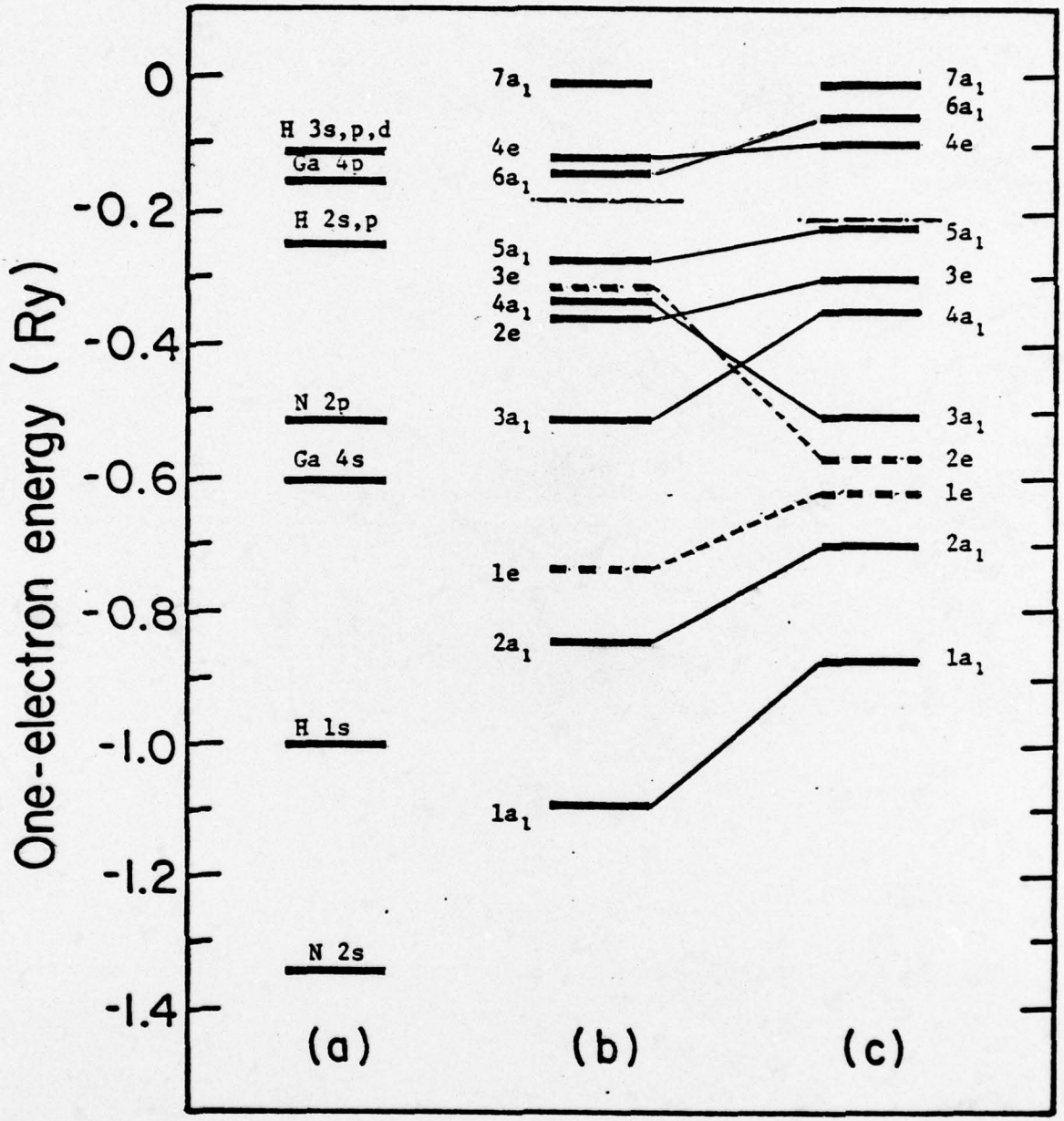
One-electron energy (Ry)
0
-0.2
-0.4
-0.6
-0.8
-1.0
-1.2
-1.4
H 3s,p,d
Ga 4p
H 2s,p
N 2p
Ga 4s
H 1s
N 2s
7a1
4e
6a1
5a1
3e
4a1
2e
3a1
1e
2a1
1a1
7a1
6a1
4e
5a1
3e
4a1
3a1
2e
1e
2a1
1a1
(a)
(b)
(c)

GaP

Fig. 4

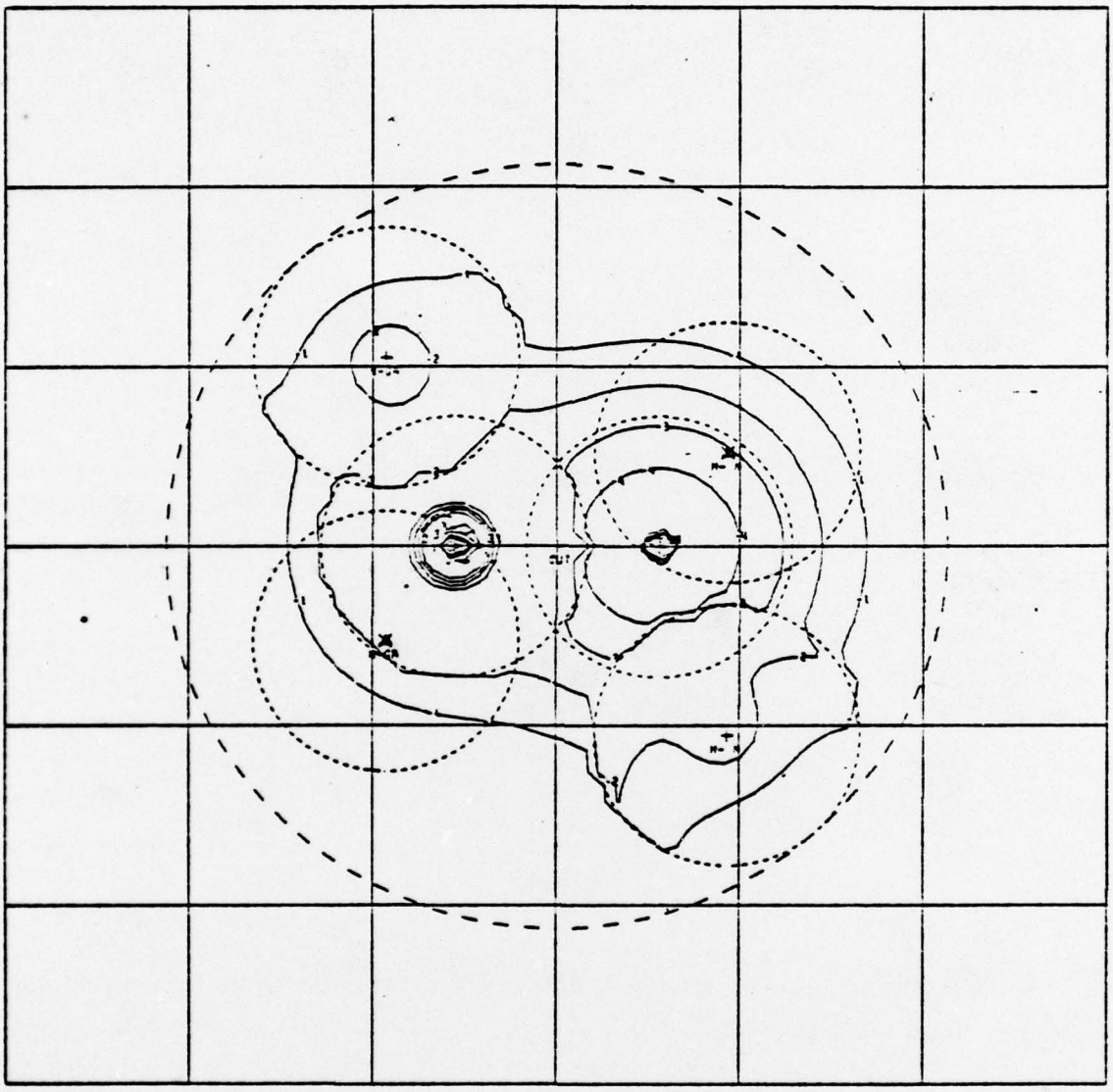

GaP

Fig. 5a

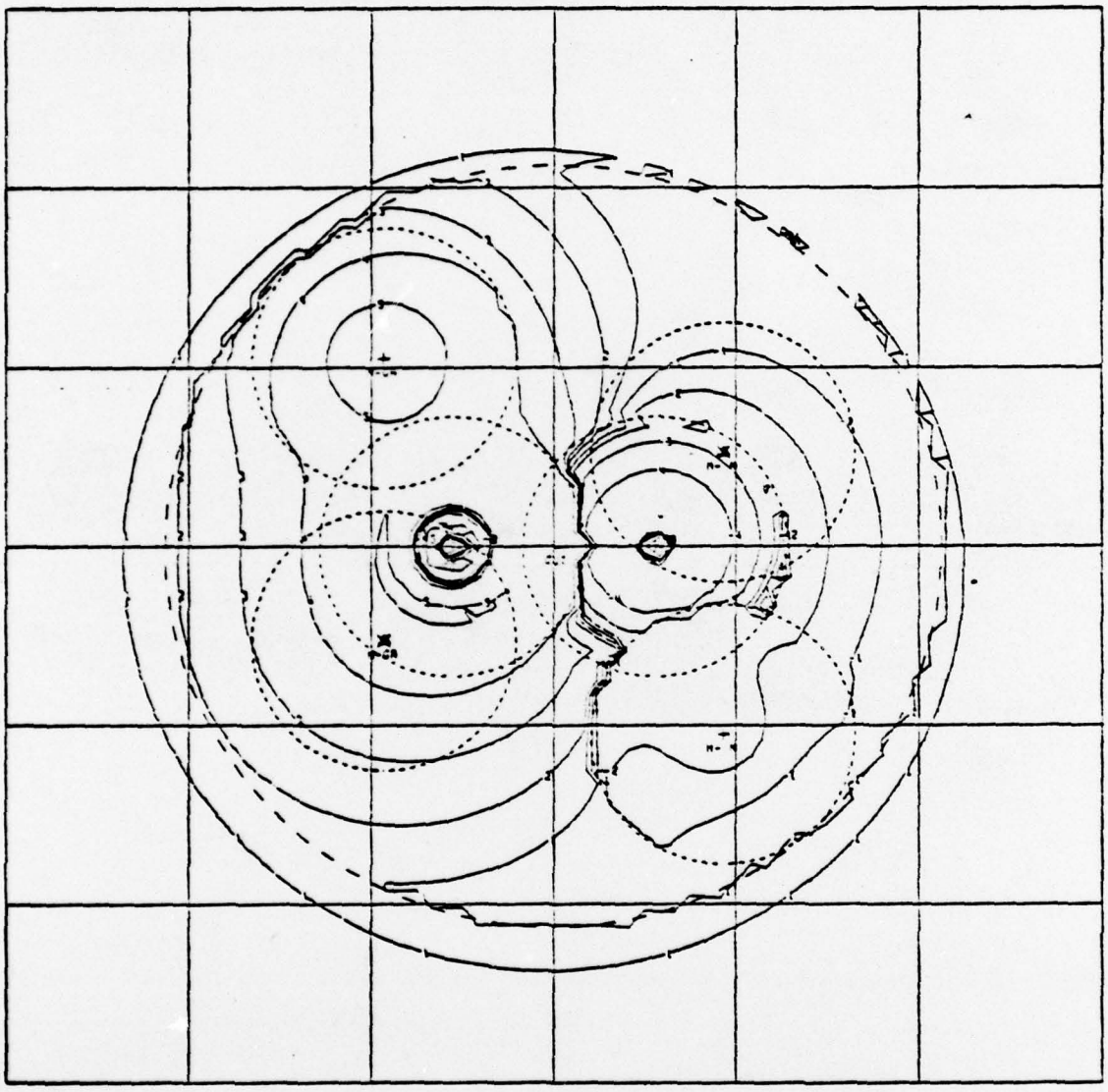

GaP

Fig. 5b

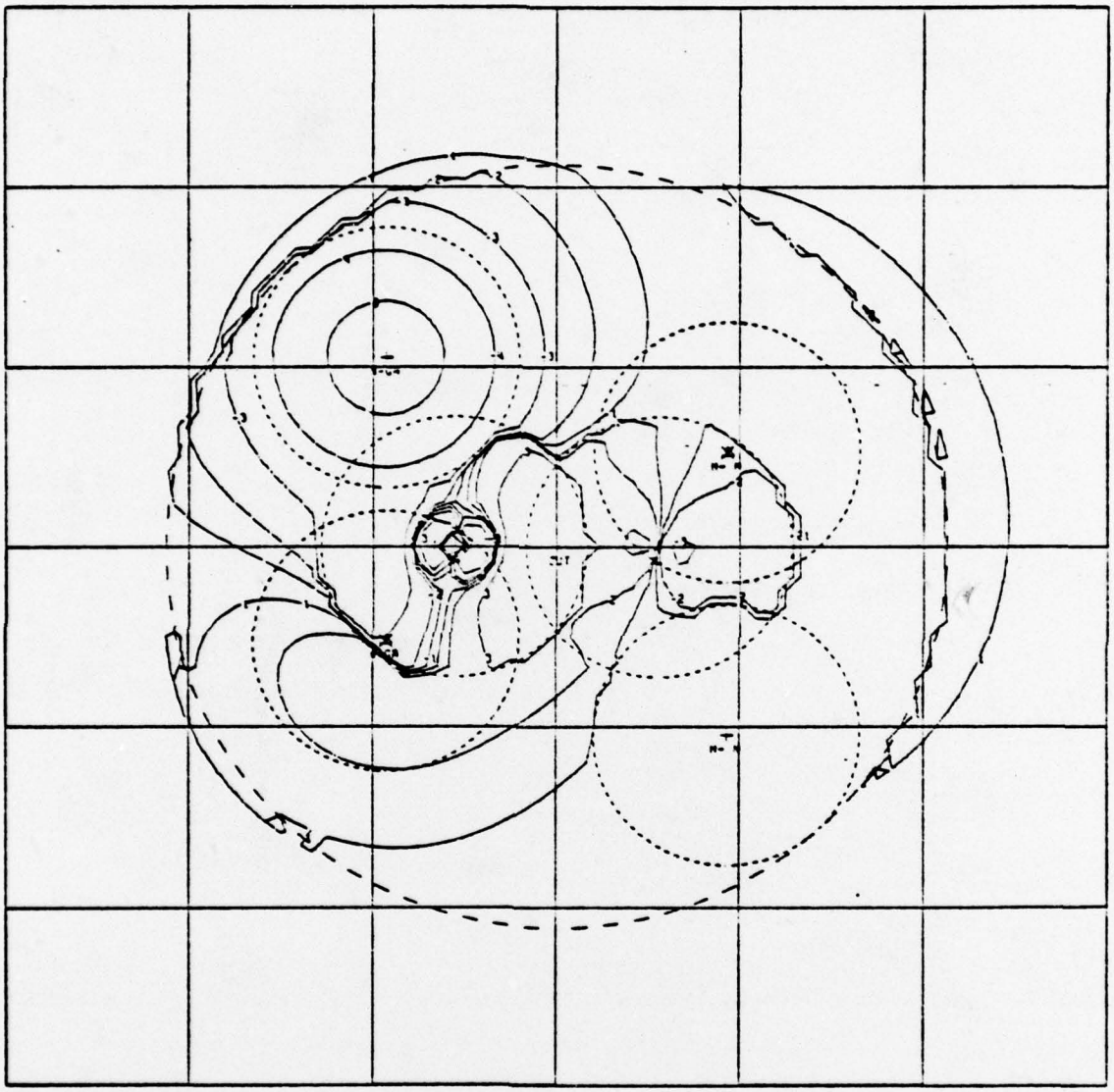

GaP

Fig. 5c

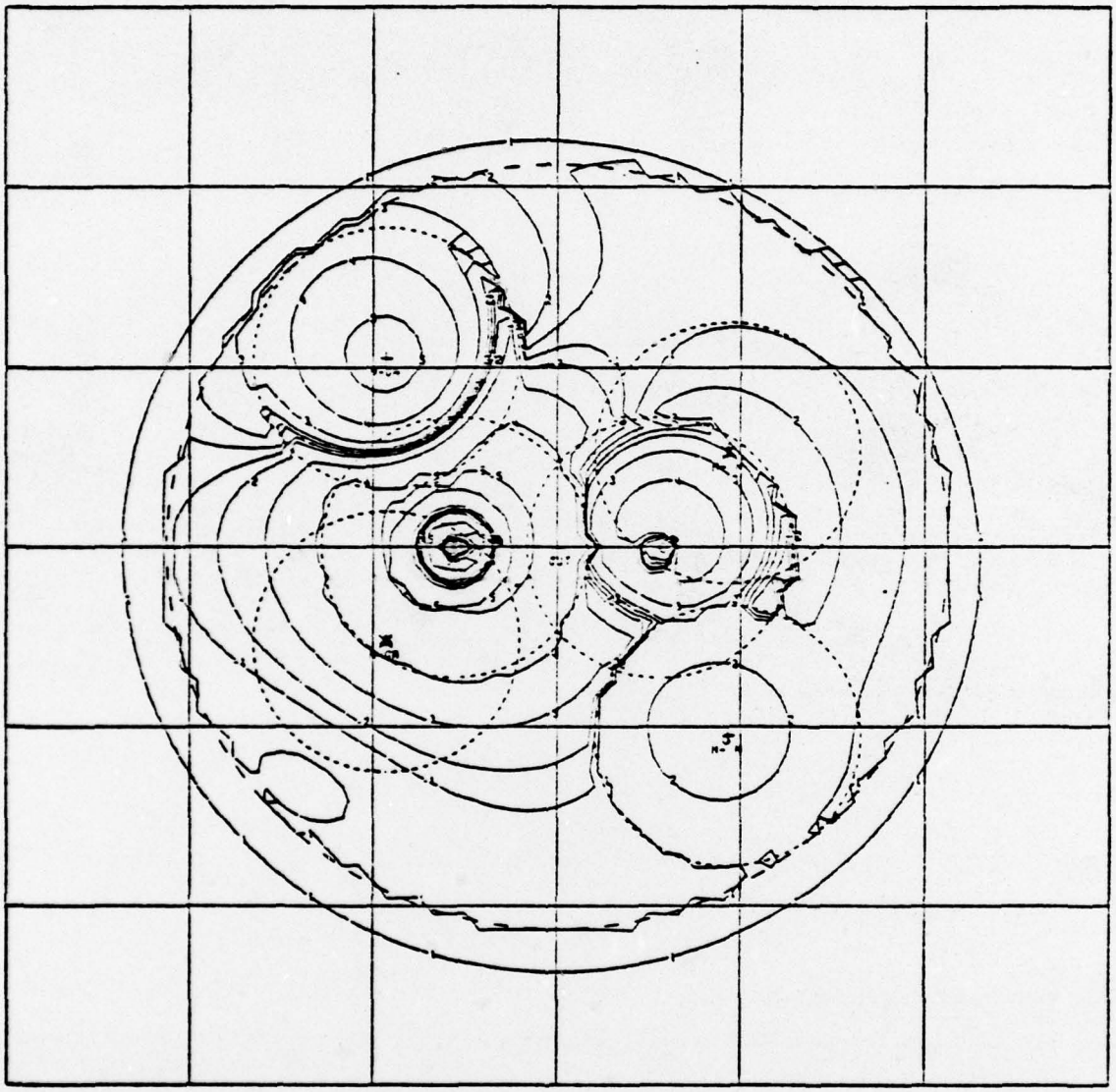

GaP

Fig. 5 d

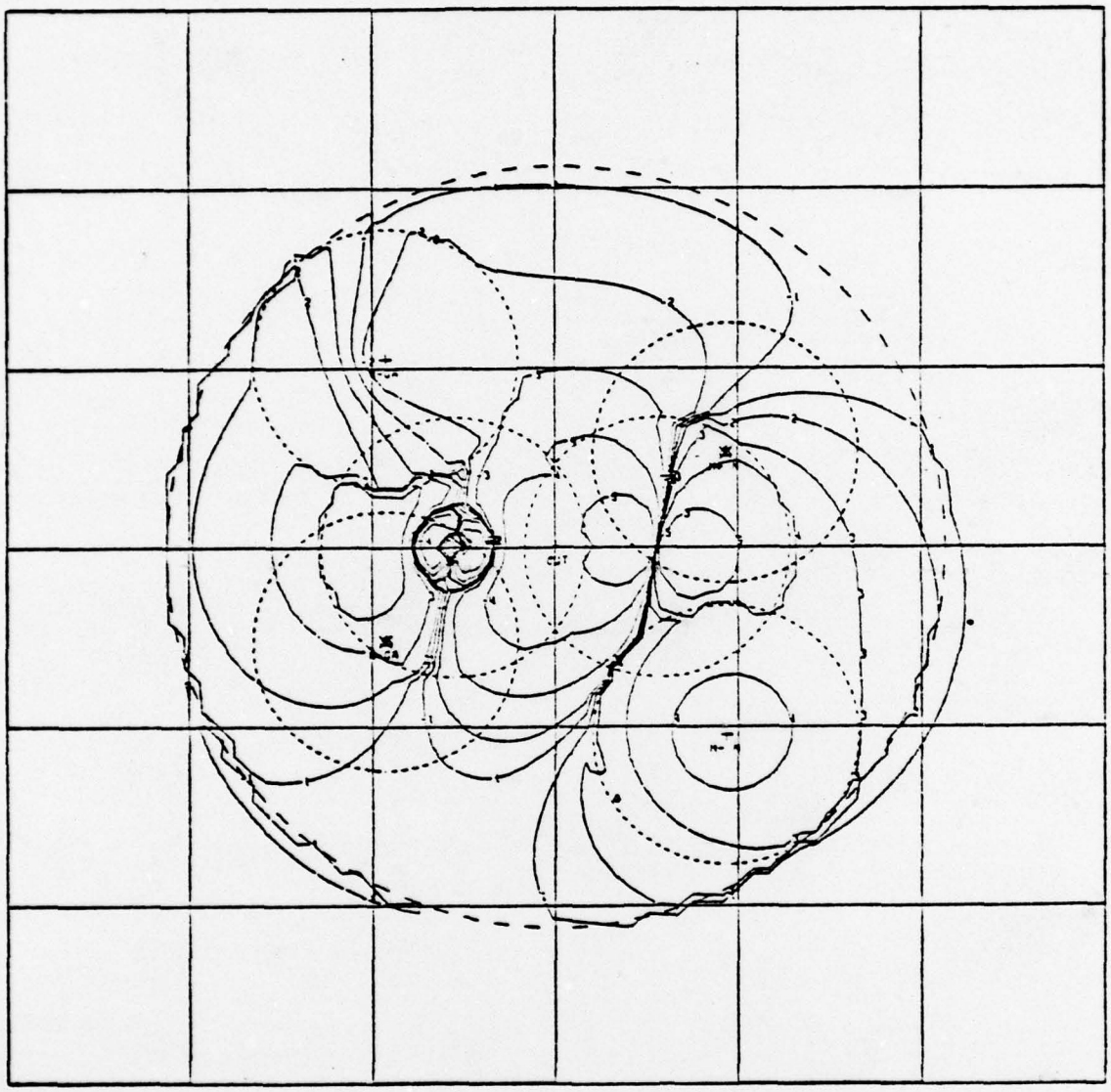

GaP

Fig. 5e

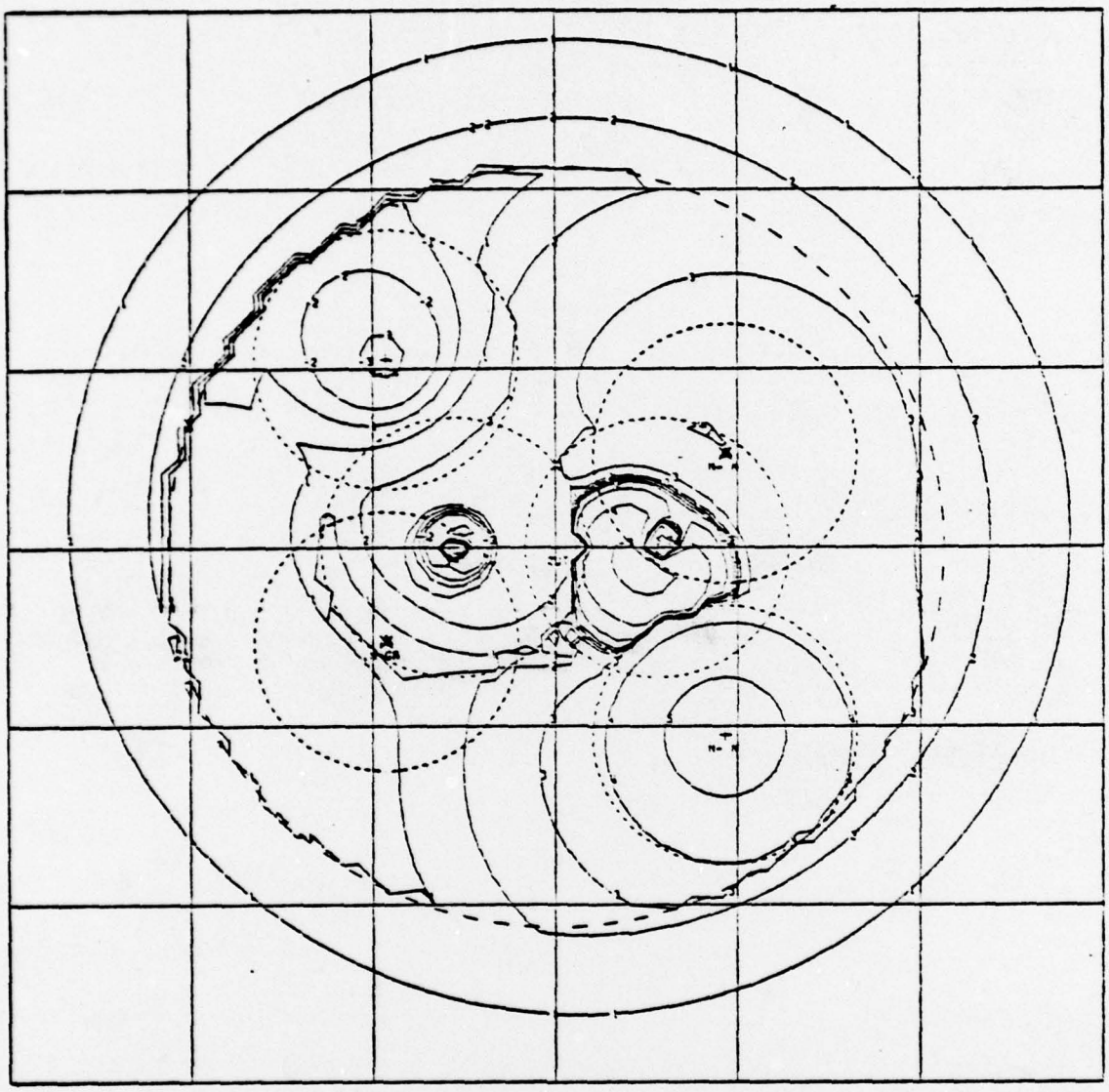

GaP

Fig. 5f

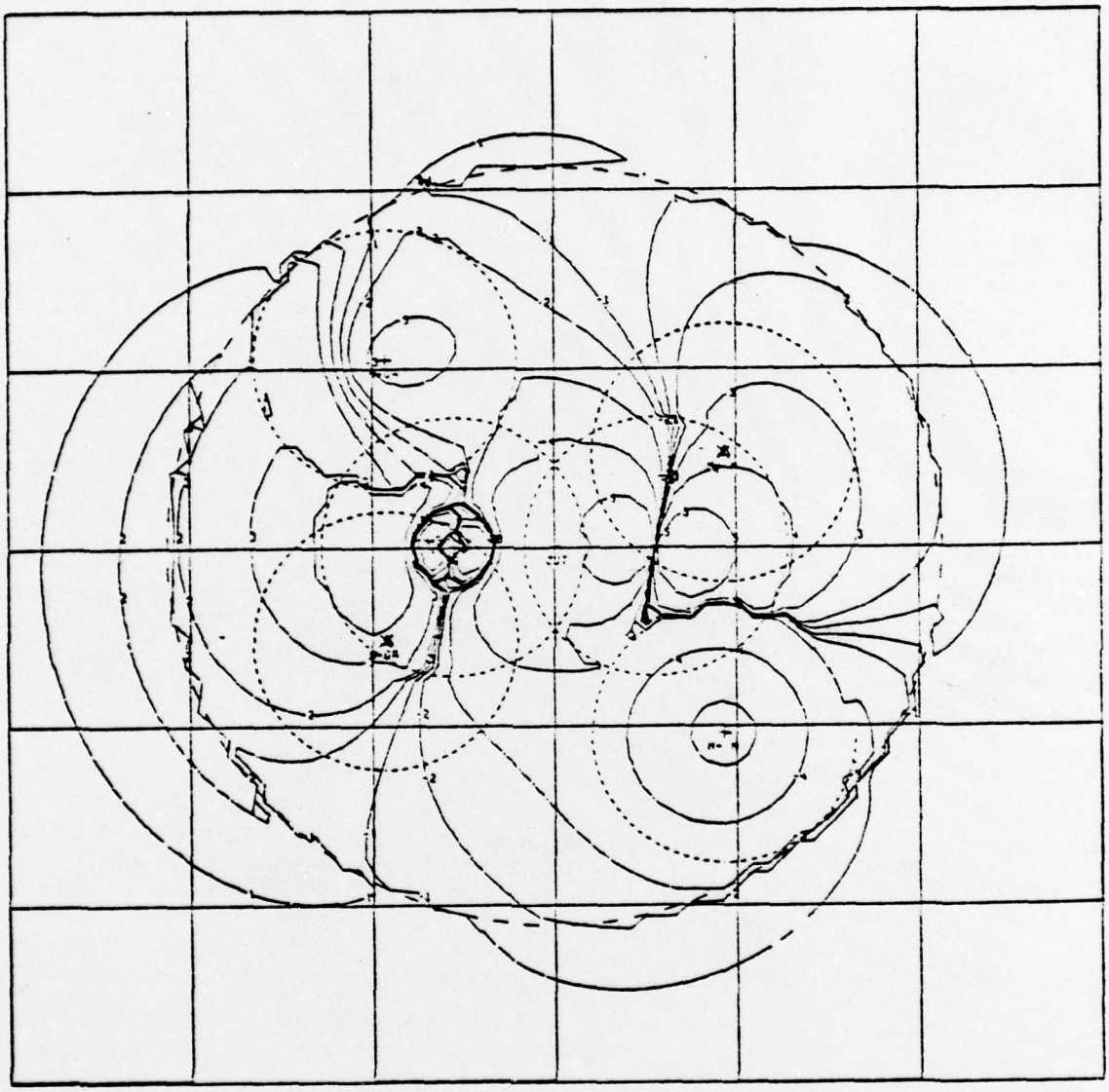

GaP

Fig. 5g

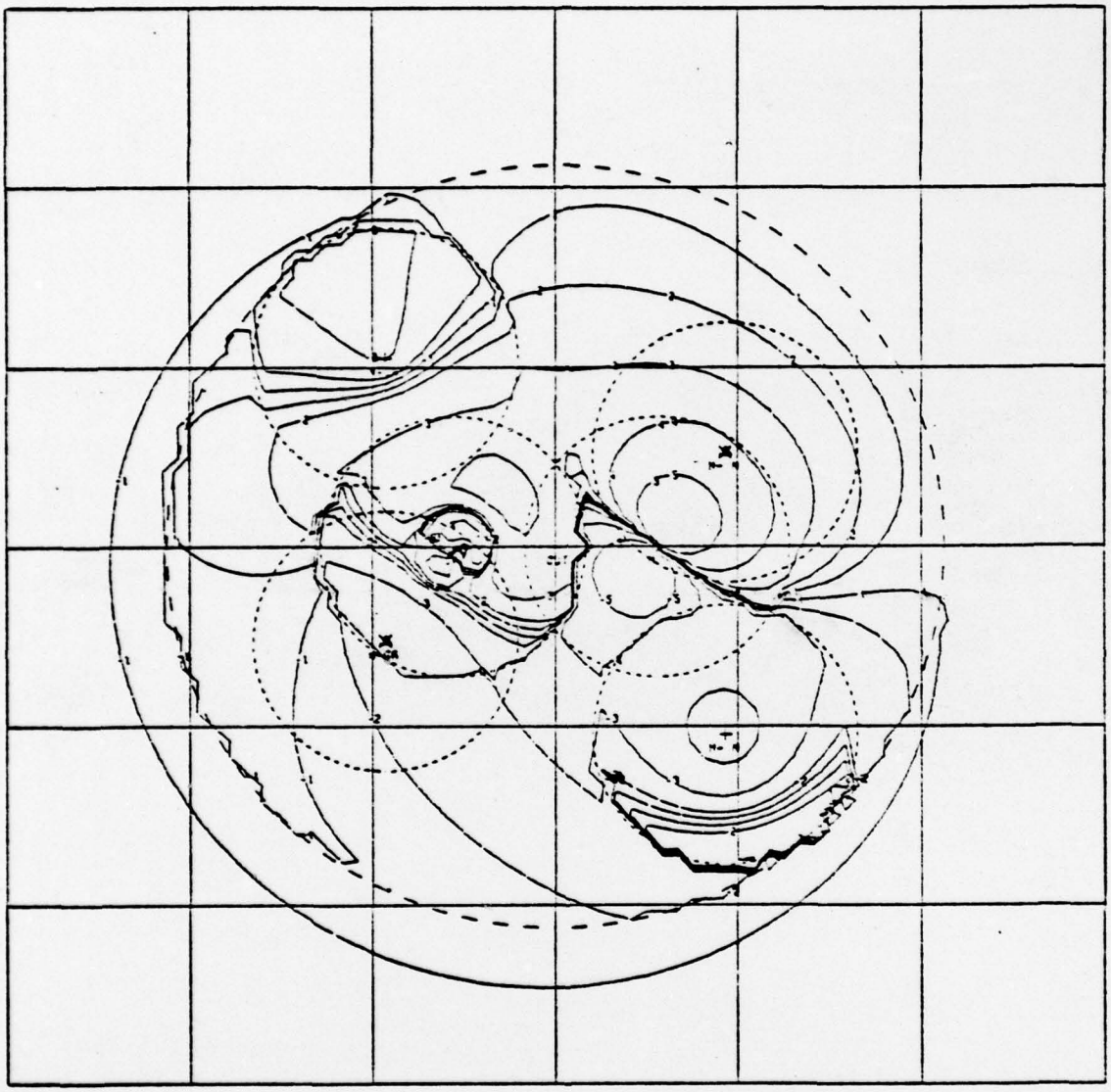

GaP

Fig. 5h

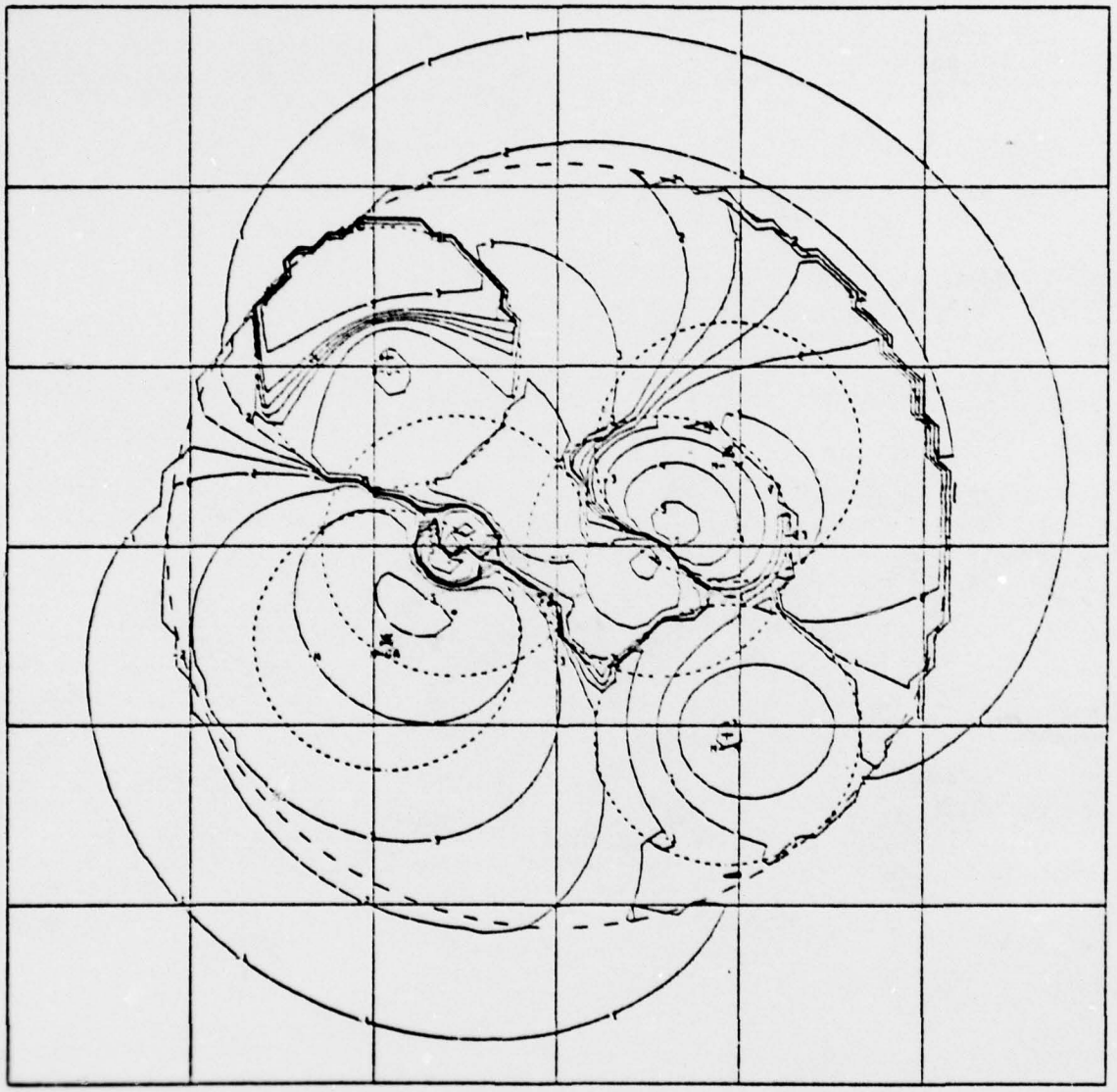

GaP

Fig 5i

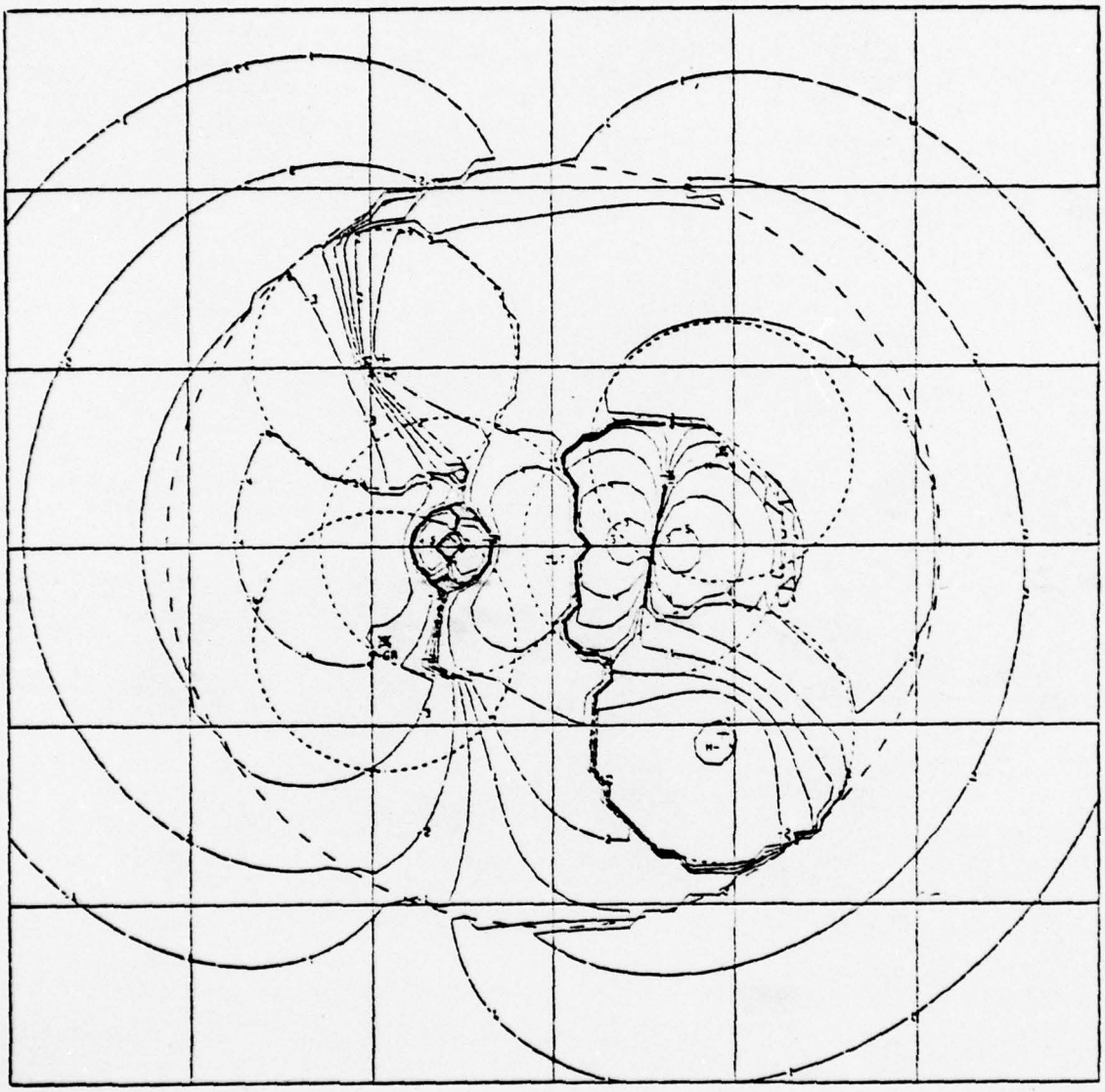

GaP

Fig. 5j

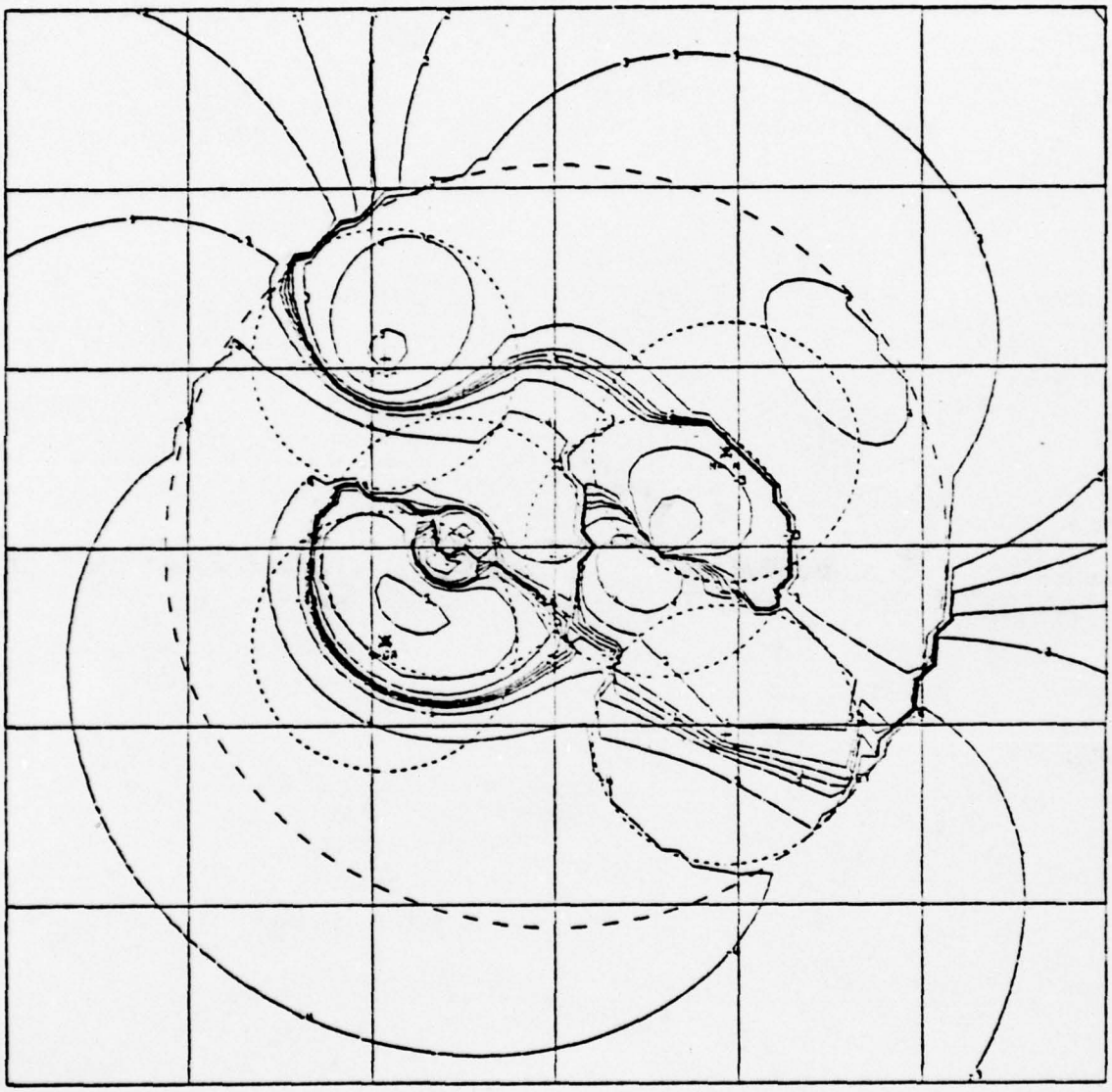

GaP

Fig. 5k